

**Functionalized Mesoporous Metal  
Oxide Spheres as Catalysts for  
Efficient Conversion of Carbohydrates  
into  
5-Hydroxymethylfurfural**

**Seyed Farshad Motevalizadeh**

ORCID: 0000-0002-3005-2181

**Submitted in total fulfilment of the requirements of the  
degree of Doctor of Philosophy**

**June 2018**

**School of Chemistry  
The University of Melbourne**

Produced on archival quality paper



Dedicated to my lovely Spouse

**Mina**

My lovely son

**Seyed Alireza**

and

**My dear parents,**

brothers, parents in law and sisters in law

## Abstract

Fossil fuels currently provide more than 90% of global energy needs and feedstocks for the chemical industry. One of the most critical challenges facing mankind is reducing emissions of carbon dioxide. Biomass is a globally accessible resource that could provide an alternative feedstock for synthesizing chemical building blocks.

5-(Hydroxymethyl)furfural (5-HMF) is a commercially useful platform molecule that can be synthesized from biomass. Solid acid catalysts such as metal oxides and modified oxides fill an important role in biomass conversion, due to advantages like carrying both Lewis and Brønsted-acid sites, where the catalytic activity occurs, as well as thermal stability and low cost. The research focus is the preparation, surface modification and characterization of zirconium oxide and binary titanium zirconium oxides spheres as solid-acid catalysts for the conversion of biomass-derived carbohydrates to 5-HMF.

In Chapter 2, mesoporous zirconia was functionalized with common di-carboxylic acids and amino acids (i.e. terephthalic acid, 2-amino terephthalic acid, adipic acid, aspartic acid, succinic acid and glutamic acid) to prepare a multifunctional acidic catalyst for conversion of carbohydrates (fructose, glucose, sucrose, cellulose and starch) to 5-HMF. A green and versatile method was utilized to introduce the functional groups on the surface of the zirconia. The final catalyst, which was grafted with terephthalic acid, exhibited acceptable activity towards the dehydration conversion of fructose to 5-HMF with a yield of 42% after 2 h in dimethyl sulfoxide (DMSO) at 150 °C, with negligible loss of activity over five consecutive catalytic recycles.

In Chapter 3, mesoporous titanium zirconium oxide spheres were prepared via sol-gel chemistry and templating using a solvothermal and calcination process with varied pore diameters (2.3-10.7 nm), surface areas (76-420 m<sup>2</sup> g<sup>-1</sup>), and surface hydroxyl group densities (4.8-7.0 nm<sup>-2</sup>). Spheres with high surface area, large pore diameter and high surface hydroxyl density were functionalized with nitrilotri(methylphosphonic acid) via a green and simple method, then used as solid-acid catalysts to produce 5-HMF through the dehydration of carbohydrates. The

impact of time, temperature, solvent and amount of catalyst on the yield of 5-HMF was systematically investigated. The recyclability of the catalyst was tested across five consecutive runs.

In Chapter 4, sulfated, mesoporous zirconium titanium oxide spheres were synthesized for the catalytic dehydration of carbohydrate to 5-HMF. Five factors affected the sulfate loading: zirconia content, solvothermal temperature, sulfuric acid concentration, duration of the acid treatment, and the post-sulfate grafting calcination temperature. After optimization, the leading catalyst had a maximum sulfate loading of 10.7 wt%, and a total surface acidity of 0.62 mmol g<sup>-1</sup>. This solid-acid catalyst demonstrated excellent results in the dehydration of fructose to 5-HMF, with a yield of 80% after 1 h in DMSO at 150 °C, and 93% after 6 h. The catalyst was reused in five consecutive cycles with only a 3% loss of activity.

Modified zirconia and mesoporous zirconium titanium binary oxide can be considered as promising solid acid catalysts to produce high-value chemicals from biomass feedstocks.

## Declaration

This is to certify that:

- i) The thesis comprises only my original work towards the PhD except there indicated in the Preface,
- ii) Due acknowledgement has been made in the text to all other material used,
- iii) The thesis is less than 100,000 words in length, exclusive of tables, figures, bibliographies and appendices.

Seyed Farshad Motevalizadeh

## Preface

The work presented in this PhD thesis was conducted on and discussed with my supervisor, Professor Rachel A. Caruso. The following contributions were also made to this work:

The XPS analysis (Chapter 4) was performed by Dr. Alex Duan at the Surface and Chemical Analysis Network, School of Chemistry, The University of Melbourne.

Dr. William McMaster (School of Chemistry, The University of Melbourne) provided editing assistance with all chapters and abstract.

## Acknowledgments

First, I would like to thank supervisor Professor Rachel A. Caruso, who guided and encouraged me through my PhD. Thank you for allowing me to work on such a rewarding project and for all the wonderful opportunities you have provided throughout this journey.

A huge thank you as well to the members of my advisory panel, Professor Francis Separovic and Associate Professor Brendan Abrahams for their guidance and support.

My appreciation goes to past and present members of the Advanced Porous Materials group, who made the laboratory an enjoyable environment to work in and in many different ways made possible the conclusion of this work: Dr. Erwin Rodriguez, Dr. Yasmina Dkhissi, Dr. Lu Cao, Dr. Hao Wei, Dr. Wuqiang Wu, Dr. Jeannie Yie Tan, Dr. Natalita Nursam and Mr. Yiqun Li. However, special thanks go to Dr. William McMaster for always being available, helpful and supportive and also for editing and commenting on this thesis. His edits and recommendations were of great help to finishing this thesis.

I would like to express my gratitude to The University of Melbourne for providing its facilities and financial support through scholarships: Melbourne International Research Scholarship and Melbourne International Fee Remission. Thanks to the Bio21 Institute (The University of Melbourne) for use of their facilities to obtain data for this study.

I would also like to convey my thanks to the members of the School of Chemistry at the University for their support: Chemistry store, IT and Science Technical staff. Also, thanks to the staff of the undergraduate teaching laboratories where I have been demonstrating: Mrs Sioe See Volaric, Dr. Young Soo Cho and Mr. Rob Ennis-Thomas.

Last, but absolutely by no means least, I am greatly indebted to my parents: Nasrin and Seyed Taghi, my brothers: Seyed Farhad, Seyed Farzad, Seyed Foad and Seyed Amirhossein, my parents in law: Fatmeh and Asadollah, my sisters in law: Shima, Parisa, Jaleh and Maryam who have provided me with continuous support and encouragement throughout my life and finally, my sincerest gratitude goes to my



lovely wife Mina for her boundless support and encouragement and my lovely son Seyed Alireza.

## Table of Contents

Abstract.....	iv
Declaration.....	vi
Preface .....	vii
Acknowledgments .....	viii
Table of Contents.....	x
List of Tables .....	xiv
List of Figures .....	xv
Chapter 1. Introduction .....	20
1.1. Lignocellulosic biomass .....	20
1.2. Principles of successful biorefinery development .....	23
1.3. 5-HMF as a platform chemical .....	23
1.4. Polymeric compounds prepared from 5-HMF and its derivatives.....	25
1.4.1. Synthesizing furandicarboxylic acid (FDCA) from 5-HMF .....	25
1.4.2. 5-HMF to diols.....	25
1.5. Fuel molecules from 5-HMF.....	26
1.5.1. Furanic materials from 5-HMF for fuel application .....	26
1.5.2. Alkanes as liquid fuel from 5-HMF.....	28
1.6. Mechanistic insight of dehydration of fructose to 5-HMF.....	28
1.7. Conversion of fructose to 5-HMF in DMSO and DMSO-containing mixtures. 31	
1.8. Conversion of fructose to 5-HMF in organic solvents other than DMSO and DMSO-containing mixtures.....	42
1.9. Conversion of fructose to 5-HMF using titanium and zirconium-based materials as solid catalysts .....	43
1.10. Motivations and aims for the research .....	49

1.11.	Aims .....	50
1.12.	Overview of chapters 2-5 .....	51
1.13.	References .....	52
Chapter 2. Modified mesoporous zirconia with dicarboxylic acids as a solid acid catalyst for dehydration of carbohydrates into 5-HMF.....		61
2.1.	Introduction .....	61
2.2.	Experimental Section .....	62
2.2.1.	Materials .....	62
2.2.2.	Preparation of zirconia spheres .....	63
2.2.3.	Functionalization of the mesoporous zirconia spheres.....	64
2.2.4.	Characterization.....	64
2.2.5.	Catalytic test .....	65
2.3.	Results and discussion.....	66
2.3.1.	Binding mode of di-carboxylic acid on zirconia particles and the quantity of loading .....	66
2.4.	Catalytic study .....	75
2.4.1.	Effect of time and temperature.....	75
2.4.2.	The effect of solvent and loading of the catalyst .....	77
2.4.3.	Conversion of other carbohydrate feedstocks to 5-HMF.....	78
2.4.4.	Reusability of the catalyst.....	78
2.5.	Conclusion .....	79
2.5.1.	Comparing the catalytic performance of Zr-Ter with other catalysts...	79
2.6.	References.....	81
Chapter 3. Phosphate-modified mesoporous zirconium titanium oxide for 5-HMF production from carbohydrates .....		85
3.1.	Introduction .....	85

3.2. Experimental Section .....	87
3.2.1. Materials .....	87
3.2.2. Catalyst preparation .....	88
3.2.3. Characterization.....	89
3.2.4. Catalytic activity test.....	89
3.3. Results and discussion.....	90
3.4. Catalytic study .....	101
3.4.1. Effect of time and temperature .....	102
3.4.2. The effect of solvent and loading of the catalyst .....	102
3.4.3. Conversion of other feedstocks to 5-HMF and reusability of the catalyst	
104	
3.5. Conclusion .....	105
3.5.1. Comparing the catalytic performance of TZ30-P with other catalysts.	
106	
3.6. References.....	108
Chapter 4. Functionalized mesoporous zirconium titanium oxide spheres as acid	
catalysts for the conversion of fructose into 5-HMF .....	112
4.1. Introduction .....	112
4.2. Experimental Section .....	114
4.2.1. Materials .....	114
4.2.2. Preparation of the TZ Spheres. ....	115
4.2.3. Characterization.....	116
4.2.4. Catalytic activity test.....	117
4.3. Results and discussion.....	118
4.3.1. Optimization of the Zr content and H <sub>2</sub> SO <sub>4</sub> treatment conditions .....	118
4.3.2. Optimization of the solvothermal and calcination temperatures.....	119

4.3.3.	Surface acidity of the TZ spheres .....	121
4.3.4.	Characterisation of TZ spheres .....	124
4.4.	Catalytic conversion of fructose to 5-HMF .....	128
4.4.1.	Solvent effects on the conversion of fructose to 5-HMF .....	129
4.4.2.	The effects of time, temperature and catalyst amount on dehydration of fructose to 5-HMF.....	129
4.4.3.	Conversion of other feedstocks to 5-HMF.....	131
4.4.4.	Investigation of the catalyst reusability.....	131
4.5.	Conclusion .....	132
4.5.1.	Comparing catalytic performance of TZ50-Solvo140-2M3h-Cl500 with other catalysts.....	133
4.6.	References.....	136
Chapter 5.	Conclusion and future work.....	140
5.1.	Research summary .....	141
5.2.	Future work.....	145
5.2.1.	Mechanism of the catalytic system .....	145
5.2.2.	Designing multifunctional catalysts that include both acidic and basic sites	145
5.2.3.	Scaling-up the process of 5-HMF production .....	145
5.3.	References.....	146

## List of Tables

Table 2-1. Grafting percentage of the different acid functional groups on the surface of Zr-Sol160 spheres. ....	68
Table 2-2. Specific surface area ( $S_{\text{BET}}$ ) and pore diameter (PD) of the mesoporous zirconia prepared at various solvothermal temperatures, and Ter functionalized Zr-Sol160 (Zr-Ter). ....	72
Table 2-3. The percentage composition of the crystal phase of the zirconia samples prepared at different solvothermal temperatures.....	74
Table 3-1. The effects of Zr percentage, solvothermal temperature, calcination temperature, ammonia treatment, and NPA functionalization on the specific surface area ( $S_{\text{BET}}$ ), pore diameter (PD), OH amount, and surface OH density.....	93
Table 3-2. A comparison of the catalytic performance of TZ30-P with reported metal phosphate catalysts. ....	107
Table 4-1. Surface acidity for TZ spheres prepared under various conditions determined from TPD-NH <sub>3</sub> measurements. ....	122
Table 4-2. Surface area and pore diameter of the mesoporous TZ spheres. ....	123
Table 4-3. A comparison of catalytic performance of the TZ50-Solvo140-2M3h-Cl500 with those of reported sulfated catalyst.....	134
Table 5-1. Comparison of the best performing solid-acid catalysts.....	144

## List of Figures

Figure 1-1. Schematic illustration of lignocellulose and its three major components. Reprinted from ref. 6. Copyright 2013 Royal Society of Chemistry. ....	22
Figure 1-2. This figure shows the range of molecules that can be synthesized from 5-HMF.....	24
Figure 1-3. The proposed mechanism for the oxidation of HMF in aqueous solution in the presence of excess base ( $\text{OH}^-$ ) and either Pt or Au catalyst. ....	26
Figure 1-4. Conversion of 5-HMF to DMF and 5-alkoxymethylfurfural ethers (R represents aliphatic or aromatic groups). ....	27
Figure 1-5. The proposed cyclic mechanism of dehydration of fructose to 5-HMF....	29
Figure 1-6. The proposed acyclic mechanism of dehydration of hexoses to 5-HMF and other products. ....	30
Figure 1-7. The role of DMSO in 5-HMF preparation from D-fructofuranose.....	31
Figure 1-8. Schematic of a sulfated metal oxide surface containing both Lewis and Brønsted-acid sites.....	45
Figure 2-1. TGA of Zr-Sol160 functionalized with di-carboxylic acids and amino acids (a); Zr-Sol160 spheres and functionalized samples with AmTer, Ter with (Zr-Ter) (b). ....	67
Figure 2-2. Possible binding modes of $\text{COOH}$ or $\text{COO}^-$ groups to the zirconia surfaces. ....	69
Figure 2-3. FT-IR of Zr-Sol160 before and after functionalization with Ter (a) and a close-up view of the peaks in the range $900\text{-}2000\text{ cm}^{-1}$ (b). ....	70
Figure 2-4. Nitrogen sorption isotherms (a), and pore size distributions (c) of zirconia samples prepared at various solvothermal temperatures. Nitrogen sorption isotherms (b), and pore size distributions (d) of Zr-Sol160 before and after (Zr-Ter) functionalization with Ter.....	71
Figure 2-5. SEM (a, b) and TEM (c-f) images of Zr-Sol160-CI500 before (a, c, e) and after (b, d, f) functionalization with Ter. ....	73
Figure 2-6. XRD patterns of zirconia samples prepared at various solvothermal temperatures, and Zr-Ter. Patterns were shifted upwards for clarity. The main peaks	

of the zirconia crystalline phases are marked as “m” and “t” for monoclinic and tetragonal, respectively. ....74

Figure 2-7. The effect of reaction temperature and time (a) on the yield of 5-HMF from the dehydration conversion of fructose in DMSO by Zr-Ter (15 mg). The effect of solvent (b) and catalyst amount (c) on the yield of 5-HMF. (d) Conversion of fructose and 5-HMF selectivity using 15 mg catalyst and fructose solution in DMSO at 150 °C. (e) The performance of catalyst on the conversion of various substrate solutions. (f) The reusability of the Zr-Ter catalyst in five consecutive runs (e). Unless the variable undergoing change, the amount of Zr-Ter was 15 mg, the solvent was DMSO, and the substrate was fructose..... 76

Figure 3-1. Nitrogen sorption isotherms: (a) TZx-Solvo140-Cl500 samples with various Zr quantities. The effect of (b) solvothermal temperature and (c) calcination temperature on TZ30-Solvoz-Clv samples. (d) The effect of solvothermal temperature on TZ30-Solvoz-Cl500 samples with the addition of 1 mL ammonia during solvothermal treatment and (e) the effect of ammonia (0, 0.5 and 1.0 mL) during solvothermal treatment. (f) TZ30-Sol160-Cl500 and after functionalization with NPA (TZ30-P).....92

Figure 3-2. Pore size distributions: (a) TZx-Solvo140-Cl500 samples with various Zr quantities. The effect of (b) solvothermal temperature and (c) calcination temperature on TZ30-Solvoz-Clv samples. (d) The effect of solvothermal temperature on TZ30-Solvoz-Cl500 samples with the addition of 1 mL ammonia during solvothermal treatment and (e) the effect of ammonia (0, 0.5 and 1.0 mL) during solvothermal treatment. (f) TZ30-Sol160-Cl500 and after functionalization with NPA (TZ30-P). ....94

Figure 3-3. The effect of solvothermal temperature on (TZ30-Solvoz-Cl500 samples) surface area (a) and pore size (b), effect of calcination temperature on pore size (TZ30-Solvo160-Clv) (c), and the effect of addition of ammonia during solvothermal treatment (TZ30-Solvo160-Cl500 samples) on pore size and surface area (d) .....95

Figure 3-4. TGA: The effect of solvothermal temperature on (a) TZ30-Solvoz-Cl500 samples and (b) TZ30-Solvoz-Cl500 samples in the presence of 1.0 mL ammonia during solvothermal treatment. TZ30-Solvo160-Clv samples (c) treated with different amounts of ammonia (0, 0.5 and 1.0 mL) and (d) calcined at different temperatures.



(e) TZ30-Solvo160-Cl500 before and after modification with NPA (TZ30-P) plus differential of TZ30-P curve. ....	97
Figure 3-5. SEM images of TZ30-Solvo160-Cl500 (a and b) and TZ30-P (c and d).....	99
Figure 3-6. TEM images of TZ30-Solvo160-Cl500 (a and b) and TZ30-P (c and d).....	100
Figure 3-7. XRD patterns (a) and FT-IR spectra (b) of TZ30-Sol160-Cl500 and TZ30-P. The XRD pattern of TZ30-Solvo160-Cl500 was shifted up the y-axis for clarity.....	101
Figure 3-8. (a)The yield of 5-HMF from fructose dehydration of reaction temperature and time (reaction condition: fructose solution in DMSO (10 mL, 1.67 mM) and 15 mg catalyst), (b) different solvents (reaction condition: fructose solution in various solvents (10 mL, 1.67 mM), 15 mg catalyst at 160 °C for 2h), and (c) the catalyst amount (reaction condition: fructose solution in DMSO (10 mL, 1.67 mM), at 160 °C for 2h). (d) Conversion of fructose and 5-HMF selectivity using 30 mg catalyst and fructose solution in DMSO at 160 °C. (e) The effect of substrate on 5-HMF yield (reaction condition: substrate solution in DMSO (10 mL, 1.67 mM), 30 mg catalyst at 160 °C for 2h). (f) The reusability of the TZ30-P catalyst in five consecutive runs....	103
Figure 4-1. TGA results of TZx-Solvo160-zMch-Cl500 samples for optimizing Zr content, H <sub>2</sub> SO <sub>4</sub> concentration and duration of the H <sub>2</sub> SO <sub>4</sub> treatment.....	120
Figure 4-2. The effect of the H <sub>2</sub> SO <sub>4</sub> concentration, duration of acidification process and Zr content on sulfate grafting percentage.....	121
Figure 4-3. TGA results for TZ50-Solvoy-2M3h-Clv samples at different solvothermal (a) and calcination (b) temperatures. ....	121
Figure 4-4. TPD-NH <sub>3</sub> curves of (a) non-acidified TZ50 and sulfated pure Ti and Zr control samples, (b) samples with different Zr percentages, the TZ50 catalyst prepared at different (c) solvothermal and (d) calcination temperatures contrasted with the TPD-NH <sub>3</sub> curve of TZ50-Solvo140-2M3h-Cl500. ....	123
Figure 4-5. (a) SEM image and (b) EDX spectrum (cps/eV is counts per second per eV) of TZ50-Solvo140-2M3h-Cl500. (c) XRD patterns of TZ50-Solvo140-2M3h-Cl500 and TZ50-Solvo140-Cl500. The XRD pattern of TZ50-Solvo140-2M3h-Cl500 was shifted up the y-axis for clarity. ....	125
Figure 4-6. TEM images of TZ50-Solvo140-2M3h-Cl500 (a and b). ....	126
Figure 4-7. Nitrogen sorption isotherms of (a) TZ samples with different Zr content and (b) the TZ50 sample before and after sulfate functionalization.....	126

Figure 4-8. XPS (a) and high-resolution XPS spectra of spectra of (b) Ti 2p, (c) Zr 3d, (d) O 1s and (e) S 2p for TZ50-Solvo140-CI500 and TZ50-Solvo140-2M3h-CI500. FT-IR spectra (f) TZ50-Solvo140-CI500 and TZ50-Solvo140-2M3h-CI500.....128

Figure 4-9. The effect of (a) different solvents, (b) reaction temperature and time and (c) the catalyst amount on the yield of production of 5-HMF. (d) Conversion of fructose and 5-HMF selectivity using 5 mg catalyst and fructose solution in DMSO at 150 °C. ....130

Figure 4-10. The effect of substrate (a) on the dehydration of fructose. (b) The reusability of the TZ50-Solvo140-2M3h-CI500 catalyst in five consecutive runs. ....132



## Chapter 1. Introduction

Carbon has been used for manufacturing chemical substances and fuels to produce for society needs during the 20<sup>th</sup> century with fossil carbon being the main source. Many technological discoveries have occurred through the development of these feedstocks such as synthesizing exceptional material with a wide range of application (e.g. carbon fiber, nanocomposites and nylon),<sup>1</sup> along with the development of porous zeolite compounds for the refinery and extraction of petroleum-sourced chemical compounds that have wide ranging applicability from human health to nutrition.<sup>2</sup> The global population has increased to about 7 billion and living requirements have also progressed appreciably, which has resulted in the faster diminution of fossil carbon reserves. The consumption of energy and demand for fuel will be increased by 30% in the next two decades due to rapid population growth, especially in semi-developed countries.<sup>3,4</sup> Consequently, it is an obligation to find an alternative for carbon sources or at least reinforce the petroleum-based chemicals. Biomass has been considered as a unique and promising option that is sustainable, abundant and biodegradable. In general, plant-derived biomass can be categorized as edible and non-edible. The global production of non-edible biomass (lignocelluloses), including forest and agricultural waste is massive and roughly estimated to be around  $1.8 \times 10^{12}$  tonnes/year.<sup>5</sup> Another ample source of plant-derived biomass is kitchen garbage which is also known as municipal solid-waste. Furthermore, chemicals can be prepared using animal-derived biomass such as chitin and chitosan. Potato, cereals, wheat, corn and rice are examples of edible biomass that mainly contain starch. However, scientist have been focused on non-edible biomass since food was dominant in the debate of food vs. chemicals. So, non-edible biomass, such as lignocellulosic biomass has gained considerable attention.

### 1.1. Lignocellulosic biomass

Lignocellulose contains three major components: cellulose, hemicellulose and lignin and Figure 1-1 illustrates the structure of these components.<sup>6</sup> The relative composition of cellulose, hemicellulose and lignin is different based on the plant type.

For instance, the percentage for dried hardwoods are 40-45%, 24-40% and 18-25% by weight for cellulose, hemicellulose and lignin, respectively.<sup>7</sup>

Cellulose consists of d-glucose molecules that are attached via  $\beta$ -1,4 linkages and it contains a high quantity of hydrogen bonds that make the hydrolysis of this compound difficult.<sup>8</sup> The hydrolysis process can be done via a dilute acid process and or an enzymatic system that make glucose molecules free.<sup>9, 10</sup> The acid process has two main drawbacks which are the need of a base to neutralize the excess acid and the formation side products, such as dehydration products of glucose.<sup>11</sup> Enzymatic hydrolysis also has disadvantages such as not being cost-effective as it required high quantity of enzyme, a difficult process for catalyst filtration from the solution and has low turnover rates.<sup>12, 13</sup>

Hemicellulose contains a mixture of various carbohydrates, mainly xylose and arabinose. Conversion of these C<sub>5</sub>-sugars to alcohol or organic acids using microorganisms (in food industry) is not an easy task compared to the C<sub>6</sub>-sugars such as glucose. However, the derived compound from xylose and arabinose can be considered as a healthy replacement for high-fructose product. For example, a mixture of xylitol, which is the product of hydrogenation of xylose, and L-arabinose have been applied as a sweetener in corn syrup-derived foods instead of fructose.<sup>14</sup> 2-3% of the above-mentioned mixture can reduce the uptake of glucose by 70% while keeping a similar level of sweetness to sucrose.<sup>14</sup> Using biomass for producing high value chemicals with application in pharmaceutical or food industries can bring motivation from an economic point of view and empower the process of commercialization of the conversion of lignocellulose. The production of furfural from the dehydration of C<sub>5</sub>-sugars is already commercialized as a high-valued chemical with applications ranging from fuel additives and resins to solvents.<sup>15, 16</sup>

Lignin is composed of cross-linked phenolic polymers and the aromatic C-O-C ether bonds found widely in the lignin structure make the process of decomposition to monomeric molecules difficult.<sup>17, 18</sup> Thus, finding an efficient method for depolymerization of lignin is still under investigation. From the fuel point of view, lignin has a high heating value due to the aromatic-based structure. But, a process of hydrogenation and/or hydrodeoxygenation is essential to make lignin a fuel.

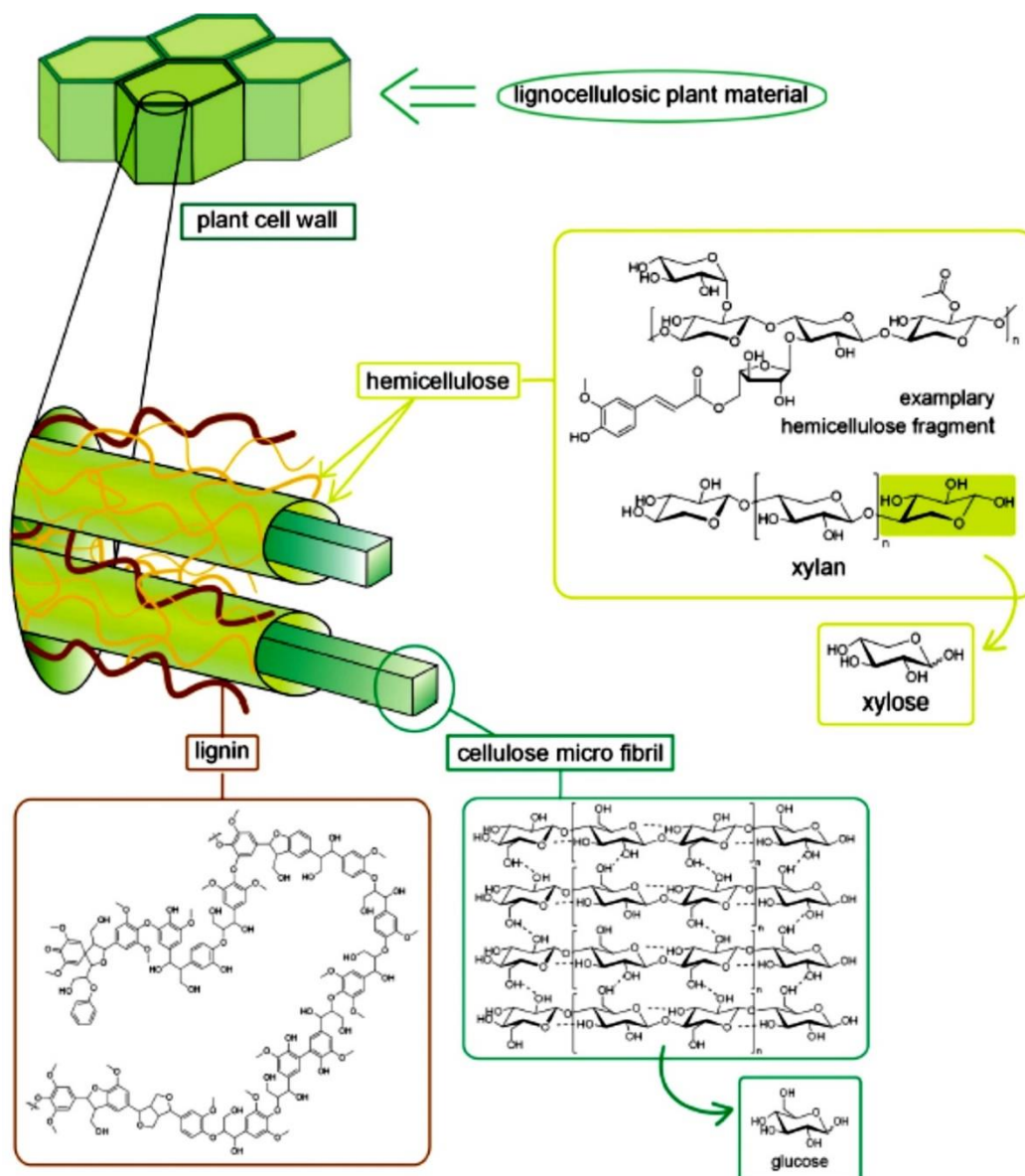


Figure 1-1. Schematic illustration of lignocellulose and its three major components. Reprinted from ref. 6. Copyright 2013 Royal Society of Chemistry.

Zhao et al. reported an effective method for decomposing lignin to the monomeric molecule in which a combination of base and boric acid were used as catalyst and capping agent.<sup>19</sup> Another study by the same group found a method to hydrogenate the monomer phenol to cycloalkane (as an ideal fuel) using a combination of Pd/C and  $H_3PO_4$ .<sup>20</sup> Dumesic et al. reported an extracted solvent from lignin during the conversion process of the cellulose and hemicellulose can be efficiently utilized in biphasic system.<sup>21</sup>

## 1.2. Principles of successful biorefinery development

Biorefinery development has two main goals which are energy and economic goals. The energy goal can be satisfied with research on biodiesel and biofuel that can be used as a replacement for gasoline and diesel. But the issue is fuel is a low value product and investment in biofuel-only systems is not economical. For example, algae has a high potential to be used as a source of biodiesel, however the process of growing and processing algal is not cost-effective.<sup>22</sup> So, the process of biorefinery requires a financial motivation. High value, low volume platform chemicals provide this motivation. A biorefinery system that produces biofuels and high value chemicals can meet the economic and energy goals.<sup>23, 24</sup> In this context, the US Department of Energy (DOE) published two reports outlining the requirements for biobased chemicals. They reported 15 chemicals that could be produced from the conversion of carbohydrates.<sup>23, 25</sup> This list of chemicals, has been used to guide research. Six years after the original report by DOE, significant progress has been made in biomass conversion to the platform chemicals and a revised list published, namely the “Top 10+4”. Several new compounds were added in which 5-(hydroxymethyl)furfural(5-HMF) was considered as one of the most important platform chemicals.

## 1.3. 5-HMF as a platform chemical

5-HMF is a natural compound that can be found in food like coffee, honey, vegetables and some beverages in low quantity.<sup>26</sup> 5-HMF can be formed as result of decomposition of carbohydrates. This compound can also be formed during caramelization and the Maillard reaction as an intermediate.<sup>27, 28</sup> Dry heating and roasting foods with a high concentration of sugars can cause caramelization. This process for fructose starts at 110 °C, while for other hexoses occurs above 160 °C. Thus, reaction can occur in various food preparations such as smoking, roasting and baking. Therefore, various food items can contain 5-HMF.

The first publication about 5-HMF was published on 1895.<sup>29</sup> 5-HMF was recognized as a high value product that has a high potential to serve as the starting material for synthesizing pharmaceuticals, polymers, fragrances, heterocycles and fuel components.<sup>5, 30, 31</sup> The most important chemicals that can be prepared from 5-HMF are shown in Figure 1-2. This high value chemical has gained considerable attention

during the past years and as identified from the number of the publications in the last 17 years. The significant interest in the preparation and application of 5-HMF is also clearly evidenced by the number of reviews.<sup>5, 30-37</sup> The global market for 5-HMF was 116750 million USD in 2016 and it is anticipated to be 123279 million USD by 2022 with a Compounded Annual Growth Rate of 0.91% during the period 2016-2021.<sup>38</sup> 5-HMF can be synthesized effectively via dehydration of hexoses such as fructose, glucose and cellulose using acid as a catalyst. In the next section the synthesis of some important chemicals from 5-HMF will be discussed.

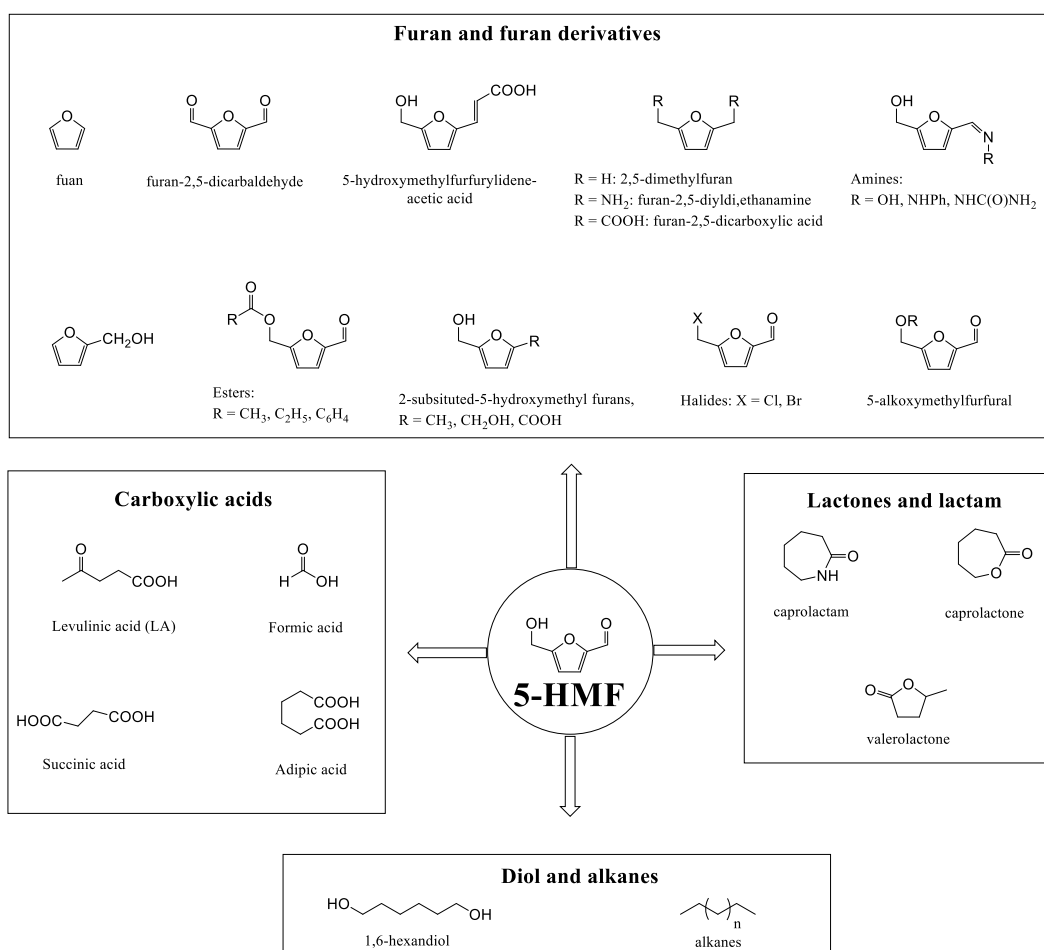


Figure 1-2. This figure shows the range of molecules that can be synthesized from 5-HMF.



## 1.4. Polymeric compounds prepared from 5-HMF and its derivatives

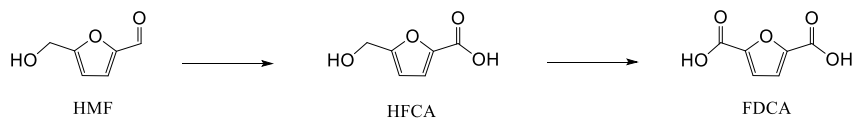
### 1.4.1. Synthesizing furandicarboxylic acid (FDCA) from 5-HMF

The physical, chemical and mechanical properties of polyethylene furanoate (PEF) is very similar to polyethylene terephthalate (PET) which is prepared from petroleum product and PEF, effectively, can be prepared from ethylene glycol and FDCA.<sup>39-41</sup> The preparation of FDCA from the oxidation of 5-HMF has been reported in homogenous and heterogeneous systems. In one study, Corma et al. synthesized FDCA with 99% yield via oxidation of 5-HMF in the presence of Au/CeO<sub>2</sub> and Au/TiO<sub>2</sub>.<sup>42</sup> Gorbanev and co-workers also used Au/TiO<sub>2</sub> as a catalyst for oxidation of 5-HMF at 30 °C and investigated the effect of base addition and oxygen pressure.<sup>43</sup> Bimetallics have been applied for 5-HMF oxidation to boost the selectivity, stability and activity of the catalyst. Abu-Omar reported on the bimetallic zinc-cobalt bromides accompanied with acetic acid, in which a yield of 60 mol% of FDCA was obtained with 1 atm oxygen.<sup>44</sup> In a study published by Davis and co-workers, biphasic oxidation systems, consisting of Pt/C, Pd/C and Au/TiO<sub>2</sub> at high pH, converted 5-HMF to FDCA successfully and gave greater than 80% yield for the Pt/C system.<sup>45</sup> The same group reported on the reaction mechanism and pathway, shown in Figure 1-3.<sup>46</sup> One of the most important drawbacks of the above-mentioned system is the necessity for the addition of extra base. To address this issue, Abu-Omar and co-worker investigated a porphyrin-based porous organic polymer-supported iron (III) catalyst with which FDCA can be obtained with 79% yield in a base-free oxidation reaction.<sup>47</sup>

### 1.4.2. 5-HMF to diols

In addition to the above-mentioned published work, conversion of 5-HMF to diols has gained considerable attention. For example, Alamillo et al. investigated hydrogenation of 5-HMF to dihydroxymethyltetrahydrofuran (DHMTFH) in which  $\gamma$ -alumina supported ruthenium was used a catalyst and the yield of the DHMTFH was about 90%.<sup>48</sup> DHMTFH was used in a wide range of applications such as monomer for polymer synthesis.<sup>49</sup>

### HMF Oxidation Scheme



### HMF Oxidation Mechanism

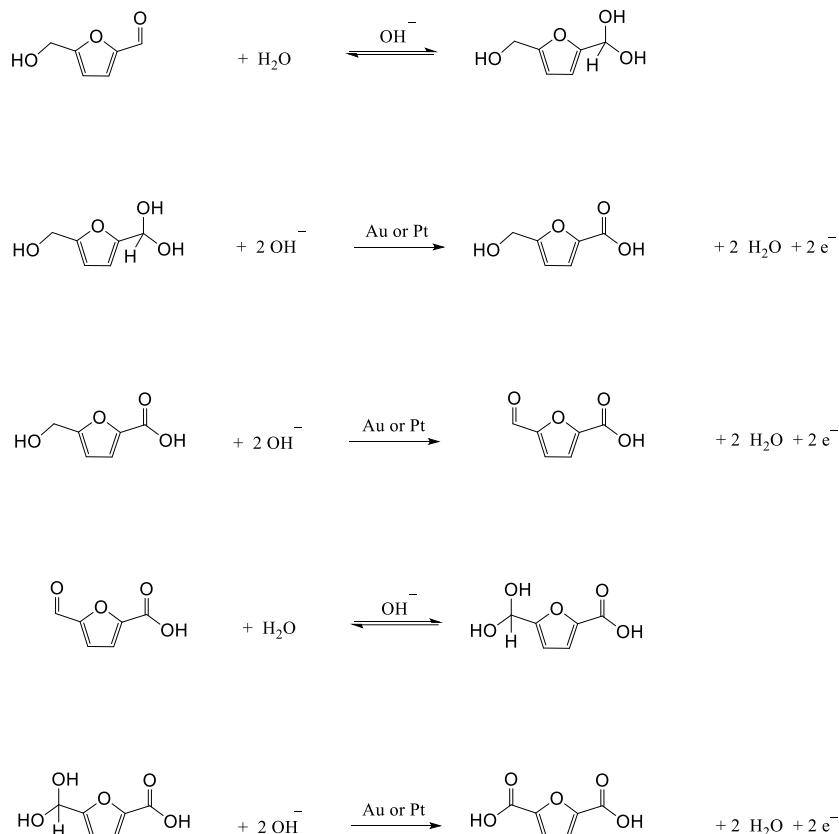


Figure 1-3. The proposed mechanism for the oxidation of HMF in aqueous solution in the presence of excess base ( $\text{OH}^-$ ) and either Pt or Au catalyst.

## 1.5. Fuel molecules from 5-HMF

### 1.5.1. Furanic materials from 5-HMF for fuel application

Two important compounds that have a high potential to be used as a fuel in transportation are 5-alkoxymethylfurfural ethers and dimethylfuran (5-DMF), which can be obtained by etherification and hydrogenolysis of 5-HMF, respectively (Figure 1-4). In one study, Bell et al. used an alcohol (as solvent and reactant) to prepare furfural ethers from 5-HMF via an acid catalyzed etherification.<sup>50</sup> By addition of Pt/C

as catalyst to the system, furfural di-ethers can be obtained as a result of reductive etherification. The heating content of these ethers are high, and they have a high potential to be applied as transportation liquid fuels. Krause and co-worker used fructose as feedstock directly in a binary system composed of hexane and sulfonic-functionalized ionic liquid, and the yield of 5-alkoxymethylfurfural ethers was greater than 50%. The activity of the catalyst was preserved after five consecutive runs.<sup>51</sup> Tsapatsis et al. reported that in a combined system including Sn-beta zeolite and Amberlyst 131 as Lewis and Brønsted acid, respectively, glucose could be directly converted to 5-alkoxymethylfurfural. In the first step, glucose underwent isomerization to produce fructose and then 5-alkoxymethylfurfural was produced with 31 mol% yield via dehydration/etherification of fructose.<sup>52</sup>

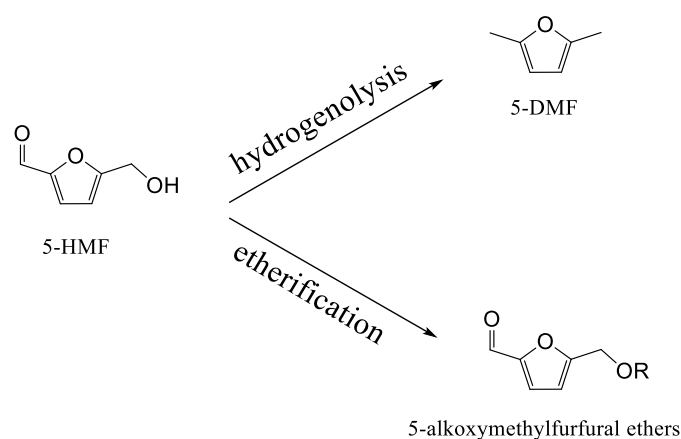


Figure 1-4. Conversion of 5-HMF to DMF and 5-alkoxymethylfurfural ethers (R represents aliphatic or aromatic groups).

Copper has drawn considerable attention for canalizing the hydrogenolysis reaction over C-C bonds, since aromatic hydrogenation could be minimized.<sup>53</sup> Thus, many copper-based catalyst systems have been prepared to synthesize 5-DMF as an interesting fuel additive from 5-HMF.<sup>54</sup> Román-Leshkov and co-workers focused on the selective hydrogenolysis of 5-HMF over copper–ruthenium catalysts that can yield over 70 mol% 5-DMF in butanol as solvent.<sup>55</sup> In 2012, Shanks et al. reported the effect of copper-chromite catalysts on C-O hydrogenolysis using a furanic model compound.<sup>53</sup> Another study by Chidambaram and co-worker reported that 5-DMF can be produced from glucose (directly) as feedstock in a two step cascade reaction using

a mixture of ionic liquid-acetonitrile as solvent.<sup>56</sup> In the first step a high quantity of 5-HMF was attained, however, the second step was less successful with just 15 mol% yield of 5-DMF over a Pd/C catalyst.<sup>56</sup>

#### 1.5.2. Alkanes as liquid fuel from 5-HMF

In one study, 5-HMF and acetone have been used in two different ratios as the substrate to produce C<sub>9</sub>, C<sub>12</sub> and C<sub>15</sub> liquid alkanes via a twostep process including condensation/hydrogenation and dehydration.<sup>57</sup> When the ratio of 5-HMF to acetone is 1:1, C<sub>9</sub> compounds are obtained that can be converted to C<sub>9</sub> alkanes through a hydrogenation/dehydration reaction. C<sub>12</sub> and C<sub>15</sub> liquid alkanes were prepared by adjusting the ratio of 5-HMF to acetone to 2:1.<sup>57</sup> This process could to be a promising alternative for fuel production if a high quantity of 5-HMF could be obtained from a cellulose-derived glucose and an inexpensive hydrogen be provided. In another study by Shen et al., several solid base catalysts were designed including MgO-ZrO<sub>2</sub>, NaY and nitrogen-substituted NaY to examine the aldol condensation reaction between acetone and furfural. They concluded that MgO-ZrO<sub>2</sub> had the best selectivity (100%) and moderate conversion (almost 50%) at 120 °C.<sup>58</sup> The same solid-base catalyst was used by Corma et al.<sup>59,60</sup> and Yang et al.<sup>61</sup> to synthesize diesel liquid alkanes from 5-HMF or furfural.

In conclusion, 5-HMF is a significant platform chemical that can be converted to a wide range of useful products with different application. Alonso et al. published a review about the biological application of 5-HMF and various preparation methods of 5-HMF.<sup>33</sup> The main barrier for scaling up the production of 5-HMF is economic. Three measures that would help to overcome this and increase the efficiency of the conversion process are: a comprehensive understanding about the dehydration of carbohydrates to 5-HMF, optimizing the process of transformation in terms of solvent, temperature etc., and designing reactors with higher quality and capability.

### 1.6. Mechanistic insight of dehydration of fructose to 5-HMF

Many researchers have devoted time to study the mechanism of carbohydrate conversion, specifically glucose and fructose to 5-HMF, but no definite conclusion had been proposed yet. However, understanding the reaction at the molecular level is

important to know about the formation of humin and other by-products and also for rational design of the catalyst in order to achieve higher efficiency on both laboratory and industrial scale. Since the dehydration of fructose to 5-HMF was used as the model reaction in this thesis, this section deals more with the mechanistic aspects of this reactions. Generally, three possible routes have been described for hexoses conversion, preferably fructose. The first mechanism is consecutive removal of three water molecules from the hexoses to produce 5-HMF. The second path for transformation is the Maillard reaction of hexoses using amino acids and amines. The third route is dehydration of hexoses via either cyclic intermediates<sup>62</sup> or acyclic intermediates.<sup>63-67</sup>

In the cyclic route, the first step is suggested to be the dehydration of D-fructofuranose at carbon-2 which produces a tertiary carbonium cation. The dehydration process continued by  $\beta$ -dehydration to form (2R,3S,4S)-2-(hydroxymethyl)-5-(hydroxyl-methylene)tetrahydrofuran-3,4-diol (Diol). The third dehydration of this process is the Diol dehydration that results in (4S,5R)-4-hydroxy-5-(hydroxymethyl)-4,5-dihydrofuran-2-carbaldehyde, which turns via a subsequent dehydration to the 5-HMF. Figure 1-5 illustrates the process of cyclic conversion of fructose to the 5-HMF.

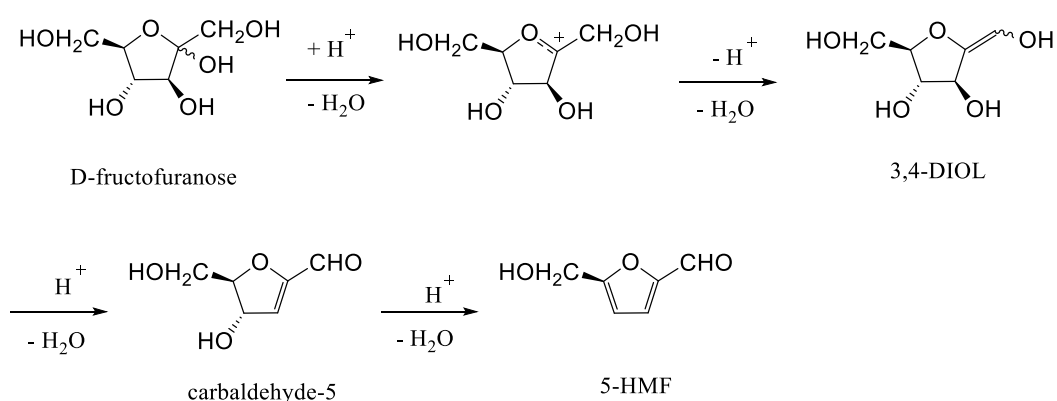


Figure 1-5. The proposed cyclic mechanism of dehydration of fructose to 5-HMF.

The proposed acyclic mechanism is well-known as the “ene-diol mechanism” since the main compound of this pathway is 1,2-enediol, which is capable of three dehydration steps to form the 5-HMF. The proposed mechanism is shown in Figure 1-6 .

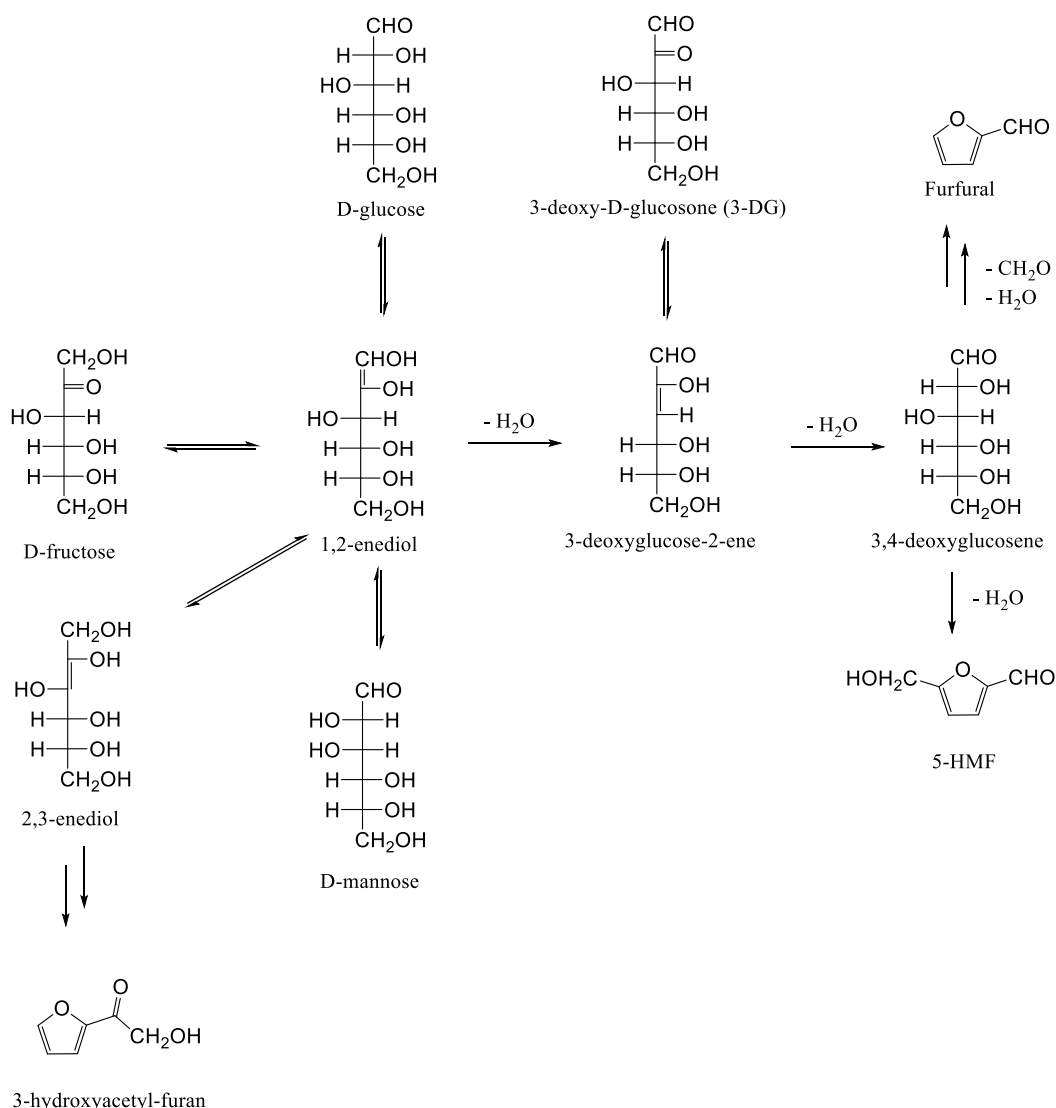


Figure 1-6. The proposed acyclic mechanism of dehydration of hexoses to 5-HMF and other products.

It is worth noting that the above-mentioned mechanisms depend on the reaction media and in most studies, water was used as the solvent.<sup>30, 31, 34</sup> For instance, Amarasekara and co-workers studied the mechanism of dehydration of fructose to 5-HMF in a catalyst-free system by <sup>1</sup>H- and <sup>13</sup>C NMR.<sup>68</sup> They explained that DMSO was used as solvent and catalyst. The final mechanism that they proposed was in good agreement with the cyclic mechanism illustrated in Figure 1-5. In another study, Weitz

et al. combined computational and experimental results to investigate dehydration of fructose to 5-HMF in DMSO with and without Brønsted acid catalysts.<sup>69</sup> They concluded that DMSO had a key role in the conversion of fructose to 5-HMF via formation of the intermediate 2-(hydroxydimethylsulfinyloxy)- $\beta$ -D-fructofuranose (Figure 1-7). One of the important results from this study is the formation of humin though the mentioned mechanism can be diminished compared to the reaction in water media under identical conditions.<sup>69</sup>

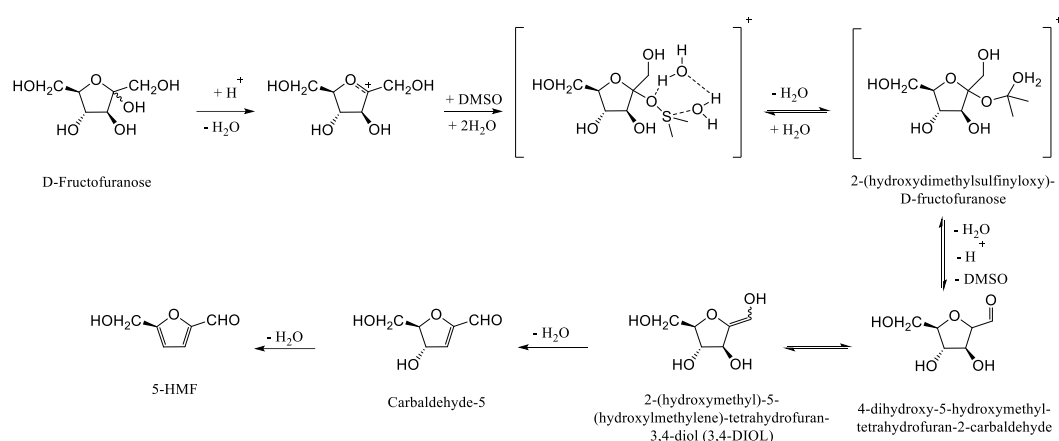


Figure 1-7. The role of DMSO in 5-HMF preparation from D-fructofuranose.

## 1.7. Conversion of fructose to 5-HMF in DMSO and DMSO-containing mixtures.

The synthesis of 5-HMF can be categorized into two periods historically, before 1970's and after. The focus of the research before 1970 was on using homogenous acid as the catalyst and water to convert C<sub>6</sub>-carbohydrates to the 5-HMF. However, several studies in 1977 and after proved the positive impact of organic solvents on the rate and yield of 5-HMF production as further conversion of 5-HMF to other products was decreased.<sup>70-73</sup> The solubility of sugars is typically low in organic solvent, except polar solvents such as DMSO. Here, the work done on DMSO will be discussed first, followed by studies on other organic solvents. Solvent systems such as ionic liquids and biphasic solvents have also been examined. But, since those systems have not been used in this thesis, they will not be discussed. Readers can find more information about those systems in the following references.<sup>5, 30, 31</sup>

Nakamura and Morikawa first reported 5-HMF preparation with 90% yield using DMSO and PK-216 ion-exchange resin as solvent and catalyst, respectively.<sup>74</sup> One year later, Szmant and Chundury produced yields of more than 90% of 5-HMF using boron trifluoride etherate as catalyst and DMSO as solvent.<sup>75</sup> They studied various catalyst concentrations, temperatures and fructose concentrations. The yield of 5-HMF ranged between 55-99% for reaction times set at 0.5-3 h. In a 1.4 M fructose solution and 25 mol% boron trifluoride 99% 5-HMF yield was obtained at 100 °C after 45 min. An interesting result was testing other solvents such as dimethylformamide (DMF) and diethylene glycol that resulted in a much lower yield of 5-HMF than DMSO. Seri et al. reported 80% 5-HMF yield in DMSO after 4 h at 100 °C with 2.5 mol% LaCl<sub>3</sub> as catalyst.<sup>76</sup> The same yield was obtained by using dimethylacetamide (DMA) and a significantly lower yield was achieved in 1-butanol and 1,4-dioxane (both ~25%) and sulfolane (~50%). Use of fructose and sorbose substrates in DMSO resulted in 93% and 61% yield of 5-HMF, respectively, at 120 °C after 2 h.<sup>76</sup> Qi et al. investigated dehydration of fructose into 5-HMF in different ratios of acetone-DMSO. The experiment was performed with 2 wt % fructose in 30:70 (w/w) DMSO-acetone in the presence of DOWEX 50WX8-100 resin as catalyst, at 140 °C, after 20 min an 88% 5-HMF yield was gained.<sup>77</sup> Reaction rate was decreased by decreasing the percentage of acetone however, selectivity and conversion remained constant. The catalysts were used in five consecutive runs and the yield of 5-HMF dropped just 2% after five runs.

Shimizu et al. reported conversion of fructose into 5-HMF in DMSO with different catalysts, such as heteropolyacids, ion exchange resins and zeolites.<sup>78</sup> The reaction conditions were set on 6 wt% catalyst, 3 wt% fructose in DMSO at 120 °C for 2 h with mild evacuation to remove water continuously. The control experiment (without any catalyst) yielded 32% while, very high yields were obtained with catalysts. Removing water from the reaction had a positive impact on the yield of 5-HMF and the quantity of 5-HMF decreased without the water removal.<sup>78</sup> An exceptional 100% yield of 5-HMF was reported by using Amberlyst 15 even without water removal, reusing catalyst for three consecutive runs and a high concentration of fructose (50 wt%). For 50 wt% fructose solution, the yield of 5-HMF reduced to below 50% when using H-BEA zeolite and FePW<sub>12</sub>O<sub>40</sub> as catalyst.<sup>78</sup>



Qi et al. published the dehydration of fructose to 5-HMF using zirconia ( $\text{ZrO}_2$ ) and sulfated zirconia ( $\text{ZrO}_2\text{-SO}_4^{2-}$ ) as catalyst.<sup>79</sup> Experiments were carried out in acetone-DMSO (70:30 w/w) with 2 wt% fructose and 20 wt% catalyst. The yield of the 5-HMF ranged between 60-66% depending on the calcination temperature. The activity of sulfated-zirconia was higher than zirconia. With bare zirconia the yield of 5-HMF was lower than 36%.<sup>79</sup>

Various ionic liquids such as N-methylpyrrolidinium ( $[\text{HNMP}]^+$ ) and N-methylimidazolium ( $[\text{HMIm}]^+$ ) ( $\text{HSO}_4^-$  and  $\text{CH}_3\text{SO}_3^-$  were utilized as anions) have been used as homogeneous catalysts by Tong and Li.<sup>80</sup>  $[\text{HNMP}]^+[\text{HSO}_4]^-$  had the highest Brønsted acidity. The effect of solvents were also studied by employing water, ethanol, carbon tetrachloride, acetonitrile, N,N-dimethylacetamide and DMSO. The highest yield of 5-HMF (72%) was obtained in DMSO by running the reaction with 7 wt% fructose 7.5 mol % of  $[\text{HNMP}]^+[\text{CH}_3\text{SO}_3]^-$  at 90 °C for 2 h.<sup>80</sup> Zakrzewska et al. reviewed the formation of 5-HMF from fructose in ionic liquid media.<sup>5</sup>

Experiments with polytungstic acid (PTA) encapsulated in MIL-101 in DMSO were reported by Zhang et al.<sup>81</sup> MIL-101 is a metal-organic framework with a chromium carboxylate cubic structure. From a 9 wt% fructose solution in DMSO in the presence of 40 wt% of catalyst a 5-HMF yield of 63% at 82% conversion was obtained after 30 min at 130 °C.<sup>81</sup> Sidhpuria et al. investigated immobilized ionic liquid on silica as a catalyst for fructose dehydration to 5-HMF.<sup>82</sup> Silica nanoparticles were prepared and functionalized with 1-(triethoxy-silylpropyl)-3-methyl imidazolium hydrogen sulfate (IL- $\text{HSO}_4$ ) to produce Si-3-IL- $\text{HSO}_4$ . A Si-3-IL- $\text{HSO}_4$  catalyst (80 wt%) was tested with an 8 wt% fructose solution in DMSO and yielded 63% at full conversion after 30 min at 130 °C.<sup>82</sup> They claimed no product was obtained in the absence of catalyst which is in contrast with other researchers.<sup>78, 83</sup>

Heteropolyacid salt catalysts were tested for 5-HMF preparation in DMSO by Huang et al.  $\text{H}_3\text{PW}_{12}\text{O}_{40}$  and  $\text{Cs}_3\text{PW}_{12}\text{O}_{40}$  yielded 94% and 73% of 5-HMF in DMSO at 120 °C for 2 h.<sup>84</sup> Mesoporous silica nanoparticles (MSN) were functionalized with sulfonic acid ( $\text{HSO}_3$ ) and ionic liquid and then activated by  $\text{CrCl}_2$  for conversion of fructose under mild conditions.<sup>85</sup> The yield of 5-HMF was 72% in DMSO after 3 h at 90 °C. The modified MSN was used four times successfully keeping the same activity.<sup>85</sup>

A green catalyst was designed based on cellulose sulfuric acid to prepare 5-HMF from fructose. Various solvents including DMSO, DMA, N-methyl-2-pyrrolidone(NMP) and DMF were used and the yield of 5-HMF was around 90% for all of them for complete conversion at 100 °C in 45 min.<sup>86</sup> A series of SO<sub>3</sub>H functionalized solid polymeric ionic liquids (FPILs) were prepared by Yang et al.<sup>87</sup> Then Cr<sup>3+</sup> was immobilized on the surface of FPILs using CrCl<sub>3</sub>·6H<sub>2</sub>O. Around 90% yield of 5-HMF with 98% conversion for fructose solution in DMSO at 120 °C for 60 min were obtained. The catalysts were separated from the solution as expected and were used in five consecutive runs with small loss of activity.<sup>87</sup> The transformation of fructose by modified carbon materials including poly(p-styrenesulfonic acid)-grafted carbon nanotubes (CNT-PSSA), poly(p-styrenesulfonic acid)-grafted carbon nanofibers, benzenesulfonic acid-grafted CMK-5, and benzenesulfonic acid-grafted carbon nanotubes with poly(p-styrenesulfonic acid) was tested by Liu et al.<sup>88</sup> The yield of 5-HMF ranged between 69-89% with more than 99% conversion for various catalysts in DMSO at 120 °C after 30 min and CNT-PSSA had the highest yield of 5-HMF. It should be noted that different substrates such as glucose and inulin were used. The CNT-PSSA was reused five times, however the loss of activity in the fifth run was noticeable and the yield of 5-HMF dropped by 15%.<sup>88</sup>

Nb<sub>2</sub>O<sub>5</sub> catalyst was developed by Dong et al.<sup>89</sup> for dehydration of fructose to 5-HMF and the effect of calcination temperature was investigated on the yield of 5-HMF by altering the calcination temperature from 300-700 °C.<sup>89</sup> The calcined sample at 400 °C had the best 5-HMF yield which was 86.2% in DMSO at 120 °C after 2 h. The catalyst recycled five times successfully with small loss in activity. It should be noted that the catalyst can be fully recovered by calcination at 120 °C for 2 h.<sup>89</sup> Inexpensive polypropylene fibre (PPF) was used as a support for ionic liquids in order to prepare a catalyst (PPFILs) for conversion of fructose to 5-HMF.<sup>90</sup> 72-86% yields of 5-HMF were achieved in DMSO at 100 °C for 1 h. The yield of 5-HMF was lower when protic solvents such as, 2-butanol, were applied. The catalyst was used in 10 successful runs keeping the same activity.<sup>90</sup> By applying Nafion-modified mesocellular silica foam as a support higher yields with outstanding selectivity were achieved at 90 °C for 2 h and the catalyst recycled five times after ion exchange.<sup>91</sup>

Estrine et al. converted carbohydrates to 5-HMF in a catalyst-free system using various heating modes, i.e. microwave irradiation and thermal heating in DMSO. The yield of 5-HMF was 92% under 900 W microwave irradiation in just 4 min from fructose as substrate.<sup>83</sup> Pidko demonstrated conversion of fructose into 5-HMF using functionalized SBA-15 sulfonic acid in DMSO and water and they showed the amount of product in water was much lower than with DMSO (120 °C, 3 h, 88%).<sup>92</sup> Modified magnetic nanoparticles with sulfonic acid were applied for dehydration of fructose to 5-HMF by Zhang et al.<sup>93</sup> The activity of the catalyst was much better than a conventional A-15 catalyst and had comparable activity to several homogeneous sulphonic acids. When the reaction condition was set at 0.02 g fructose in DMSO at 100 °C for 3 h under Ar, the highest yield of 5-HMF was achieved which was 82%.<sup>93</sup> A series of metal-organic frameworks (MOFs) were designed by Chen et al.<sup>94</sup> and then functionalized with sulfonic acid. Very high yield (90%) was achieved by MIL-101(Cr)-SO<sub>3</sub>H in DMSO at 120 °C after 1 h. By replacing Cr with Zr, and Al, the yields of 5-HMF were 85% and 79%, respectively. MIL-101(Cr)-SO<sub>3</sub>H was recycled five times with a small loss of activity.<sup>94</sup> Various types of pyridinium-based dicationic ionic-liquid catalysts were reported by Kim et al. for the dehydration of fructose into 5-HMF.<sup>95</sup> Two catalysts including 1,1'-hexane-1,6-diylbis (3-methylpyridinium) tetrachloronickelate (II) [C<sub>6</sub>(Mpy)<sub>2</sub>][NiCl<sub>4</sub>]<sup>2-</sup> in DMSO and 1,1'-decane-1,10-diylbis (3-ethylpyridinium) dibromide [C<sub>10</sub>(Epy)<sub>2</sub>]<sup>2+</sup>2Br<sup>-</sup> without DMSO had the best results. The yield of 5-HMF was 96% for [C<sub>6</sub>(Mpy)<sub>2</sub>][NiCl<sub>4</sub>]<sup>2-</sup> in DMSO after 1 h at 110 °C and 87% for [C<sub>10</sub>(Epy)<sub>2</sub>]<sup>2+</sup>2Br<sup>-</sup> after 90 min at 100 °C.<sup>95</sup>

Ionic-liquid polyoxometalate salts (IL-POM) were designed for conversion of fructose to 5-HMF and ethyl levulinate (EL) by Chen et al.<sup>96</sup> Phosphotungstic acid-derived IL-POM ([3·2H]<sub>3</sub>[PW<sub>12</sub>O<sub>40</sub>]<sub>2</sub>) had the highest catalytic performance for 5-HMF and EL. The yield of 5-HMF was 92% with optimized conditions of 50 mg fructose in 2 mL DMSO at 100 °C after 1 h. Other feedstocks were used as substrates (e.g., inulin, sucrose, and cellobiose) and a reasonable yield of 5-HMF was obtained. The catalyst was reused 5 times; however, the loss of activity was noticeable, at the fifth run just 62% yield of 5-HMF was achieved.<sup>96</sup> Hexachlorocyclotriphosphazene (HCCp) and cyanuric chloride (CNC) were tested as homogenous catalysts for dehydration of fructose to 5-HMF by

Xu et al.<sup>97</sup> P-Cl and C-Cl bonds had an crucial role for dehydration reaction. HCCP, CNC and other inorganic acids such as HCl were used to compare the yield of the catalysts and reactions performed on 12.5 g fructose in DMSO at 90 °C for 2 h. HCCP resulted the highest yield (91%) and conversion (99%) of 5-HMF in comparison with other catalysts.<sup>97</sup>

Liu et al. prepared a chromium-exchanged zirconium phosphate (ZrP-Cr) catalyst for the fructose dehydration under mild conditions.<sup>98</sup> With almost 99% fructose conversion, ZrP-Cr gave a yield of 86% and 94% in DMSO and in ionic liquids 1-butyl-3-methylimidazolium chloride ([Bmim]Cl) at 120 °C after 2 h. The catalyst activity was stable after 6 consecutive runs.<sup>98</sup> Mesoporous zirconium oxophosphate with different P/Zr mole ratios was prepared for the conversion of fructose to 5-HMF.<sup>99</sup> Reasonable yield (69%) with almost 91% fructose conversion were achieved with M-ZrPO-0.75 in DMSO at 120 °C after 1.5 h. The catalyst was recycled 12 times with small loss of catalyst activity.<sup>99</sup> A carbonaceous solid acid catalyst based on sulfonic acid functionalized  $\beta$ -cyclodextrin ( $\beta$ -cyclodextrin-SO<sub>3</sub>H) was reported by Raju and Vrushali for conversion of carbohydrates to 5-HMF.<sup>100</sup> Remarkable yield (94%) was achieved with 100 mg fructose in 10 mL DMSO at 140 °C after 2 h.<sup>100</sup>

Catalysts with a magnetic core that could be easily separated from solution, were also investigated. A porous magnetic lignin-derived solid acid carbonaceous catalyst was synthesized via an impregnation–carbonization–sulfonation process by Hu et al.<sup>101</sup> The catalyst presented activity towards fructose dehydration with a yield of 81 % for a fructose solution in DMSO at 130 °C after 40 min. The catalyst was separated from the reaction mixture using an external magnet and reused 5 times.<sup>101</sup> Core-shell nanoparticles of chromium-exchanged hydroxyapatite  $\gamma$ -Fe<sub>2</sub>O<sub>3</sub> were prepared by Lan and Zhang.<sup>102</sup> The catalyst was used for 5-HMF synthesis from fructose and presented a yield of 88.9% in DMSO at 120 °C after 240 min. The catalyst was recycled 6 times with negligible loss of activity.<sup>102</sup> Sulfonated nanoporous polytriphenylamine (SPPTPA-1) was prepared and used as a catalyst for conversion of carbohydrates to 5-HMF in DMSO.<sup>103</sup> The catalyst had high surface area (1437 m<sup>2</sup> g<sup>-1</sup>) and acidic groups on the surface and it was applied in microwave-assisted reactions. In just 20 min, the yield of 5-HMF was 94% in DMSO at 140 °C, with a turnover number of 6.11.<sup>103</sup> An excellent

5-HMF yield of 97% and 99% conversion was obtained using sulfonated two-dimensional crystalline covalent organic frameworks, in DMSO at 100 °C after 60 min. The catalyst was used for three consecutive runs without any loss in activity.<sup>104</sup>

Shen et al. investigated high internal phase emulsions (HIPEs) for conversion of carbohydrates to 5-HMF.<sup>105</sup> The catalyst contained both Brønsted and Lewis acidic sites via  $-\text{SO}_3\text{H}$  and Cr(III) species, respectively. When the reaction conditions were optimized, an 81% yield of 5-HMF was achieved from fructose conversion in DMSO at 120 °C. The catalyst was also used for glucose and cellulose and 58 and 37% yields of 5-HMF were obtained.<sup>105</sup> A sulfonic acid-functionalized KIT-6, prepared for conversion of fructose to 5-HMF gave a fructose conversion with 100% and 84% yield of 5-HMF in DMSO at 165 °C after 30 min.<sup>106</sup> The catalyst was applied in five consecutive runs and the loss of activity was only 4%.<sup>106</sup> Sulfonic acid-functionalized mesoporous carbon/silica was synthesized and utilized as catalyst for the conversion of fructose to 5-HMF.<sup>107</sup> The yield of 5-HMF was 70% from 0.5 g of fructose in 6 mL of DMSO at 130 °C after 90 min.<sup>107</sup> A solid-base catalyst, formyl-modified polyaniline synthesized by Zhu et al. for fructose conversion into 5-HMF.<sup>108</sup> A high yield of 5-HMF (90%) was obtained from a 45 mg fructose in 1 mL DMSO at 140 °C after 4 h. They mentioned that the amide site of the catalyst was responsible for catalytic activity and a mechanism for fructose conversion also was proposed. The catalyst maintained its activity for four runs successfully.<sup>108</sup>

Two hierarchically porous MOFs with strong Brønsted acidity were prepared: NUS-6 that contains either zirconium (Zr) or hafnium (Hf) clusters.<sup>109</sup> The catalysts were synthesized at low temperature (80 °C) with both micropores and mesopores in their porous structures. Both catalysts provided a high yield of HMF, however NUS-6(Hf) gave an outstanding 98% yield of 5-HMF with 99% fructose conversion in DMSO at 100 °C after 1 h. NUS-6(Hf) was also used with high fructose concentrations up to 20 wt%. Both catalysts were recycled for five times with very small loss in their activity.<sup>109</sup> Yang et al. synthesized acidic silica nanoparticles with varied surface hydrophobicity in three steps including an alkali co-condensation method, oxidation procedure and acidification process, for dehydration of fructose to 5-HMF.<sup>37</sup> The results indicated that an increase in hydrophobicity of the sample has a positive effect on the yield of

the 5-HMF. The most hydrophobic solid acid (SiNP-SO<sub>3</sub>H-C<sub>16</sub>) gave the highest yield of 5-HMF (87%) in a DMSO/H<sub>2</sub>O (V/V, 4:1) mixture or pure DMSO at 120 °C after 3 h. SiNP-SO<sub>3</sub>H-C<sub>16</sub> kept its initial activity after five consecutive runs.<sup>37</sup> Sulfonated graphene oxide (SGO) was prepared by Hou et al. via a one-pot method and was applied for 5-HMF production from fructose.<sup>110</sup> A superior 5-HMF yield up to 94% and 100% fructose conversion was achieved in a mixture of ionic liquid 1-allyl-3-methyl-methylimidazolium chloride and DMSO (w/w 1:1) at 120 °C after 1 h. An acceptable yield of 67% was obtained with a high-concentration fructose (20 wt%) solution. The catalyst was reused for five cycles and in the fifth run, the 5-HMF yield and the conversion of fructose were 81% and 85%, respectively.<sup>110</sup>

Spherical fibrous KCC-1 silica were synthesized, functionalized with sulfonic acid (KCC-1-Pr-SO<sub>3</sub>H) and applied as solid-acid catalyst for the production of 5-HMF from fructose in DMSO.<sup>111</sup> The effect of solvents was studied by using the catalyst in dimethylformamide (DMF), dimethylacetamide (DMAC), N-methyl-2-pyrrolidone (NMP) and ethylene glycol, however DMSO gave the best yield of 5-HMF. After optimization of the reaction conditions (162 °C, 30 min) 68% selectivity, 99% fructose conversion and 67% yield for the 5-HMF was obtained. KCC-1-Pr-SO<sub>3</sub>H was reused in four consecutive runs and no significant loss of activity was observed.<sup>111</sup> A silicoaluminophosphate molecular sieve (SAPO) named SAPO-34 was prepared by Wang and co-worker as a solid-acid catalyst in the dehydration of fructose into 5-HMF.<sup>112</sup> Using mesoporous nanoplate-like SAPO-34 as catalyst, gave an acceptable yield of 5-HMF (73.0%) with 100% conversion of fructose at 130 °C after 2.5 h in DMSO under a N<sub>2</sub> atmosphere.<sup>112</sup>

Two different catalysts based on KIT-5 were prepared, namely Al-KIT-5 and KIT-5-SO<sub>3</sub>H which contain Lewis and Brønsted-acid sites, respectively for conversion of fructose to 5-HMF.<sup>113</sup> Both catalysts resulted in a high yield of 5-HMF, however, KIT-5-SO<sub>3</sub>H showed a better catalytic activity due to the Brønsted-acid sites. The yield of 5-HMF for reaction conditions including 40 mg KIT-5-SO<sub>3</sub>H in DMSO at 125 °C after 45 min was 94%, while 50 mg of Al-KIT-5 in DMSO at 130 °C after 60 min yielded 88%. Both catalysts were recycled for five times, however, the loss of activity was noticeable. The yield of 5-HMF gradually dropped by 10% using KIT-5-SO<sub>3</sub>H and diminished from 88 to

71% using Al-KIT-5 as catalyst.<sup>113</sup> Liu et al. reported the preparation of polyvinylpyrrolidone (PVP) functionalized halloysite nanotubes (HNTs) as a support for immobilizing various amount of acidic MOFs of UiO-66-SO<sub>3</sub>H.<sup>114</sup> The obtained catalysts (PVP-HNTs@UiO-66-SO<sub>3</sub>H-X where X stands for the amounts of immobilized acidic MOFs) were tested for transformation of fructose to the 5-HMF. When PVP-HNTs@UiO-66-SO<sub>3</sub>H-2 was applied as catalyst, 92.4% 5-HMF yield was obtained at 120 °C after 2 h in DMSO. Five experiments were run under optimized conditions and no significant difference in 5-HMF yield was observed that indicates good stability of the catalyst.<sup>114</sup>

Souza and co-workers tested heteropolyacid compounds namely phosphotungstic acid (HPW) and Cs-exchanged phosphotungstic acid (HCsPW) for 5-HMF synthesis from fructose and glucose.<sup>115</sup> These catalysts have strong acidity and well-defined structures. Promising results were obtained with HPW, achieving 92% yield of HMF and 100% conversion of fructose in DMSO at 120 °C after 30 min. However, HPW could not be recycled since it is soluble in DMSO. To overcome this issue, HPW was immobilized on MCM-41 (HPW/MCM-41) and after optimizing the reaction conditions 100% conversion of fructose and 80% yield of 5-HMF in DMSO at 120 °C after 60 min were achieved. HCsPW were also prepared by exchanging protons by Cs in HPW, which resulted in a lower yield (80% yield of 5-HMF in DMSO at 120 °C after 40 min) compared to HPW and similar yield of 5-HMF as HPW/MCM-41 in shorter time. It should be noted that HCsPW was heterogeneous in DMSO.<sup>115</sup>

Three layered transition metal oxides including HNbMoO<sub>6</sub>, HNbWO<sub>6</sub> and HTaWO<sub>6</sub> were produced via ion-exchange and solid-state reaction. HTaWO<sub>6</sub> has been investigated systematically for dehydration of fructose to 5-HMF.<sup>116</sup> Under optimized conditions in DMSO, 99% fructose conversion and 67% 5-HMF yield were attained at 140 °C after 30 min. The catalyst was recycled three times successfully however, in the fourth run noticeable loss of activity was observed due to the leaching of active acid sites.<sup>116</sup> Bhaumik and co-workers prepared mesoporous bifunctionalized organosilica (MPBOS) via synthesizing SBA-15, functionalizing with (3-chloropropyl)triethoxysilane and replacing of the chloro group with amine species by an S<sub>N</sub>2 substitution reaction, for conversion of carbohydrates to 5-HMF.<sup>117</sup> The 5-HMF yield from a fructose solution

in DMSO microwave heated by irradiation was 74% at 135 °C after just 20 min. The reusability of the catalyst was also investigated by recycling MPBOS in five consecutive runs and the catalyst showed very good stability in which the decreasing yield of 5-HMF in the fifth run was about 5%.<sup>117</sup> A series of cyclopentanone-based acidic resins were prepared by Tang et al. in a one-step process and sulfated cyclopentanone-formaldehyde condensate (SCFC) showed the best activity for dehydration of fructose to 5-HMF in DMSO.<sup>118</sup> An outstanding yield (97%) of 5-HMF was obtained under mild conditions (120 °C, 1.5 h). No deactivation was observed when five times recycling the catalyst. Conversion of inulin, glucose and sucrose to 5-HMF yielded above 80% for all substrates under identical condition.<sup>118</sup>

Raveendra and co-workers synthesized SnO<sub>2</sub> via a hydrothermal method and then loaded different quantities of WO<sub>3</sub> on it.<sup>119</sup> Specifically, the effect of WO<sub>3</sub> loading and the calcination temperature were evaluated for the dehydration of fructose to 5-HMF in DMSO. The 20% WO<sub>3</sub>/SnO<sub>2</sub> catalyst presented the best catalytic performance under mild conditions, e.g. the yield of 5-HMF can reach 93% at 120 °C after 2 h. Higher loading of WO<sub>3</sub> resulted in lower acid site concentration. The 20% WO<sub>3</sub>/SnO<sub>2</sub> was calcined at 400 °C as exceeding this temperature lead to the monoclinic phase, which was inactive for conversion of fructose to 5-HMF. The catalyst was reused five times and maintained the initial activity indicating the high activity of the catalyst for dehydration of fructose into 5-HMF.<sup>119</sup> MOF-derived carbon (MDC) was functionalized with sulfonic acid and applied as catalyst for production of 5-HMF from fructose.<sup>120</sup> For the catalyst preparation, MOF-5 was converted to MDC via a simple heat-treatment process and subsequently, -SO<sub>3</sub>H groups were grafted on the surface through a sulfonation process. The resulting catalyst, MDC-SO<sub>3</sub>H was used for dehydration of fructose to 5-HMF and the highest yield of 5-HMF was 89% in solvent mixture of isopropanol and DMSO (isopropanol: 4.5 mL, DMSO: 0.5 mL) at 120 °C after 2 h. The catalyst was recycled five times and the yield of 5-HMF dropped by 10% in the fifth run.<sup>120</sup>

A series of sulfonated carbon solid acid catalysts were synthesized using fructose and zinc chloride with different ratios and were applied for conversion of fructose to 5-HMF under microwave irradiation.<sup>121</sup> The prepared catalysts, e.g. C<sub>1</sub>, C<sub>2</sub>, C<sub>3</sub>, and C<sub>4</sub>



(based on the fructose and  $\text{ZnCl}_2$  weight ratios i.e. 1:1, 1:2, 1:3, and 1:4, respectively) were functionalized with  $-\text{SO}_3\text{H}$  using sulfuric acid solution in a hydrothermal process at  $180\text{ }^\circ\text{C}$  and the final materials referred to as  $\text{C}_1\text{-SO}_3\text{H}$ ,  $\text{C}_2\text{-SO}_3\text{H}$ ,  $\text{C}_3\text{-SO}_3\text{H}$  and  $\text{C}_4\text{-SO}_3\text{H}$ . The highest yield of 5-HMF and fructose conversion were 87% and 99%, respectively, in DMSO at  $170\text{ }^\circ\text{C}$  after 3 min using  $\text{C}_2\text{-SO}_3\text{H}$  as catalyst. The catalyst was reused four times, however, the yield of 5-HMF decreased noticeably to about 60%.<sup>121</sup> An insoluble and reusable heteropolyacid ( $\text{H}_x\text{Zr}_{3-x}\text{PW}_{12}\text{O}_{40}$ ) was synthesized via exchanging  $\text{H}_3\text{PW}_{12}\text{O}_{40}$  with Zr at different ratios for selective dehydration of fructose to 5-HMF in DMSO.<sup>122</sup>  $\text{H}_2\text{Zr}_1\text{PW}_{12}\text{O}_{40}$  had the highest acidity and at optimized reaction conditions, the yield of 5-HMF and fructose conversion were 85 and 100%, respectively, at  $140\text{ }^\circ\text{C}$  in just 10 min. The catalyst was reusable compared to the  $\text{H}_3\text{PW}_{12}\text{O}_{40}$  and recycled three times with very small loss of activity.<sup>122</sup>

Aquivion@silica solid acid was applied for production of 5-HMF from fructose by Cao and co-workers.<sup>123</sup> Aquivion perfluorosulfonic acid resin (PFSA) is well-known for its amphiphilic properties and strong acidity. PFSA was used as a template and acidic agent for the preparation of mesoporous silica via sol-gel chemistry. Based on the incorporation of Aquivion resin in mesoporous silica three samples were produced e.g. 10%Aquivion@silica, 20%Aquivion@silica and 30%Aquivion@silica. After optimizing of conditions reaction, the 10%Aquivion@silica catalyst gave 85% yield of 5-HMF and 100% conversion of fructose at  $90\text{ }^\circ\text{C}$  after 2 h in DMSO. The catalyst was recycled four times and a slight decrease (less than 5%) in the yield of 5-HMF and conversion of fructose were observed.<sup>123</sup>

Emre Kiliç et al. prepared various sulfated catalysts including  $\text{SO}_4/\text{TiO}_2\text{-SiO}_2$ ,  $\text{SO}_4/\text{ZrO}_2$ , and  $\text{SO}_4/\text{SiO}_2$  for dehydration of fructose to 5-HMF.<sup>124</sup> Sulfur leaching was not observed from  $\text{SO}_4/\text{ZrO}_2$  and  $\text{SO}_4/\text{TiO}_2\text{-SiO}_2$ , catalysts in the reaction tests.  $\text{SO}_4/\text{TiO}_2\text{-SiO}_2$  had the highest amount of Lewis and Brønsted acidity. Under optimized conditions, 89 and 77 % of selectivity and conversion were obtained from dehydration of fructose using  $\text{SO}_4/\text{TiO}_2\text{-SiO}_2$  as catalyst in DMSO at  $110\text{ }^\circ\text{C}$ . The catalyst showed no loss in activity after four times reuse.<sup>124</sup>

## 1.8. Conversion of fructose to 5-HMF in organic solvents other than DMSO and DMSO-containing mixtures.

The dehydration of fructose is better in DMSO and DMSO mixtures reaction media,<sup>35</sup> however the conversion of fructose has been investigated in other organic solvents as well. Hafnium(IV) chloride was utilized as a catalyst for conversion of carbohydrates into 5-HMF in different solvents including DMF.<sup>125</sup> 60% yield of 5-HMF was achieved from 100 mg of fructose at 100 °C after 2 h in DMF. The highest quantity of 5-HMF (80%) was obtained in 1-butyl-3-methylimidazolium bromide; [Bmim]Cl at similar temperature and after 30 min.<sup>125</sup> DMAC and NMP were used as solvents in the conversion of fructose to 5-HMF using a waste by-product of the paper industry, liginosulfonic acid.<sup>126</sup> The 5-HMF yield were 52 and 39 % for NMP and DMAC, respectively for 0.2 g of fructose at 100 °C after 60 min. The best yield of 5-HMF (94.3%) and conversion of fructose (98%) were obtained in [Bmim]Cl at identical reaction conditions after 10 min.<sup>126</sup> Kuo et al. prepared acidic TiO<sub>2</sub> nanoparticles as heterogeneous catalysts for the dehydration of fructose into 5-HMF.<sup>127</sup> Various protic and aprotic solvents were used including THF, acetonitrile, DMSO, DMAC, DMF, ethanol, n-propanol, isopropanol, n-butanol, 2-butanol and t-butanol. THF gave the highest yield (42%) at 150 °C after 3 h. Almost no 5-HMF was obtained from alcohols however, a reasonable yield of 5-HMF-derived ethers were obtained under identical conditions.<sup>127</sup>

A combination of heteropolyacid and ionic liquid (1-(3-sulfonicacid)propyl-3-methylimidazoliumphosphotungstate([MIMPS]<sub>3</sub>PW<sub>12</sub>O<sub>40</sub>)) was used as a catalyst for dehydration of fructose to 5-HMF in various protic and aprotic solvents including n-butanol, sec-butanol, iso-butanol, DMSO and methylisobutylketone (MIBK).<sup>84</sup> The conversion of fructose was above 95% in all solvents and the highest (99%) and lowest (17%) yield of 5-HMF occurred in the sec-butanol and MIBK, at 120 °C after 2 h respectively. When the temperature increased to 160 °C the yield of 5-HMF reached 90% in 30 min using sec-butanol as solvent. The catalyst was recycled 6 times successfully without noticeable loss in activity.<sup>84</sup> Functionalized polyvinyl alcohol (PVA) (DIC<sub>A</sub>T-1) was prepared by Pawar and Lali as a solid acid catalyst to convert fructose to 5-HMF.<sup>128</sup> The effect of solvents on the yield of 5-HMF was studied by using

isopropanol, t-butanol, THF, acetone, acetonitrile, DMF, and DMSO. 95% fructose conversion and an 85% yield of 5-HMF were obtained in isopropanol at 120 °C after 2 min under microwave irradiation. DMSO and DMF also resulted in high fructose conversion of 100% and 88%, respectively, but lower 5-HMF yields. In acetonitrile almost no fructose conversion was achieved. DIC<sub>A</sub>T-1 was used in four runs successfully; however, the yield of 5-HMF dropped by 4% over the next two runs.<sup>128</sup>

### 1.9. Conversion of fructose to 5-HMF using titanium and zirconium-based materials as solid catalysts

During the past decades, 5-HMF was produced using mineral acids, such as sulfuric acid and HCl.<sup>129</sup> However, serious issues related to the use of these homogenous catalysts, for example, safe handling and reactor corrosion, have led to the use of solid acid heterogeneous catalysts as alternatives. Advantages of solid catalysts are transferring protons and electrons during chemical reaction, high selectivity and reactivity, being recoverable and reusable, having long shelf-life, producing less toxic waste, and an overall lower processing cost. Therefore, solid acid catalysts have emerged as powerful tools for 5-HMF production. Moreover, the further conversion of 5-HMF into levulinic acid and formic acid can be prevented using solid acid catalysts when the dehydration reaction is conducted at high temperature.<sup>130</sup> A broad range of carbohydrates such as fructose, glucose, sucrose and cellobiose can be converted to 5-HMF using solid-acid catalysts. However, the efficient dehydration of lignocellulosic biomass has not yet been reported, a fact that can be associated with weak acidic sites on the surface of the solid catalyst, and low accessibility of catalytic sites for substrates.<sup>129</sup>

Among the solid acid catalysts, metal oxides play an important role in biomass conversion,<sup>127, 131-136</sup> due to advantages like thermal stability, low cost, and most importantly an ability to carry both Lewis and Brønsted-acid sites. Along with catalytic applications, the synthesis and characterization of these compounds has been well-researched.<sup>127, 136-140</sup> Metal oxides, specifically based on early transition metals such as titanium, have been used successfully in acid-catalyzed reactions for preparing 5-HMF.<sup>34, 127</sup> Numerous studies have demonstrated the successful application of TiO<sub>2</sub>

and ZrO<sub>2</sub>, separately, in combination, or as modified metal oxides as solid acid catalysts for 5-HMF synthesis.<sup>33, 127, 134, 135, 141-155</sup>

Qi et al. tested TiO<sub>2</sub> and ZrO<sub>2</sub> for the dehydration of fructose and glucose to 5-HMF in hot compressed water and under microwave heating.<sup>156</sup> The yield of 5-HMF and fructose conversion in compressed water were 38% and 83% after 5 min reaction, respectively, using TiO<sub>2</sub> as the catalyst, while 30% and 83% resulted, respectively, in the presence of ZrO<sub>2</sub>. Additionally, ZrO<sub>2</sub> promoted the isomerization of glucose to fructose, in which glucose conversion and selectivity of fructose to glucose were respectively 50% and 60% after just 1 min of reaction. To investigate the effect of microwave heating, the catalytic reaction was initially run in a sand bath. Fructose conversion and 5-HMF yield were 27% and 12%, respectively, using 0.05 g of TiO<sub>2</sub> at 200 °C after 3 min, whereas under microwave irradiation, 73% and 35% resulted, respectively.<sup>156</sup> It was concluded that titania and zirconia can halt the conversion of 5-HMF into levulinic acid and formic acid.<sup>156</sup> Qi et al. did not compare their results with a control reaction (i.e. reaction without catalyst), nor did they study the reusability of the catalysts. McNeff et al. applied porous zirconia and titania to the continuous production of 5-HMF using a fixed bed catalytic reactor for conversion of various sugars.<sup>157</sup> When glucose was treated in a mixture of MIBK and water (10:1), yields of 5-HMF were 29 and 21% using TiO<sub>2</sub> and ZrO<sub>2</sub> as the catalyst, respectively, at 180 °C after 2 min. Interestingly, under identical conditions, the yield of 5-HMF was 26% from a honey solution using TiO<sub>2</sub> as the catalyst at 170 °C after 2 min.<sup>157</sup> The authors also modified the surface of the zirconia with phosphoric acid; however, the yield of 5-HMF was lower than bare zirconia. A cellulose solution in a mixture of MIBK and water (5:1) gave a 35% yield of 5-HMF at 270 °C after 60 min; the titania catalyst was recycled three times, and the yield of 5-HMF dropped by 2%.<sup>157</sup> Dutta et al. reported the dehydration of fructose and glucose to 5-HMF using mesoporous titania as a catalyst under microwave irradiation. Yields of 54 and 36% 5-HMF were obtained from a fructose solution in DMSO and water, respectively, at 140 °C after 15 min. By comparison, the yield of 5-HMF was 20% when no catalyst was used under similar conditions. Other carbohydrates were also investigated: glucose, sucrose, cellobiose and maltose solutions gave 5-HMF yields of 37, 21, 18 and 14% in that order. The

catalyst was reused 4 times and the loss of activity was just 2%.<sup>158</sup> TiO<sub>2</sub> and ZrO<sub>2</sub> were used as catalysts by Chareonlimkun et al. for dehydrating glucose and xylose in hot compressed water.<sup>159</sup> When TiO<sub>2</sub> was the catalyst yields of 5-HMF were 27 and 62% for glucose and xylose at 250 °C after 5 min, while yields of 17 and 52% were obtained for ZrO<sub>2</sub> under identical conditions. For TiO<sub>2</sub> and glucose as catalyst and substrate, prolonging the reaction to 10 min reduced the yield to 24%. When no catalyst was added, just 4% 5-HMF was achieved. The catalysts were recycled 5 times and almost no loss of activity was observed for both TiO<sub>2</sub> and ZrO<sub>2</sub>.<sup>159</sup> From the preceding discussion, it can be seen that bare titania and zirconia, can successfully convert carbohydrates to 5-HMF; however, yields are comparatively low, and specific conditions such as compressed hot water, microwave heating or high temperatures were necessary to obtain decent yields of 5-HMF. As a result, modification of the surface of these solid acid catalysts to increase the strength of the acid on the catalyst surface has been investigated.

In this context, sulfated zirconia and titania are typical solid acids that have been used for 5-HMF synthesis. Compared with sulfonated resins that have only Brønsted-acid sites, sulfated metal oxides contain both Lewis and Brønsted-acid sites (Figure 1-8). Metal atoms comprise the Lewis acidic sites, while the protons of surface hydroxyl groups that are coordinated with sulfated metal oxides provide Brønsted acidic sites.<sup>160-164</sup> The acidity of hydroxyl groups is extremely weak. After functionalization with sulfate, the S-O bond of sulfuric acid attaches strongly to a metal atom, while the S=O

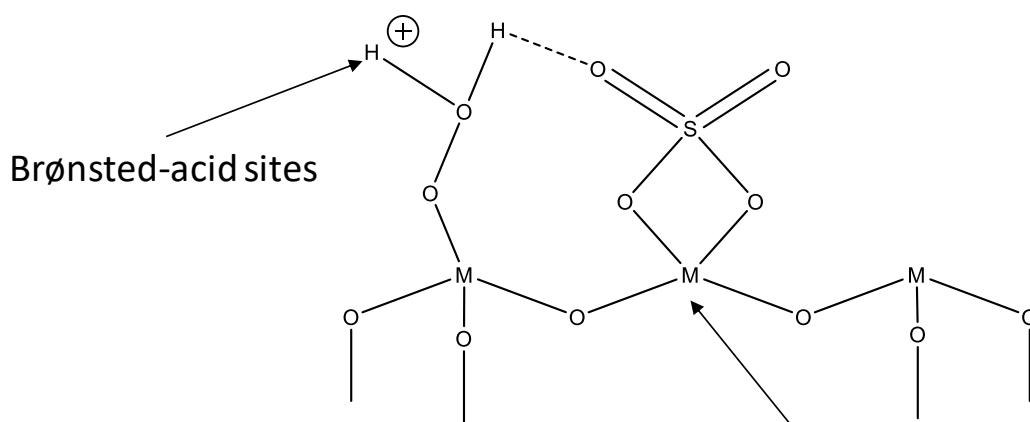


Figure 1-8. Schematic of a sulfated metal oxide surface containing both Lewis and Brønsted-acid sites.

bond is coordinated with the hydrogens of surface hydroxyl groups, and the result of grafting process is strong Brønsted acidic sites.

Brønsted acidic strength depends on the metal type. For instance, the strength of the Brønsted acidic site of  $\text{SO}_4^{2-}/\text{SnO}_2$  and  $\text{SO}_4^{2-}/\text{ZrO}_2$  are more than  $\text{SO}_4^{2-}/\text{TiO}_2$  because of the lower electronegativities of Zr and Sn compared to Ti, which can lead to easier proton release.<sup>160</sup> Therefore, sulfated zirconia has been used as a catalyst for the dehydration of carbohydrates to 5-HMF, owing to its bi-functionality. Shimizu, Uozumi and Satsuma investigated a broad range of catalysts including sulfated zirconia (SZ) and  $\text{WO}_3/\text{ZrO}_2$  for the conversion of fructose to 5-HMF under mild evacuation.<sup>78</sup> Fructose conversion of 100% and respective yields of 92 and 94% resulted from using SZ and  $\text{WO}_3/\text{ZrO}_2$  as catalysts at 120 °C after 2 h. Mild evacuation removed the water that was a side product of the dehydration process, preventing hydrolysis of 5-HMF to levulinic acid and suppressing any possible formation of humin. A 100% yield of 5-HMF and 100% fructose conversion were obtained under similar conditions using Amberlite-15 as the catalyst.<sup>78</sup> SZ was used in combination with [Bmim]Cl for the dehydration of fructose to 5-HMF.<sup>165</sup> Under optimized conditions, a 5-HMF yield of 88% and fructose conversion of 95% were obtained at 100 °C after 30 min. The catalyst and ionic liquid were used in 6 consecutive runs with no loss of activity, but the yield of 5-HMF gradually decreased to 60% when the catalyst was used for another four runs.<sup>165</sup>

Osatiashtiani et al. investigated the ideal ratio of basic and Lewis–Brønsted acid sites on SZ as a bifunctional catalyst for conversion of glucose to 5-HMF.<sup>135</sup> The dehydration of glucose to 5-HMF is a two-step process. First is the isomerization of glucose to fructose, which is a rate-determining step, while the second step is dehydration of fructose to 5-HMF. For the first step, a Lewis acid or Brønsted base catalyst is necessary, whereas in the second step an acid catalyst is crucial.<sup>135</sup> After optimization of the quantity of the sulfate on the surface, in a reaction run at 120 °C for 6 h, the results were 42% glucose conversion and a selectivity for 5-HMF of just 11%, which could be considered low in comparison with other reports.<sup>135</sup> It can be speculated that the unimpressive results were due to the low reaction temperature and using water

as solvent. Although water is a green and cheap solvent, it can accelerate the conversion of 5-HMF to levulinic acid and formic acid.

SZ and  $\text{SO}_4^{2-}/\text{ZrO}_2\text{-Al}_2\text{O}_3$  with various Zr:Al mole ratios of 9:1, 7:3, 1:1, 3:7, and 1:9 were prepared for the conversion of glucose to 5-HMF by Yan et al.<sup>166</sup> The yields of 5-HMF from glucose solution in DMSO under a nitrogen atmosphere at 130 °C after 4 h were 19 and 47.6% for SZ and  $\text{SO}_4^{2-}/\text{ZrO}_2\text{-Al}_2\text{O}_3$  (Zr:Al 1:1), respectively. When fructose was used as the substrate, 67.7 and 56.6% 5-HMF yields were achieved for SZ and  $\text{SO}_4^{2-}/\text{ZrO}_2\text{-Al}_2\text{O}_3$ . The  $\text{SO}_4^{2-}/\text{ZrO}_2\text{-Al}_2\text{O}_3$  catalyst was recycled 5 times for glucose conversion, with the yield of 5-HMF decreasing by 14% in the fifth run.<sup>166</sup> Yang et al. made use of the same catalyst, i.e.  $\text{SO}_4^{2-}/\text{ZrO}_2\text{-Al}_2\text{O}_3$  (Zr:Al 1:1), for the conversion of starch, which is a more complex carbohydrate than glucose.<sup>167</sup> A 5-HMF yield of 55% was obtained in a mixture of DMSO and water at 150 °C after 6 h.<sup>167</sup>

Tungstated zirconia oxides containing 1–21 wt.%  $\text{WO}_3$  (denoted as m- $\text{WO}_3/\text{ZrO}_2$ , where m is wt.%  $\text{WO}_3$ ) were prepared as amphoteric catalysts to investigate the relationship between surface acidity and fructose conversion for 5-HMF production.<sup>168</sup> The highest yield of 5-HMF (12%) was obtained from fructose solution in water when 16.8- $\text{WO}_3/\text{ZrO}_2$  was used as the catalyst, and the catalytic reaction was performed at 130 °C for 4 h. By increasing the percentage of  $\text{WO}_3$ , the surface area (108 and 37  $\text{m}^2/\text{g}$  for 20.9- $\text{WO}_3/\text{ZrO}_2$  and bare  $\text{ZrO}_2$ , respectively) and acidity of the surface increased, which favored the dehydration of fructose; however, selectivity towards 5-HMF peaked when the quantity of  $\text{WO}_3$  was 9.8 wt.%. As was logical, the basicity of the surface declined with increasing quantity of  $\text{WO}_3$ . It was concluded that a small quantity of surface basic sites are crucial for improving selectivity and reducing the formation of by-products.<sup>168</sup>

In the conversion of high fructose corn syrup to 5-HMF, two important factors for preparing sulfated titania ( $\text{SO}_4^{2-}/\text{TiO}_2$ ) as a solid acid catalyst were investigated by Zhang, Wu and Li.<sup>169</sup> The first factor was sulfuric acid concentration. It was concluded that 0.5 M was the concentration that produced the highest quantity of acidic sites on the  $\text{TiO}_2$  surface. The other factor was calcination temperature, which was optimized at 500 °C. The optimized catalyst was used in reaction, and a 33% yield of 5-HMF was

obtained at 175 °C after 1 h. The catalyst was recycled five times; however, in the fifth run the yield of 5-HMF dropped 20%.

High surface area Sn-based catalysts, SnO<sub>2</sub>-ZrO<sub>2</sub> and SO<sub>4</sub><sup>2-</sup>/SnO<sub>2</sub>-ZrO<sub>2</sub>, were applied to the 5-HMF production from hexose.<sup>170</sup> Materials with various Sn:Zr ratios (0.1, 0.2, 0.03, or 0.05 g/g) were synthesized. After grafting sulfate on the surface, the catalyst with a Sn:Zr ratio of 0.05 had the highest quantity of surface acidic sites. Under optimized conditions, a 75% yield of 5-HMF was obtained from a fructose solution in DMSO at 120 °C after 2.5 h. The catalyst was stable, and after reusing five times no loss of activity was observed.<sup>170</sup> In conclusion, sulfated metal oxides have been used successfully for the conversion of biomass to 5-HMF.

The other option to increase the strength of acidity on the surface of titania and zirconia is modifying the catalyst material with either phosphate or phosphonic acid and its derivatives. Porous titanium phosphate (MTiP-1) was prepared for the conversion of carbohydrates to 5-HMF under microwave irradiation.<sup>171</sup> At optimized conditions, the yield of 5-HMF was 44% from fructose in a DMA solvent mixture containing 10 wt.% LiCl at 140 °C after 5 min. When the solvent was changed to water, MIBK or a mixture of water and MIBK, gave 5-HMF yields of 29, 34 and 35%, respectively. The same catalytic reaction was performed with other substrates, e.g. glucose, mannose, sucrose and cellulose, which resulted in 22, 23, 27 and 17% yields of 5-HMF. The reusability of the MTiP-1 catalyst was also investigated by recycling the catalyst five times. In the fifth run, the yield of 5-HMF dropped by 8%.<sup>171</sup>

Nakajima et al. studied the transformation of glucose to 5-HMF using titania and phosphate-titania as solid acid catalysts.<sup>172</sup> For the latter catalyst, TiO<sub>2</sub> nanoparticles were first synthesized, then modified with phosphate via immersion in 1 M phosphoric acid for 2 h. The final sample was washed several times with water and dried at 120 °C. Phosphate-titania exhibited high activity for the production of 5-HMF from glucose in a THF/water (90/10 vol.%) solution, with an 81% yield of 5-HMF and 98% glucose conversion obtained at 120 °C after 2 h. Bare TiO<sub>2</sub> resulted in just 8.5% yield, but with 99% glucose conversion under identical conditions. Phosphoric acid was also tested for catalytic reaction, the 5-HMF yield and glucose conversion were 9.2 and 1.2%,



respectively. Phosphate-titania was a stable catalyst. After five times recycling the catalyst, no loss of activity was observed.<sup>172</sup>

Atanda et al. also reported the conversion of glucose to 5-HMF using phosphate-titania.<sup>173</sup> The phosphate content was varied from 5 to 25 wt% to investigate the effect of phosphate quantity on 5-HMF yield. It was revealed that by increasing the phosphate quantity the surface area increased and peaked at 15 wt% phosphate content, giving an acidic site coverage of 2.36 mmol/g. Under optimal reaction conditions, the yield of 5-HMF and glucose conversion from glucose solution in a water/n-butanol mixture were 81 and 97%, respectively, at 175 °C after 3 h. The catalyst showed fair stability and was used for 6 runs; however, the yield of 5-HMF dropped 10% after the third run.<sup>173</sup> Hattori, Kamataa and Hara immobilized phosphate on the surface of titania for direct conversion of glucose to 5-HMF.<sup>174</sup> The phosphate group was attached to the surface of the titania via esterification between the phosphoric acid and surface terminal OH groups on the titania. Since the quantity of OH groups on the surface of the titania is restricted, this limits the grafting of the phosphate moieties (surface atomic ratio of P/Ti was 0.65). In this report, the process of phosphate grafting was performed under fluorescent light irradiation in order to increase the density of OH groups on titania. Under optimal conditions, the selectivity of 5-HMF and glucose conversion were 80 and 84%, respectively, from a glucose solution in a mixture of water and 2-sec-butylphenol (1:3 V/V) at 135 °C after 4 h. The highly stable catalyst was recycled three times with only a very small loss of activity (less than 3% 5-HMF selectivity).<sup>174</sup> In summary, phosphated metal oxides can be considered as an option for dehydration of carbohydrates to the 5-HMF.

In conclusion, sulfated and phosphated metal oxides can be considered as a promising option for conversion of fructose to 5-HMF.

### 1.10. Motivations and aims for the research

To summarize the previous sections, global issues about fossil fuels were discussed, with biomass being a promising alternative for fuel and chemical production (refer to sections 1.1 and 1.2). Among the top 14 chemical species targeted by U.S DOE for production from biomass conversion, 5-HMF and its derivatives are high-value

chemicals that may make biorefining commercially viable (sections 1.3 to 1.5). The mechanism of biomass conversion to 5-HMF is a multistep catalytic reaction (section 1.6), for which an acid catalyst is essential. However, problems with reactor corrosion and handling of mineral acids as homogenous catalysts to convert biomass have created opportunities for heterogeneous solid acid catalysts. The conversion of fructose to 5-HMF has been used as a model reaction to investigate the capabilities of new solid acid catalysts. The performance of solid acid catalysts in the dehydration of fructose to 5-HMF in a range of organic solvents was reviewed in sections 1.7 and 1.8. The former focused on DMSO and DMSO-containing solvents, and the latter on non-DMSO solvent mixtures. Consequently, one of the best options as solid acid catalysts for 5-HMF production are sulphated and phosphated metal oxides, particularly those based on early transition metals such as titanium and zirconium (section 1.9).

Through a review of relevant literature the following knowledge deficiencies were identified: 1) The effect of the concentration of sulfuric acid and the duration of treatment on sulfate grafting have not been investigated deeply. 2) The effect of elemental composition on sulfate grafting is not clear. 3) The quantity of acidic sites were low due to the low surface area of the metal oxide materials employed. 4) When grafting sulfate a calcination process is necessary, but how calcination temperature affects sulfate modification has not been investigated deeply. 5) One serious barrier for extending the application of phosphated metal oxides, specifically titanium and zirconium-based ones, is low surface area. The percentage of phosphate grafting depends on the density of OH groups on the surface, but the surface area of crystalline titania and zirconia materials is limited ( $<200 \text{ m}^2\text{g}^{-1}$ ) because of the calcination process used to induce crystallization. So, a procedure that can either increase the surface area, or the quantity of the OH groups on the surface is highly required.

The objectives of this thesis are to *prepare, functionalize and characterize mesoporous titania, zirconia and binary titanium zirconium oxides for the conversion of carbohydrates to 5-HMF*. The following aims satisfy the objectives of the thesis.

### 1.11. Aims

This thesis has six research aims:

- i. Synthesise zirconium dioxide spheres by controlling the physical properties of pore diameter and surface area, then modify the zirconia surface with aliphatic di-carboxylic acids, aromatic di-carboxylic acids or amino acids to prepare a multifunctional catalyst that contains both Lewis and Brønsted acid and base sites for the conversion of sugars to 5-HMF.
- ii. Control the crystal structure of zirconia to tune the acid strength of the surface.
- iii. Prepare mesoporous titanium zirconium oxide spheres and control the physicochemical properties of pore diameter, surface area and surface hydroxyl group density, and study the effect of Ti:Zr ratio, solvothermal temperature and calcination temperature on the physicochemical properties.
- iv. Functionalize the surface of high surface area mesoporous titanium zirconium oxide spheres with phosphonic acid derivatives to prepare a multifunctional solid acid catalyst for the dehydration of carbohydrates to 5-HMF.
- v. Graft sulfate groups on the surface of the mesoporous titanium zirconium oxide spheres to prepare a solid acid catalyst for the conversion of carbohydrates to 5-HMF, studying the effect of sulfuric acid concentration, duration of acid treatment, calcination temperature and Ti:Zr ratio on the grafting percentage of sulfate on the surface.
- vi. Apply the prepared solid acid catalysts for the conversion of fructose to 5-HMF, and study the effect of time, temperature, solvent, substrate and loading of the catalyst on the 5-HMF yield.

### 1.12. Overview of chapters 2-5

Chapter 2 focuses on the preparation of mesoporous zirconia via a sol-gel method. The pore diameter is controlled by tuning the solvothermal processing temperature. The optimized zirconia sample is functionalized with aliphatic di-carboxylic acids, aromatic di-carboxylic acids or amino acids through a simple and green process. Finally, the compound with the highest quantity of functional groups is applied as a solid acid catalyst for carbohydrate dehydration to 5-HMF. Factors such as solvent, temperature, time, and the amount of the catalyst are optimized.

In chapter 3 a synthesis for mesoporous titanium zirconium oxide (TZ) spheres with high surface area is presented. The Ti:Zr ratio, solvothermal and calcination temperatures were optimized to find the TZ spheres with high surface area, mesopore size and a high quantity of surface hydroxyl groups, before functionalization with phosphonic acid derivatives to create a solid acid catalyst. The modified compound is used as a solid acid catalyst for conversion of fructose to 5-HMF in a model reaction. The catalytic reaction conditions of time, temperature, solvent, and the amount of catalyst are optimized. Substrates other than fructose, and the reusability of the catalyst are also investigated.

Sulfated zirconium titanium binary oxide as a solid-acid catalyst for 5-HMF production from sugars are examined in chapter 4. The effects of acid concentration, duration of acid treatment, surface area and zirconia content on the percentage of sulfate grafting are investigated. The sample with the highest loading of sulfate groups is then utilized as a solid acid catalyst for the conversion of fructose to 5-HMF.

Chapter 5 summarizes the research findings from this work and closes with an outlook for future studies.

## 1.13. References

1. M. E. Davis, *Nature*, 2002, **417**, 813.
2. G. W. Stone, S. G. Ellis, D. A. Cox, J. Hermiller, C. O'shaughnessy, J. T. Mann, M. Turco, R. Caputo, P. Bergin and J. Greenberg, *New England Journal of Medicine*, 2004, **350**, 221-231.
3. J. A. Geboers, S. Van de Vyver, R. Ooms, B. O. de Beeck, P. A. Jacobs and B. F. Sels, *Catalysis Science & Technology*, 2011, **1**, 714-726.
4. H. Kobayashi, H. Ohta and A. Fukuoka, *Catalysis Science & Technology*, 2012, **2**, 869-883.
5. M. E. Zakrzewska, E. Bogel-Łukasik and R. Bogel-Łukasik, *Chemical Reviews*, 2011, **111**, 397-417.
6. M. Moller and U. Schroder, *RSC Advances*, 2013, **3**, 22253-22260.
7. H. Kobayashi and A. Fukuoka, *Green Chemistry*, 2013, **15**, 1740-1763.
8. N. Mosier, C. Wyman, B. Dale, R. Elander, Y. Y. Lee, M. Holtzaple and M. Ladisch, *Bioresource Technology*, 2005, **96**, 673-686.
9. R. Rinaldi and F. Schüth, *ChemSusChem*, 2009, **2**, 1096-1107.
10. R. H.-Y. Chang, J. Jang and K. C. W. Wu, *Green Chemistry*, 2011, **13**, 2844-2850.

11. J. Zaldivar, A. Martinez and L. O. Ingram, *Biotechnology and Bioengineering*, 1999, **65**, 24-33.
12. C. E. Wyman, B. E. Dale, R. T. Elander, M. Holtzapple, M. R. Ladisch and Y. Y. Lee, *Bioresource Technology*, 2005, **96**, 1959-1966.
13. A. Takimoto, T. Shiomi, K. Ino, T. Tsunoda, A. Kawai, F. Mizukami and K. Sakaguchi, *Microporous and Mesoporous Materials*, 2008, **116**, 601-606.
14. I. Krog-Mikkelsen, O. Hels, I. Tetens, J. J. Holst, J. R. Andersen and K. Bukhave, *The American Journal of Clinical Nutrition*, 2011, **94**, 472-478.
15. A. S. Mamman, J.-M. Lee, Y.-C. Kim, I. T. Hwang, N.-J. Park, Y. K. Hwang, J.-S. Chang and J.-S. Hwang, *Biofuels, Bioproducts and Biorefining*, 2008, **2**, 438-454.
16. J.-P. Lange, E. van der Heide, J. van Buijtenen and R. Price, *ChemSusChem*, 2012, **5**, 150-166.
17. A. Corma, S. Iborra and A. Velty, *Chemical Reviews*, 2007, **107**, 2411-2502.
18. J. Zakzeski, P. C. A. Bruijninx, A. L. Jongorius and B. M. Weckhuysen, *Chemical Reviews*, 2010, **110**, 3552-3599.
19. C. Zhao, Y. Kou, A. A. Lemonidou, X. Li and J. A. Lercher, *Chemical Communications*, 2010, **46**, 412-414.
20. C. Zhao, J. He, A. A. Lemonidou, X. Li and J. A. Lercher, *Journal of Catalysis*, 2011, **280**, 8-16.
21. P. Azadi, R. Carrasquillo-Flores, Y. J. Pagan-Torres, E. I. Gurbuz, R. Farnood and J. A. Dumesic, *Green Chemistry*, 2012, **14**, 1573-1576.
22. Y. Chisti, *Biotechnology Advances*, 2007, **25**, 294-306.
23. J. E. Holladay, J. F. White, J. J. Bozell and D. Johnson, *Top value-added chemicals from biomass-Volume II—Results of screening for potential candidates from biorefinery lignin*, Pacific Northwest National Laboratory (PNNL), Richland, WA (US), 2007.
24. J. J. Bozell, *CLEAN—Soil, Air, Water*, 2008, **36**, 641-647.
25. T. Werpy, G. Petersen, A. Aden, J. Bozell, J. Holladay, J. White, A. Manheim, D. Eliot, L. Lasure and S. Jones, *Top value added chemicals from biomass. Volume 1-Results of screening for potential candidates from sugars and synthesis gas*, Department of Energy Washington DC, 2004.
26. A. Kulkarni, H. Modak, S. Jadhav and R. Khan, *Journal of scientific & industrial research*, 1988.
27. S. I. Martins and M. A. Van Boekel, *Food Chemistry*, 2005, **92**, 437-448.
28. M. Van Boekel, *Biotechnology Advances*, 2006, **24**, 230-233.
29. G. Düll, *Chem. Ztg*, 1895, **19**, 216-220.
30. B. Saha and M. M. Abu-Omar, *Green Chemistry*, 2014, **16**, 24-38.
31. X. Zheng, X. Gu, Y. Ren, Z. Zhi and X. Lu, *Biofuels, Bioproducts and Biorefining*, 2016, **10**, 917-931.
32. J. B. Binder, A. V. Cefali, J. J. Blank and R. T. Raines, *Energy & Environmental Science*, 2010, **3**, 765-771.
33. D. M. Alonso, J. Q. Bond and J. A. Dumesic, *Green Chemistry*, 2011, **13**, 754-793.
34. R.-J. van Putten, J. C. van der Waal, E. de Jong, C. B. Rasrendra, H. J. Heeres and J. G. de Vries, *Chemical Reviews*, 2013, **113**, 1499-1597.
35. T. Wang, M. W. Nolte and B. H. Shanks, *Green Chemistry*, 2014, **16**, 548-572.

36. P. K. Rout, A. D. Nannaware, O. Prakash, A. Kalra and R. Rajasekharan, *Chemical Engineering Science*, 2016, **142**, 318-346.
37. Z. Yang, W. Qi, R. Huang, J. Fang, R. Su and Z. He, *Chemical Engineering Journal*, 2016, **296**, 209-216.
38. <http://www.decisiondatabases.com/>, Global 5-Hydroxymethylfurfural (CAS 67-47-0) Market by Manufacturers, Countries, Type and Application, Forecast to 2022., (accessed June, 2017).
39. A. Gandini and M. N. Belgacem, *Progress in Polymer Science*, 1997, **22**, 1203-1379.
40. A. Eerhart, A. Faaij and M. K. Patel, *Energy & Environmental Science*, 2012, **5**, 6407-6422.
41. M. G. Gert-Jan, S. Laszlo and D. Matheus Adrianus, *Combinatorial Chemistry & High Throughput Screening*, 2012, **15**, 180-188.
42. O. Casanova, S. Iborra and A. Corma, *ChemSusChem*, 2009, **2**, 1138-1144.
43. Y. Y. Gorbanev, S. K. Klitgaard, J. M. Woodley, C. H. Christensen and A. Riisager, *ChemSusChem*, 2009, **2**, 672-675.
44. B. Saha, S. Dutta and M. M. Abu-Omar, *Catalysis Science & Technology*, 2012, **2**, 79-81.
45. S. E. Davis, L. R. Houk, E. C. Tamargo, A. K. Datye and R. J. Davis, *Catalysis Today*, 2011, **160**, 55-60.
46. S. E. Davis, B. N. Zope and R. J. Davis, *Green Chemistry*, 2012, **14**, 143-147.
47. B. Saha, D. Gupta, M. M. Abu-Omar, A. Modak and A. Bhaumik, *Journal of Catalysis*, 2013, **299**, 316-320.
48. R. Alamillo, M. Tucker, M. Chia, Y. Pagán-Torres and J. Dumesic, *Green Chemistry*, 2012, **14**, 1413-1419.
49. H. Cai, C. Li, A. Wang and T. Zhang, *Catalysis Today*, 2014, **234**, 59-65.
50. M. Balakrishnan, E. R. Sacia and A. T. Bell, *Green Chemistry*, 2012, **14**, 1626-1634.
51. G. A. Kraus and T. Guney, *Green Chemistry*, 2012, **14**, 1593-1596.
52. C. M. Lew, N. Rajabbeigi and M. Tsapatsis, *Industrial & Engineering Chemistry Research*, 2012, **51**, 5364-5366.
53. K. L. Deutsch and B. H. Shanks, *Journal of Catalysis*, 2012, **285**, 235-241.
54. X. Tong, Y. Ma and Y. Li, *Applied Catalysis A: General*, 2010, **385**, 1-13.
55. Y. Román-Leshkov, C. J. Barrett, Z. Y. Liu and J. A. Dumesic, *Nature*, 2007, **447**, 982.
56. M. Chidambaram and A. T. Bell, *Green Chemistry*, 2010, **12**, 1253-1262.
57. G. W. Huber, J. N. Chheda, C. J. Barrett and J. A. Dumesic, *Science*, 2005, **308**, 1446-1450.
58. W. Shen, G. A. Tompsett, K. D. Hammond, R. Xing, F. Dogan, C. P. Grey, W. C. Conner Jr, S. M. Auerbach and G. W. Huber, *Applied Catalysis A: General*, 2011, **392**, 57-68.
59. A. Corma, O. de la Torre and M. Renz, *ChemSusChem*, 2011, **4**, 1574-1577.
60. A. Corma, O. de la Torre and M. Renz, *Energy & Environmental Science*, 2012, **5**, 6328-6344.
61. J. Yang, N. Li, G. Li, W. Wang, A. Wang, X. Wang, Y. Cong and T. Zhang, *ChemSusChem*, 2013, **6**, 1149-1152.

62. M. J. Antal Jr, W. S. Mok and G. N. Richards, *Carbohydrate Research*, 1990, **199**, 91-109.
63. B. Kuster, *Starch-Stärke*, 1990, **42**, 314-321.
64. F. Newth, in *Advances in Carbohydrate Chemistry*, Elsevier, 1951, vol. 6, pp. 83-106.
65. E. Anet, in *Advances in Carbohydrate Chemistry*, Elsevier, 1964, vol. 19, pp. 181-218.
66. C. Moreau, R. Durand, S. Razigade, J. Duhamet, P. Faugeras, P. Rivalier, P. Ros and G. Avignon, *Applied Catalysis A: General*, 1996, **145**, 211-224.
67. M. S. Feather and J. F. Harris, in *Advances in Carbohydrate Chemistry and Biochemistry*, Elsevier, 1973, vol. 28, pp. 161-224.
68. A. S. Amarasekara, L. D. Williams and C. C. Ebede, *Carbohydrate Research*, 2008, **343**, 3021-3024.
69. L.-K. Ren, L.-F. Zhu, T. Qi, J.-Q. Tang, H.-Q. Yang and C.-W. Hu, *ACS catalysis*, 2017, **7**, 2199-2212.
70. B. F. M. Kuster, *Carbohydrate Research*, 1977, **54**, 177-183.
71. B. F. M. Kuster and H. S. van der Baan, *Carbohydrate Research*, 1977, **54**, 165-176.
72. B. F. M. Kuster and H. M. G. Temmink, *Carbohydrate Research*, 1977, **54**, 185-191.
73. H. Van Dam, A. Kieboom and H. Van Bekkum, *Starch-Stärke*, 1986, **38**, 95-101.
74. Y. Nakamura and S. Morikawa, *Bulletin of the Chemical Society of Japan*, 1980, **53**, 3705-3706.
75. H. H. Szmant and D. D. Chundury, *Journal of Chemical Technology and Biotechnology*, 1981, **31**, 135-145.
76. S. Kei-ichi, I. Yoshihisa and I. Hitoshi, *Chemistry Letters*, 2000, **29**, 22-23.
77. X. Qi, M. Watanabe, T. M. Aida and R. L. Smith, *Industrial & Engineering Chemistry Research*, 2008, **47**, 9234-9239.
78. K.-i. Shimizu, R. Uozumi and A. Satsuma, *Catalysis Communications*, 2009, **10**, 1849-1853.
79. X. Qi, M. Watanabe, T. M. Aida and R. L. Smith, *Catalysis Communications*, 2009, **10**, 1771-1775.
80. X. Tong and Y. Li, *ChemSusChem*, 2010, **3**, 350-355.
81. Y. Zhang, V. Degirmenci, C. Li and E. J. M. Hensen, *ChemSusChem*, 2011, **4**, 59-64.
82. K. B. Sidhpuria, A. L. Daniel-da-Silva, T. Trindade and J. A. P. Coutinho, *Green Chemistry*, 2011, **13**, 340-349.
83. S. Despax, C. Maurer, B. Estrine, J. Le Bras, N. Hoffmann, S. Marinkovic and J. Muzart, *Catalysis Communications*, 2014, **51**, 5-9.
84. Y. Qu, C. Huang, J. Zhang and B. Chen, *Bioresource Technology*, 2012, **106**, 170-172.
85. Y.-Y. Lee and K. C. W. Wu, *Physical Chemistry Chemical Physics*, 2012, **14**, 13914-13917.
86. B. Liu, Z. Zhang and K. Huang, *Cellulose*, 2013, **20**, 2081-2089.
87. H. Li, Q. Zhang, X. Liu, F. Chang, Y. Zhang, W. Xue and S. Yang, *Bioresource Technology*, 2013, **144**, 21-27.

88. R. Liu, J. Chen, X. Huang, L. Chen, L. Ma and X. Li, *Green Chemistry*, 2013, **15**, 2895-2903.
89. F. Wang, H.-Z. Wu, C.-L. Liu, R.-Z. Yang and W.-S. Dong, *Carbohydrate Research*, 2013, **368**, 78-83.
90. X.-L. Shi, M. Zhang, Y. Li and W. Zhang, *Green Chemistry*, 2013, **15**, 3438-3445.
91. Z. Huang, W. Pan, H. Zhou, F. Qin, H. Xu and W. Shen, *ChemSusChem*, 2013, **6**, 1063-1069.
92. W. N. P. van der Graaff, K. G. Olvera, E. A. Pidko and E. J. M. Hensen, *Journal of Molecular Catalysis A: Chemical*, 2014, **388-389**, 81-89.
93. X. Zhang, M. Wang, Y. Wang, C. Zhang, Z. Zhang, F. Wang and J. Xu, *Chinese Journal of Catalysis*, 2014, **35**, 703-708.
94. J. Chen, K. Li, L. Chen, R. Liu, X. Huang and D. Ye, *Green Chemistry*, 2014, **16**, 2490-2499.
95. A. Chinnappan, A. H. Jadhav, H. Kim and W.-J. Chung, *Chemical Engineering Journal*, 2014, **237**, 95-100.
96. J. Chen, G. Zhao and L. Chen, *RSC Advances*, 2014, **4**, 4194-4202.
97. Z. Huang, Y. Pan, Y. Chao, W. Shen, C. Wang and H. Xu, *RSC Advances*, 2014, **4**, 13434-13437.
98. B. Liu, C. Ba, M. Jin and Z. Zhang, *Industrial Crops and Products*, 2015, **76**, 781-786.
99. H. Xu, Z. Miao, H. Zhao, J. Yang, J. Zhao, H. Song, N. Liang and L. Chou, *Fuel*, 2015, **145**, 234-240.
100. R. S. Thombal and V. H. Jadhav, *Applied Catalysis A: General*, 2015, **499**, 213-216.
101. L. Hu, X. Tang, Z. Wu, L. Lin, J. Xu, N. Xu and B. Dai, *Chemical Engineering Journal*, 2015, **263**, 299-308.
102. J. Lan and Z. Zhang, *Journal of Industrial and Engineering Chemistry*, 2015, **23**, 200-205.
103. S. Mondal, J. Mondal and A. Bhaumik, *ChemCatChem*, 2015, **7**, 3570-3578.
104. Y. Peng, Z. Hu, Y. Gao, D. Yuan, Z. Kang, Y. Qian, N. Yan and D. Zhao, *ChemSusChem*, 2015, **8**, 3208-3212.
105. Y. Shen, Y. Zhang, Y. Chen, Y. Yan, J. Pan, M. Liu and W. Shi, *Energy Technology*, 2016, **4**, 600-609.
106. H. Hafizi, A. Najafi Chermahini, M. Saraji and G. Mohammadnezhad, *Chemical Engineering Journal*, 2016, **294**, 380-388.
107. X. Tian, Z. Jiang, Y. Jiang, W. Xu, C. Li, L. Luo and Z.-J. Jiang, *RSC Advances*, 2016, **6**, 101526-101534.
108. L. Zhu, J. Dai, M. Liu, D. Tang, S. Liu and C. Hu, *ChemSusChem*, 2016, **9**, 2174-2181.
109. Z. Hu, Y. Peng, Y. Gao, Y. Qian, S. Ying, D. Yuan, S. Horike, N. Ogiwara, R. Babarao, Y. Wang, N. Yan and D. Zhao, *Chemistry of Materials*, 2016, **28**, 2659-2667.
110. Q. Hou, W. Li, M. Ju, L. Liu, Y. Chen and Q. Yang, *RSC Advances*, 2016, **6**, 104016-104024.
111. A. Najafi Chermahini, F. Shahangi, H. A. Dabbagh and M. Saraji, *RSC Advances*, 2016, **6**, 33804-33810.



112. H. Yang, X. Liu, G. Lu and Y. Wang, *Microporous and Mesoporous Materials*, 2016, **225**, 144-153.
113. A. Najafi Chermahini, H. Hafizi, N. Andisheh, M. Saraji and A. Shahvar, *Research on Chemical Intermediates*, 2017, **43**, 5507-5521.
114. M. Liu, Y. Zhang, E. Zhu, P. Jin, K. Wang, J. Zhao, C. Li and Y. Yan, *ChemistrySelect*, 2017, **2**, 10413-10419.
115. F. N. D. C. Gomes, F. M. T. Mendes and M. M. V. M. Souza, *Catalysis Today*, 2017, **279**, 296-304.
116. J. Zhong, Y. Guo and J. Chen, *Journal of Energy Chemistry*, 2017, **26**, 147-154.
117. P. Bhanja, A. Modak, S. Chatterjee and A. Bhaumik, *ACS Sustainable Chemistry & Engineering*, 2017, **5**, 2763-2773.
118. H. Tang, N. Li, F. Chen, G. Li, A. Wang, Y. Cong, X. Wang and T. Zhang, *Green Chemistry*, 2017, **19**, 1855-1860.
119. G. Raveendra, M. Surendar and P. S. Sai Prasad, *New Journal of Chemistry*, 2017, **41**, 8520-8529.
120. P. Jin, Y. Zhang, Y. Chen, J. Pan, X. Dai, M. Liu, Y. Yan and C. Li, *Journal of the Taiwan Institute of Chemical Engineers*, 2017, **75**, 59-69.
121. Q. Wang, J. Hao and Z. Zhao, *Australian Journal of Chemistry*, 2018, **71**, 24-31.
122. N. L. Mulik, P. S. Niphadkar, K. V. Pandhare and V. V. Bokade, *ChemistrySelect*, 2018, **3**, 832-836.
123. Y. Dou, S. Zhou, C. Oldani, W. Fang and Q. Cao, *Fuel*, 2018, **214**, 45-54.
124. E. Kılıç and S. Yılmaz, *Industrial & Engineering Chemistry Research*, 2015, **54**, 5220-5225.
125. Z. Zhang, B. Liu and Z. K. Zhao, *Starch - Stärke*, 2012, **64**, 770-775.
126. H. Xie, Z. K. Zhao and Q. Wang, *ChemSusChem*, 2012, **5**, 901-905.
127. C.-H. Kuo, A. S. Poyraz, L. Jin, Y. Meng, L. Pahalagedara, S.-Y. Chen, D. A. Kriz, C. Guild, A. Gudz and S. L. Suib, *Green Chemistry*, 2014, **16**, 785-791.
128. H. S. Pawar and A. M. Lali, *Energy Technology*, 2016, **4**, 823-834.
129. L. Hu, G. Zhao, W. Hao, X. Tang, Y. Sun, L. Lin and S. Liu, *RSC Advances*, 2012, **2**, 11184-11206.
130. W. Deng, Q. Zhang and Y. Wang, *Science China Chemistry*, 2015, **58**, 29-46.
131. J. L. Roperro-Vega, A. Aldana-Pérez, R. Gómez and M. E. Niño-Gómez, *Applied Catalysis A: General*, 2010, **379**, 24-29.
132. T. Y. Kim, D. S. Park, Y. Choi, J. Baek, J. R. Park and J. Yi, *Journal of Materials Chemistry*, 2012, **22**, 10021-10028.
133. Z. Li, R. Wnetrzak, W. Kwapinski and J. J. Leahy, *ACS Applied Materials & Interfaces*, 2012, **4**, 4499-4505.
134. J. B. Joo, A. Vu, Q. Zhang, M. Dahl, M. Gu, F. Zaera and Y. Yin, *ChemSusChem*, 2013, **6**, 2001-2008.
135. A. Osatiashtiani, A. F. Lee, D. R. Brown, J. A. Melero, G. Morales and K. Wilson, *Catalysis Science & Technology*, 2014, **4**, 333-342.
136. J. Li, Y. Ma, L. Wang, Z. Song, H. Li, T. Wang, H. Li and W. Eli, *Catalysts*, 2016, **6**, 1.
137. D. Chen, L. Cao, F. Huang, P. Imperia, Y.-B. Cheng and R. A. Caruso, *Journal of the American Chemical Society*, 2010, **132**, 4438-4444.
138. F. Huang, D. Chen, X. L. Zhang, R. A. Caruso and Y.-B. Cheng, *Advanced Functional Materials*, 2010, **20**, 1301-1305.

139. D. Chen and R. A. Caruso, *Advanced Functional Materials*, 2013, **23**, 1356-1374.
140. X. Wang, D. Chen, L. Cao, Y. Li, B. J. Boyd and R. A. Caruso, *ACS Applied Materials & Interfaces*, 2013, **5**, 10926-10932.
141. Y. Zhang, J. Zhang and D. Su, *Journal of Energy Chemistry*, 2015, **24**, 548-551.
142. R. Vivani, F. Costantino and M. Taddei, in *Metal Phosphonate Chemistry: From Synthesis to Applications*, The Royal Society of Chemistry, 2012, DOI: 10.1039/9781849733571-00045, pp. 45-86.
143. S. S. Joshi, A. D. Zodge, K. V. Pandare and B. D. Kulkarni, *Industrial & Engineering Chemistry Research*, 2014, **53**, 18796-18805.
144. L. Wang, H. Wang, F. Liu, A. Zheng, J. Zhang, Q. Sun, J. P. Lewis, L. Zhu, X. Meng and F.-S. Xiao, *ChemSusChem*, 2014, **7**, 402-406.
145. N. Wang, Y. Yao, W. Li, Y. Yang, Z. Song, W. Liu, H. Wang, X.-F. Xia and H. Gao, *RSC Advances*, 2014, **4**, 57164-57172.
146. H. Xu, Z. Miao, H. Zhao, J. Yang, J. Zhao, H. Song, N. Liang and L. Chou, *Fuel*, 2015, **145**, 234-240.
147. F. Forato, H. Liu, R. Benoit, F. Fayon, C. Charlier, A. Fateh, A. Defontaine, C. Tellier, D. R. Talham, C. Queffelec and B. Bujoli, *Langmuir*, 2016, **32**, 5480-5490.
148. S. A. Paniagua, A. J. Giordano, O. N. L. Smith, S. Barlow, H. Li, N. R. Armstrong, J. E. Pemberton, J.-L. Brédas, D. Ginger and S. R. Marder, *Chemical Reviews*, 2016, **116**, 7117-7158.
149. D. Geldof, M. Tassi, R. Carleer, P. Adriaenssens, A. Roevens, V. Meynen and F. Blockhuys, *Surface Science*, 2017, **655**, 31-38.
150. U. Ciesla, M. Fröba, G. Stucky and F. Schüth, *Chemistry of Materials*, 1999, **11**, 227-234.
151. W. Li, F. Ma, F. Su, L. Ma, S. Zhang and Y. Guo, *ChemCatChem*, 2012, **4**, 1798-1807.
152. M. Petit and J. Monot, in *Chemistry of Organo-Hybrids*, John Wiley & Sons, Inc., 2014, DOI: 10.1002/9781118870068.ch5, pp. 168-199.
153. C. A. S. Lanziano, S. F. Moya, D. H. Barrett, E. Teixeira-Neto, R. Guirardello, F. d. S. d. Silva, R. Rinaldi and C. B. Rodella, *ChemSusChem*, 2018, **11**, 872-880.
154. K. Nakajima, R. Noma, M. Kitano and M. Hara, *The Journal of Physical Chemistry C*, 2013, **117**, 16028-16033.
155. R. Noma, K. Nakajima, K. Kamata, M. Kitano, S. Hayashi and M. Hara, *The Journal of Physical Chemistry C*, 2015, **119**, 17117-17125.
156. X. Qi, M. Watanabe, T. M. Aida and R. L. Smith Jr, *Catalysis Communications*, 2008, **9**, 2244-2249.
157. C. V. McNeff, D. T. Nowlan, L. C. McNeff, B. Yan and R. L. Fedie, *Applied Catalysis A: General*, 2010, **384**, 65-69.
158. S. Dutta, S. De, A. K. Patra, M. Sasidharan, A. Bhaumik and B. Saha, *Applied Catalysis A: General*, 2011, **409-410**, 133-139.
159. A. Chareonlimkun, V. Champreda, A. Shotipruk and N. Laosiripojana, *Fuel*, 2010, **89**, 2873-2880.
160. W. Li, F. Ma, F. Su, L. Ma, S. Zhang and Y. Guo, *ChemSusChem*, 2011, **4**, 744-756.
161. A. M. Alsalme, P. V. Wiper, Y. Z. Khimyak, E. F. Kozhevnikova and I. V. Kozhevnikov, *Journal of Catalysis*, 2010, **276**, 181-189.
162. B. M. Reddy and M. K. Patil, *Chemical Reviews*, 2009, **109**, 2185-2208.

163. K. Arata, *Green Chemistry*, 2009, **11**, 1719-1728.
164. C. Gannoun, A. Turki, H. Kochkar, R. Delaigle, P. Eloy, A. Ghorbel and E. M. Gaigneaux, *Applied Catalysis B: Environmental*, 2014, **147**, 58-64.
165. X. Qi, H. Guo and L. Li, *Industrial & Engineering Chemistry Research*, 2011, **50**, 7985-7989.
166. H. Yan, Y. Yang, D. Tong, X. Xiang and C. Hu, *Catalysis Communications*, 2009, **10**, 1558-1563.
167. Y. Yang, X. Xiang, D. Tong, C. Hu and M. M. Abu-Omar, *Bioresource Technology*, 2012, **116**, 302-306.
168. R. Kourieh, V. Rakic, S. Bennici and A. Auroux, *Catalysis Communications*, 2013, **30**, 5-13.
169. J. Zhang, S. B. Wu and B. Li, *Advanced Materials Research*, 2013, **666**, 131-142.
170. Y. Wang, X. Tong, Y. Yan, S. Xue and Y. Zhang, *Catalysis Communications*, 2014, **50**, 38-43.
171. A. Dutta, A. K. Patra, S. Dutta, B. Saha and A. Bhaumik, *Journal of Materials Chemistry*, 2012, **22**, 14094-14100.
172. K. Nakajima, R. Noma, M. Kitano and M. Hara, *Journal of Molecular Catalysis A: Chemical*, 2014, **388-389**, 100-105.
173. L. Atanda, S. Mukundan, A. Shrotri, Q. Ma and J. Beltramini, *ChemCatChem*, 2015, **7**, 781-790.
174. M. Hattori, K. Kamata and M. Hara, *Physical Chemistry Chemical Physics*, 2017, **19**, 3688-3693.



## Chapter 2. Modified mesoporous zirconia with dicarboxylic acids as a solid acid catalyst for dehydration of carbohydrates into 5-HMF

### 2.1. Introduction

As it was mentioned in chapter 1 section 1.1 and 1.2, biomass has evolved as the most promising alternative fuel source due to its high abundance, being a sustainable source of organic carbon and a primary energy carrier.<sup>1</sup> Of the products obtained after biomass conversion, it is 5-hydroxymethylfurfural (5-HMF) which has gained considerable attention due to its importance as an intermediate feedstock for the production of fine chemicals, polymer precursors, and fuels. 5-HMF can be produced by the acid catalyzed dehydration of hexose.<sup>2</sup> This process is often carried out using solid super-acid catalysts such as anion-modified metal oxides (e.g.  $\text{TiO}_2$  or  $\text{ZrO}_2$ ),<sup>3-5</sup> or binary metal oxides (e.g.  $\text{TiO}_2\text{-SiO}_2$ ,  $\text{Al}_2\text{O}_3\text{-ZrO}_2$  or  $\text{TiO}_2\text{-ZrO}_2$ ).<sup>6-9</sup>

Mesoporous zirconia has been applied to water treatment, drug delivery and catalysis on account of the super acid, high surface area, and structural stability properties that can be obtained.<sup>10-13</sup> Since the first reports nearly forty years ago on the super acidic properties of sulfated-zirconia,<sup>14-16</sup> the preparation and catalysis of this class of catalyst has been intensely studied.<sup>11, 17-19</sup> Sulfated-zirconia has been used in many chemical reactions such as condensation, esterification and dehydration.<sup>20, 21</sup> The advantageous properties of sulfated-zirconia are not only the strength of the acid, but also the type of acidity, both Brønsted and Lewis. As a result, sulfated-zirconia catalysts are capable of high activity and selectivity.<sup>21, 22</sup> Chemical reactions typically occur at the surface of the catalyst, and rational design can maximize the capacity the catalytically active surface area. Sulfated-zirconia is conventionally prepared by post-functionalization of mesoporous zirconia using concentrated sulfuric acid, followed by calcination at temperatures above 500 °C. However, both steps of this process have their drawbacks, being energy intensive and non-green chemistry.

Functionalizing metal oxides with carboxylic acids has been researched extensively, with a focus on long chain aliphatic carboxylic acids, since these are capable to form close-packed, highly organized monolayer films.<sup>23-26</sup> Three methods have been used to graft carboxylic groups onto the surface of the metal oxides, namely Langmuir-Blodgett techniques, attachment from dilute solution, and gas-phase techniques.<sup>27-30</sup> The power of the carboxylate attachment is dependent on the substrate, carboxylic acid, and preparation conditions.<sup>31-33</sup> For example, Dobson and McQuillan studied the adsorption of aromatic carboxylic acids on TiO<sub>2</sub>, Ta<sub>2</sub>O<sub>5</sub>, Al<sub>2</sub>O<sub>3</sub>, and ZrO<sub>2</sub> from aqueous solutions by in-situ IR spectroscopy. They concluded that benzoic acid strongly attached to ZrO<sub>2</sub>, but showed only a weak tendency towards TiO<sub>2</sub> and Ta<sub>2</sub>O<sub>5</sub>.<sup>31</sup>

In this chapter, mesoporous zirconia was prepared via a sol-gel and templating process. The pore size was tuned by controlling solvothermal temperature. The mesoporous zirconia was functionalized with aliphatic and aromatic di-carboxylic acids, as well as amino acids, via a simple aqueous method followed by washing and heating to remove unattached functional groups. The di-carboxylic acids were chosen to study the effect of molecular structure on the quantity of functional group grafted to the zirconia surface. The highest functional group loading was achieved with terephthalic acid. This sample was applied as a catalyst for the dehydration of D-fructose to 5-HMF. Factors such as solvent, temperature, time, and amount of the catalyst that affect the yield of 5-HMF were studied. Good control over the porosity of zirconia, the simple and green method of functionalization, and good dispersity in polar solvent are advantages of the final catalyst.

## 2.2. Experimental Section

### 2.2.1. Materials

Zirconium(IV) propoxide (ZrP, 70% in 1-propanol), hexadecylamine (HDA, 90%), D-fructose (>99%), glucose (>99%), sucrose (>99%), cellulose, starch, terephthalic acid (Ter, >99%), 2-amino terephthalic acid (Am-Ter, >99%), adipic acid (Adi, >99%), aspartic acid (Asp, >99%), succinic acid (Suc, >99%), glutamic acid (Glu, >99%), potassium chloride (AR) and dimethyl sulfoxide (DMSO) were obtained from

Sigma–Aldrich. Absolute ethanol (>99.7%), tetrahydrofuran (THF), methanol (HPLC grade), and dimethylformamide (DMF), acetone and acetonitrile were from Merck. Milli-Q water was collected from a Millipore Academic system with a resistivity higher than 18.2 MΩ cm. All chemicals and solvents were used as received.

#### 2.2.2. Preparation of zirconia spheres

The preparation of the mesoporous zirconia spheres is a two-step process.

##### 1. Synthesis of non-porous zirconia spheres

An amorphous precursor of zirconia was prepared via a sol-gel and templating method using HDA as a structure directing agent. KCl was used to control the size of the beads by adjusting the ionic strength of the solution.<sup>34</sup> In a typical preparation, 7.95 g of HDA was dissolved in 800 mL of ethanol, followed by the addition of 3.20 mL of KCl solution (0.1 M) and 5.44 mL water. This solution was stirred vigorously for 30 min, then 26.50 mL ZrP was added and stirred for 1 min. The resulting milky white precursor suspension was kept static at room temperature overnight. The spheres were separated from solution by centrifugation (Beckman Coulter Allegra 25R, 6000 rpm for 15 min) and washed with ethanol three times. Finally, the as-prepared amorphous zirconia spheres were left in a fume cupboard at ambient temperature for 6 days to dry.

##### 2. Solvothermal treatment and calcination of mesoporous zirconia spheres

To prepare mesoporous crystalline zirconia a solvothermal process was carried out. 1.6 g of as-prepared amorphous beads were dispersed in 20 mL ethanol and 10 mL water and stirred for 30 min. The resulting mixture was sealed within a 50 mL Teflon-lined steel autoclave and heated at 100, 140, 160, 180 or 200 °C for 16 h in a Labec fan-forced oven. The products were collected by centrifugation, washed with ethanol three times and dried in an oven at 60 °C overnight. It is worth mentioning that without the solvothermal process no mesoporous zirconia could be obtained. The samples were calcined at 500 °C (ramp rate of 1.6 °C min<sup>-1</sup> from room temperature) for 2 h in air to obtain mesoporous crystalline zirconia. The final samples were labelled Zr-Solx where x is the temperature of solvothermal treatment.

### 2.2.3. Functionalization of the mesoporous zirconia spheres

A green and effective method was used to introduce acidic groups on the surface of the zirconia in order to prepare a multifunctional catalyst. Various dicarboxylic acids and amino acids were used to functionalize the mesoporous zirconia spheres. In a typical procedure, 1.56 mmol of dicarboxylic acid or amino acid was dissolved in 10 mL of water and then 0.1 g of Zr-Sol160 was added. The mixture was sonicated for 5 min in an ultrasonic bath followed by stirring overnight at ambient temperature. The spheres were separated by centrifugation (7000 rpm 20 min), washed several times with water and once with ethanol, then dried in an oven at 100 °C overnight.

### 2.2.4. Characterization

Scanning electron microscopy (SEM) was conducted to observe the morphology and particle size of the samples using a FEI Quanta 200 environmental scanning electron microscope under low vacuum mode, and with an accelerating voltage of 15 kV. SEM images were obtained without metal sputter coating. Transmission electron microscopy (TEM) images were obtained on a FEI Tecnai F20 transmission electron microscope operated at 200 kV. Powder X-ray diffraction (XRD) patterns were obtained using a Bruker D8 Advance Diffractometer with Cu K $\alpha$  radiation. The diffractometer was set at a 40 kV working voltage and 40 mA working current, with samples scanned from 5 to 80° 2 $\theta$  at a step size of 0.02° and a scan-step time of 4 s. Phase identification was completed using DIFFRAC.EVA v4.1 software with the ICDD PDF4+ 2018 database, while Quantitative Rietveld analysis of identified crystalline phases was carried out using Bruker DIFFRAC.SUITE TOPAS software. Thermogravimetric analysis (TGA) measurements were carried out on a Mettler Toledo TGA/SDTA 851<sup>e</sup> Thermogravimetric Analyzer with a heating ramp of 10 °C min<sup>-1</sup> under 30 mL min<sup>-1</sup> flowing nitrogen from 25 to 900 °C. Nitrogen gas sorption isotherms were obtained at 77 K using a Micromeritics Tristar 3000 Surface Area and Porosity Analyzer. Before the measurement, samples were degassed at 160 °C for 18 h on a vacuum line. The specific surface area was calculated by a standard multipoint Brunauer-Emmett-Teller (BET) method using adsorption data in the P/P<sub>0</sub> range from 0.05 to 0.20. The Barrett-Joyner-Halenda (BJH) model was applied to the adsorption branch of the isotherm to determine pore size distributions. Fourier transform



infrared spectroscopy (FTIR) was carried out on a Perkin Elmer IR Spectrum ASCII PEDS 1.60 FTIR spectrometer. Spectra were acquired as the average of 8 scans.

#### 2.2.5. Catalytic test

The catalytic activity of the functionalized zirconia was tested by the dehydration reaction of fructose to 5-HMF. Typically, 15 mg of catalyst was added to a solution of fructose (3 mg) dissolved in DMSO (10 mL, 1.67 mM) in a 25 mL round-bottom flask in an oil bath, with the catalyst well-dispersed by ultrasonication for 5 min. Then reaction mixture was heated at 120, 130, 140, 150 or 160 °C for 1, 2, 3 or 5 h. The catalysts were collected by centrifugation (7000 rpm 20 min), then the supernatant examined using reverse phase preparatory high-performance liquid chromatography (HPLC) on an Agilent 1200 series HPLC system. Fructose disappearance was monitored by a UV detector ( $\lambda = 285$  nm) after sample elution from an Eclipse Plus C18 column (150 mm x 2.1 mm x 5  $\mu$ m), using an 88:12 water: methanol (v/v) gradient at a flow rate of 0.25 mL min<sup>-1</sup>. It was assumed that the volume changes were negligible after the dehydration reaction for all experiments. The 5-HMF yield was calculated as moles of 5-HMF produced based on a 5-HMF external standards curve. Variations in experiments using different solvents (acetone, acetonitrile, THF, ethanol and DMF), amounts of catalyst (5, 10, 30 and 45 mg) or the carbohydrate substrate (glucose, sucrose, cellulose and starch) followed the above procedure. The mass spectroscopy (MS) analyses were performed using an Agilent 6500 Q-TOF LC/MS system in negative ion mode to calculate fructose conversion and 5-HMF selectivity. The 5-HMF yield, fructose conversion, and 5-HMF selectivity were calculated based on Equations 1, 2 and 3, respectively as follows:

$$5 - \text{HMF yield (\%)} = \frac{\text{moles of 5-HMF obtained}}{\text{moles of initial fructose}} \times 100 \quad (1)$$

$$\text{Fructose conversion (\%)} = \frac{\text{moles of reacted fructose}}{\text{moles of initial fructose}} \times 100 \quad (2)$$

$$5 - \text{HMF selectivity (\%)} = \frac{\text{moles of 5-HMF obtained}}{\text{moles of reacted fructose}} \times 100 \quad (3)$$

Catalyst reusability tests: After each catalytic cycle (150 °C for 2 h), the catalyst (15 mg) was separated by centrifugation, washed thoroughly with ethanol and dried in an oven at 60 °C overnight.

## 2.3. Results and discussion

Amorphous zirconia spheres were prepared via a sol-gel and templating process, where HDA was used as the structure directing agent. This was followed by a solvothermal process carried out at temperatures between 100 and 200 °C. The mesoporous zirconia spheres were obtained after calcination at 500 °C for 2 h. The zirconia samples were functionalized by dispersing in dilute aqueous solutions of different di-carboxylic acids and amino acids to introduce functional groups onto the surface of the samples, followed by heating to remove functional group species that were only physically adsorbed.

### 2.3.1. Binding mode of di-carboxylic acid on zirconia particles and the quantity of loading

The yield of the functional groups was quantified via TGA. The results for neat and functionalized Zr-Sol160 are shown in Figure 2-1, from which was extracted data about mass loss due to the decomposition of organic species present on the surface of the zirconia spheres (Table 2-1). The grafting percentage was calculated from the mass percentage decrease over the temperature range 120 to 900 °C. Thermal analysis of neat zirconia spheres indicated only one main mass loss across 120 to 900 °C, which was related to physically adsorbed water and surface hydroxyl groups (Figure 2-1 a). Figure 2-1 a presents TGA results for Zr-Sol160 functionalized with amino acids, and both aliphatic and aromatic dicarboxylic acids. The grafting percentage of the amino acids (i.e., Asp and Glu) was higher than the aliphatic dicarboxylic acids (i.e., Adi and Suc), but the aromatic dicarboxylic acid, Ter, had the highest grafting percentage of 8.7 wt% (Figure 2-1 a and Table 2-1). In aqueous solutions at pH values between 2.5 and 4, the amino groups of Asp and Glu can gain a proton from the neighboring carboxylic acid group to form a zwitterion,  ${}^{-}\text{OOC-CH}(\text{NH}_3^{+})\text{-R-COOH}$  (R could be an aliphatic or aromatic chain).<sup>35</sup> This process can facilitate the adsorption of amino acids onto the surface of the zirconia due to the positive surface charge of the zirconia sample <sup>13</sup>, and would account for the higher grafting percentage of Asp and Glu

compared with the aliphatic dicarboxylic acids. As shown in Table 2-1, the amount of functional groups grafted onto the samples functionalized with aromatic dicarboxylic acids was greater than with aliphatic dicarboxylic acids (Figure 2-1 b), findings which are in agreement with previous reports.<sup>31, 36</sup> Moreover, this difference can be explained by the stabilizing effect the aromatic ring has on the carboxylate group (i.e.  $^-OOC-R-COO^-$ ).

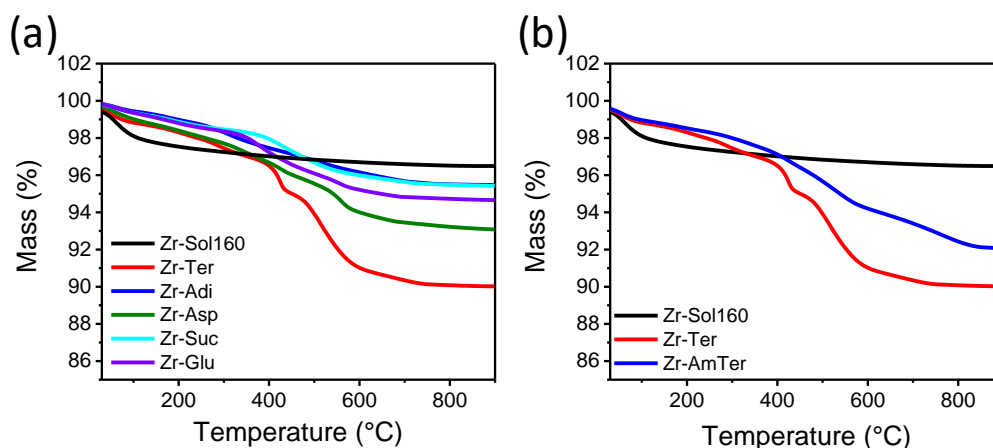
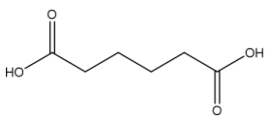
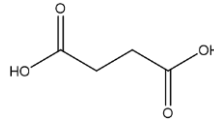
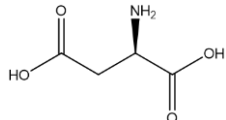
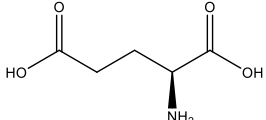
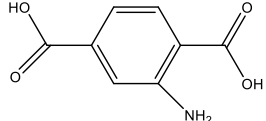
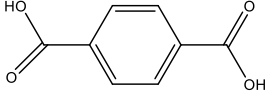


Figure 2-1. TGA of Zr-Sol160 functionalized with di-carboxylic acids and amino acids (a); Zr-Sol160 spheres and functionalized samples with AmTer, Ter with (Zr-Ter) (b).

Amino acids have been used as an effective and green catalyst for the isomerization of fructose to glucose in water.<sup>37</sup> Furthermore, in the conversion of glucose to 5-HMF, isomerization of glucose to fructose is the determining step, and requires either a base or Lewis acid as a catalyst.<sup>38</sup> Consequently, some researchers have tried to prepare multifunctional catalysts that contain both basic and acidic groups.<sup>3, 38</sup> In this study, by using a simple and green method amino acids were grafted successfully to the surface of the zirconia. This means acidic and basic groups, as well as the Lewis acidity of the zirconia are all present on the one particle, preparing a multifunctional catalyst. However, since the grafting percentage was low (Table 2-1) due to the relatively low surface area of the Zr-Sol160 spheres, the catalytic conversion of glucose to 5-HMF was not the focus of this research. Since Ter had the highest grafting percentage on the surface of the zirconia spheres, the Ter-functionalized mesoporous zirconia sample was selected as the catalyst for the dehydration of fructose to 5-HMF, and is a major focus of the remainder of this chapter.

Table 2-1. Grafting percentage of the different acid functional groups on the surface of Zr-Sol160 spheres.

Functional group	Functional molecule Structure	Grafting percentage <sup>(a)</sup> (wt %)
Adipic acid (Adi)		3.9
Succinic acid (Suc)		3.8
Aspartic acid (Asp)		5.8
Glutamic acid (Glu)		4.6
2-aminoterephthalic acid (AmTer)		6.8
Terephthalic acid (Ter)		8.7

<sup>(a)</sup> The grafting percentage is the mass percentage of the grafted functional group component which calculated from the mass percentage decrease over the temperature range 120 to 900 °C.

There are several binding modes that could describe the attachment of di-acids on the surface of zirconia including simple adsorption (i.e. electrostatic attraction and hydrogen bonding) and chemical adsorption (ester linkage, bridging, and chelating), as shown in Figure 2-2.<sup>31, 36</sup> FT-IR was carried out to study the binding modes of the attached Ter carboxylic acid on the surface of zirconia (Figure 2-3) The strong bands

at 1539 and 1384  $\text{cm}^{-1}$  were assigned to the asymmetric and symmetric stretching band of carboxylate anion ( $\text{COO}^-$ ) due to splitting of carboxylate group complexed with Zr atoms, while the peak at 1589  $\text{cm}^{-1}$  was attributed to ring stretch vibration (Figure 2-3 b). The bands at 1508 and 1434  $\text{cm}^{-1}$ , and at 1147 and 1018  $\text{cm}^{-1}$  were related to ring stretch modes and ring C–H bend modes, respectively. The strong peak at 1712  $\text{cm}^{-1}$  was linked to the C=O band of carboxylic acid.<sup>31, 39, 40</sup> As Ter is a di-carboxylic acid when it functionalized Zr-Sol160 one carboxylic group was attached to the surface and the other carboxylic acid group was free. The binding mode of carboxylic acids on the  $\text{ZrO}_2$  particles can be characterized by the separation between asymmetric and symmetric stretching band of carboxylate anion ( $\Delta(\nu_{\text{as}}-\nu_{\text{s}})$ ). Generally, the band separation for monodentate binding, bidentate bridging and bidentate chelating is 350-500  $\text{cm}^{-1}$ , 150-180  $\text{cm}^{-1}$  and 60-100  $\text{cm}^{-1}$ , respectively.<sup>31</sup> In our case, the value of  $\Delta(\nu_{\text{as}}-\nu_{\text{s}})$  is 155  $\text{cm}^{-1}$  and from these results, it was concluded that a bridging bidentate species had formed on the surface of the zirconia (option (e) in Figure 2-2).

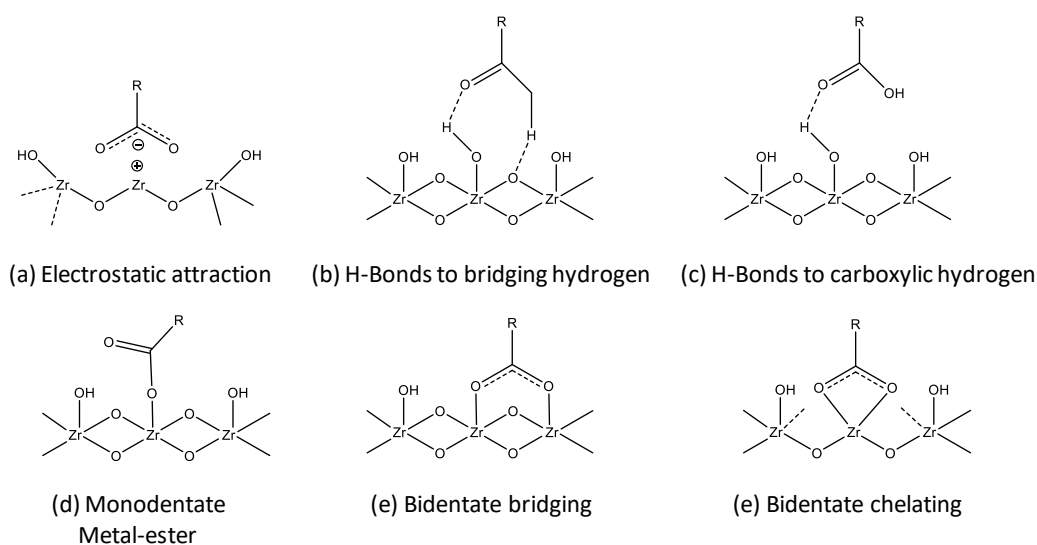


Figure 2-2. Possible binding modes of  $\text{COOH}$  or  $\text{COO}^-$  groups to the zirconia surfaces.

The mesoporosity of the zirconia spheres prepared at different solvothermal temperatures and following calcination at 500  $^{\circ}\text{C}$ , and Ter functionalized zirconia using Zr-Sol160 was examined by nitrogen gas porosimetry. The sorption isotherms shown in Figure 2-4 all type IV isotherms, indicating that all samples were mesoporous. The BJH pore-size distribution curves indicate that mesopore size of the zirconia increased

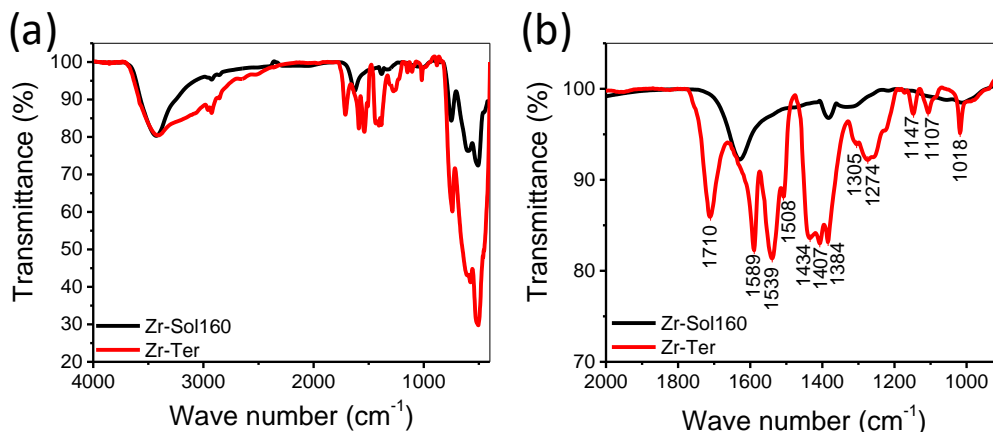


Figure 2-3. FT-IR of Zr-Sol160 before and after functionalization with Ter (a) and a close-up view of the peaks in the range 900-2000  $\text{cm}^{-1}$  (b).

with increasing solvothermal temperature from 100 to 200  $^{\circ}\text{C}$ , and was accompanied by an increase in associated mesopore volume (Fig. 3d). The BET surface area and BJH pore diameters at maximum pore volume are summarized in Table 2-2. Specific surface area (SBET) and pore diameter (PD) of the mesoporous zirconia prepared at various solvothermal temperatures, and Ter functionalized Zr-Sol160 (Zr-Ter). By increasing the solvothermal temperature from 100 to 140  $^{\circ}\text{C}$ , the surface area changed from 61 to 84  $\text{m}^2 \text{g}^{-1}$ , an increase of 38%, while the pore diameter enlarged by 0.9 nm to 3.8 nm. Further increases in the solvothermal temperature reduced the zirconia surface area, but the pore diameter was enhanced. The surface area of Zr-Sol200 was slightly higher than that of Zr-Sol180 (68 and 66  $\text{m}^2 \text{g}^{-1}$ , respectively), due to the presence of micropores in the former. The highest surface area and pore diameter were achieved with Zr-Sol140 (84  $\text{m}^2 \text{g}^{-1}$ ) and Zr-Sol200 (9 nm), respectively. Pore morphology and porosity can influence the activity of a catalyst.<sup>19</sup> Functionalizing the surface of mesoporous material will cause surface area and pore size to be reduced. Consequently, surface area and pore size for catalytic application must be optimized. On the one hand, by increasing the surface area more functional groups could be introduced on the surface of the catalyst, but pore size would be smaller which could negatively affect diffusion of the substrate and product. On the other hand, by increasing pore size, surface area would be reduced, and that could influence the number of functional groups present. In order to balance these considerations, Zr-Sol160 was selected as the zirconia support for Ter functionalization. Compared with the zirconia sample solvothermally treated at 140  $^{\circ}\text{C}$ , the surface area of Zr-Sol160

decreased from 84 to 75  $\text{m}^2\text{g}^{-1}$ , but the pore size grew by 60% to 6.1 nm (Table 2-2). After functionalizing with Ter, the surface area was reduced to 67  $\text{m}^2\text{g}^{-1}$ , and pore diameter to 5.2 nm (Table 2-2). This reduction in textural properties was attributed to the chemically bound Ter both shielding the zirconia surface and occupying space in the mesopore cavity. It should be noted that Zr-Ter displays a type IV isotherm, indicating that mesoporosity was preserved after functionalization (Figure 2-4).

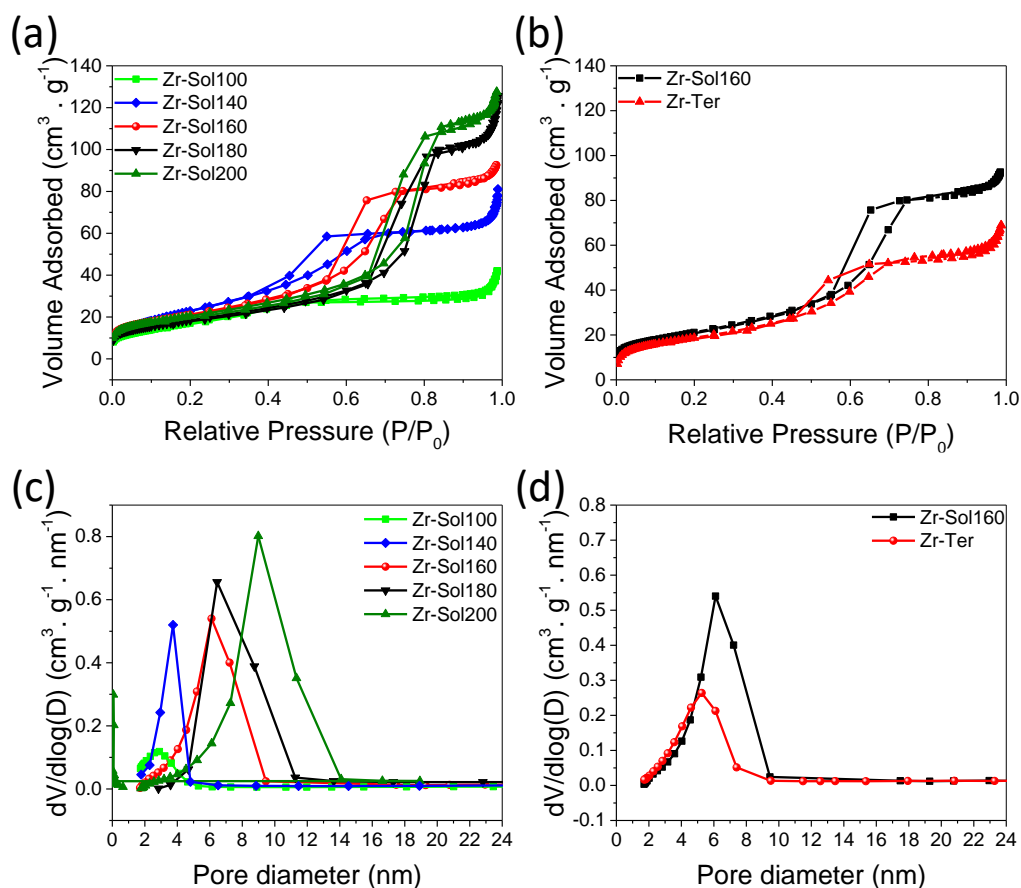


Figure 2-4. Nitrogen sorption isotherms (a), and pore size distributions (c) of zirconia samples prepared at various solvothermal temperatures. Nitrogen sorption isotherms (b), and pore size distributions (d) of Zr-Sol160 before and after (Zr-Ter) functionalization with Ter.

Table 2-2. Specific surface area ( $S_{\text{BET}}$ ) and pore diameter (PD) of the mesoporous zirconia prepared at various solvothermal temperatures, and Ter functionalized Zr-Sol160 (Zr-Ter).

Sample	$S_{\text{BET}}^{(a)}$ ( $\text{m}^2\text{g}^{-1}$ )	$PD^{(b)}$ (nm)
Zr-Sol100	61	2.9
Zr-Sol140	84	3.8
Zr-Sol160	75	6.1
Zr-Sol180	66	6.5
Zr-Sol200	68	9.0
Zr-Ter	67	5.2

- <sup>(a)</sup>  $S_{\text{BET}}$  = BET surface area obtained from adsorption data in the  $P/P_0$  range 0.05-0.20.
- <sup>(b)</sup> PD = pore diameter determined by using BJH model from the adsorption branch.

SEM and TEM were used to study the morphology of samples before and after Ter functionalization as displayed in Figure 2-5. The zirconia sample consisted of spherical particles with an average diameter between 300-400 nm (Fig. 4a and b), with the spherical shape of Zr-Sol160 being preserved after functionalization (Fig. 4d and e). High-resolution TEM (HRTEM) images show the presence of lattice fringes both before and after functionalization. The porous nature of the materials was also evident from TEM observation (Figure 2-5 e and f), which is in keeping with the nitrogen sorption results (Figure 2-4).

The preparation of mesoporous zirconia is widely described in the literature.<sup>17, 41-47</sup> It is well-known that as-prepared samples are amorphous and a transition to crystalline forms (tetragonal and monoclinic) is possible by calcination. The transition to the tetragonal phase normally happens at about 450 °C, while the transition to monoclinic phase begins at 600 °C and is completed at about 800 °C.<sup>45, 46</sup> Doping or incorporating other elements may change the crystal phase of zirconia too. For example, Freris et al. showed that doping zirconia with either  $\text{Eu}^{3+}$  or  $\text{Er}^{3+}$  ions can affect the phase composition of zirconia.<sup>48</sup> The crystal structure may also be affected by grafting



functional groups such as sulfate.<sup>3</sup> In this study the effect of solvothermal temperature on the XRD phase composition of the final zirconia samples, i.e. after calcination at 500 °C, was examined. The as-prepared zirconia samples were amorphous (data are not shown). The XRD patterns of all samples indicated that they

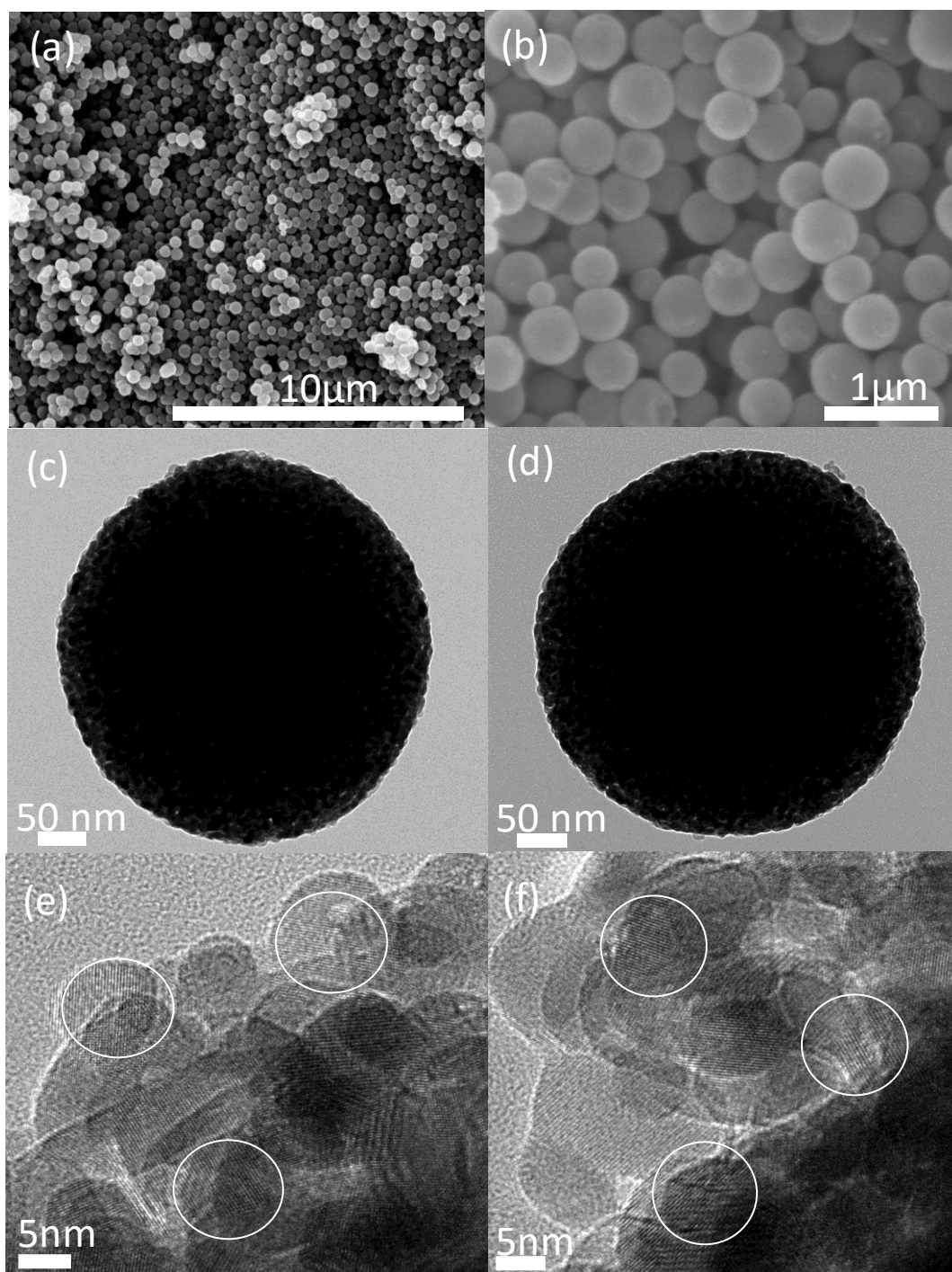


Figure 2-5. SEM (a, b) and TEM (c-f) images of Zr-Sol160-Cl500 before (a, c, e) and after (b, d, f) functionalization with Ter.

were composed of a mixture of tetragonal and monoclinic zirconia phases.<sup>49</sup> Quantitative Rietveld analysis established that solvothermal temperature affected the phase composition (Table 2-3). By increasing solvothermal temperature from 100 to 160 °C, monoclinic zirconia content increased from 33% to 61%, while the tetragonal

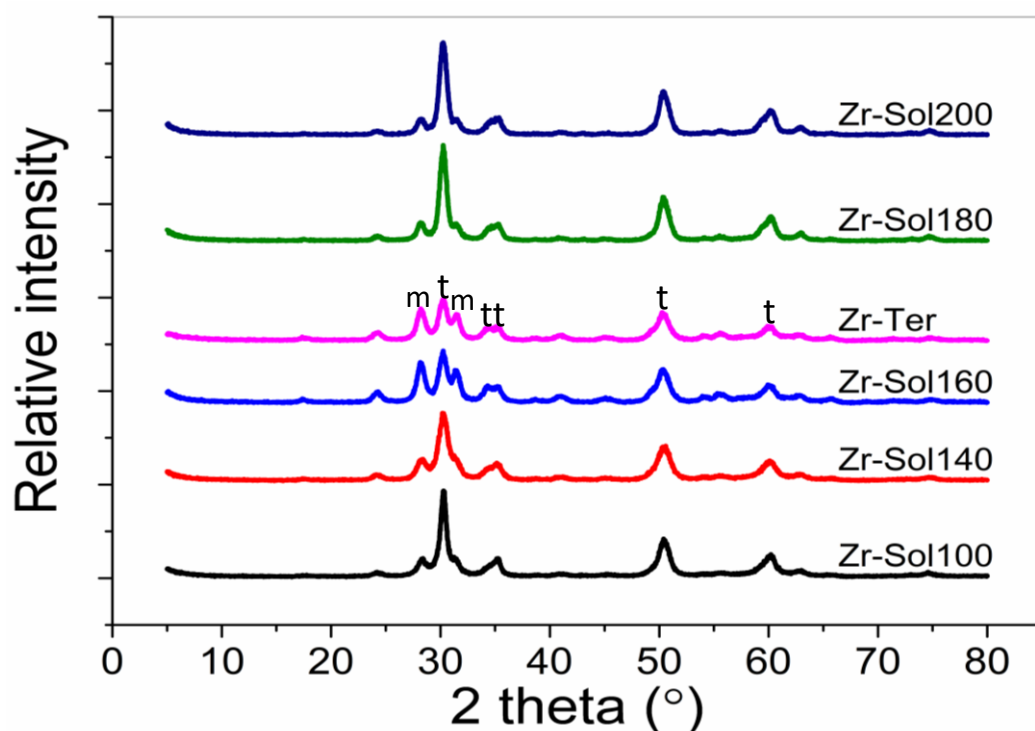


Figure 2-6. XRD patterns of zirconia samples prepared at various solvothermal temperatures, and Zr-Ter. Patterns were shifted upwards for clarity. The main peaks of the zirconia crystalline phases are marked as “m” and “t” for monoclinic and tetragonal, respectively.

Table 2-3. The percentage composition of the crystal phase of the zirconia samples prepared at different solvothermal temperatures.

Solvothermal temperature (°C)	Monoclinic phase	Tetragonal phase
100	33	67
140	39	61
160	61	39
180	26	74
200	23	77

content decreased by 28%. Interestingly, further increasing the solvothermal temperature to 200 °C caused the monoclinic content to decrease to just 23% (Table 2-3). Zirconia is an amphoteric metal oxide that can exhibit Lewis basicity and varying degrees of Lewis or Brønsted acidity depending on the crystalline phase. Monoclinic

zirconia is reported to show predominantly Lewis acidity.<sup>50-52</sup> Thus, surface acidity and crystal phase composition were tuned by the solvothermal temperature.<sup>3, 49</sup> Like Zr-Sol160, the XRD pattern of Zr-Ter also consisted of both tetragonal and monoclinic zirconia nanocrystals.<sup>49</sup> Therefore, the zirconia crystal structure was not altered after grafting Ter on the surface.

## 2.4. Catalytic study

The prepared catalyst, Zr-Ter, where the zirconia spheres were Zr-Sol160, was evaluated for the dehydration of fructose to 5-HMF. Zr-Ter was selected for its high surface area, mesoporous spherical structure, mesopore size, and high quantity of the acidic group grafted on its surface. Time, temperature, solvent and catalyst loading are all factors that can affect the yield of 5-HMF. The yield of 5-HMF was determined by HPLC-UV monitoring of the disappearance of fructose and a 5-HMF external standards curve.

### 2.4.1. Effect of time and temperature

Figure 2-7 a shows the effects of temperature and reaction time on the conversion of fructose to 5-HMF using 15 mg of Zr-Ter as the catalyst, and DMSO as the solvent. The yield of 5-HMF depended on both time and temperature, with higher temperatures and longer reaction times generally producing higher yields. The minimum temperature at which a meaningful yield of 5-HMF could be obtained was 130 °C, but only after 5 h of reaction. When the reaction time was kept steady at 1 h, a yield of 2 % was achieved at 120 °C, little more at both 130 and 140 °C, was enhanced dramatically to 32 % at 150 °C, but decreased to 26 % at 160 °C (Figure 2-7 a). Similar trends resulted when the reaction time was extended to 2 h, with a peak 5-HMF yield of 42 % at 150 °C, and then to 3 h, although this longer time was sufficient to produce a significant yield at 140 °C. When the reaction was prolonged to 5 h, approximately even yields were obtained from 130 to 160 °C. From these results it was concluded that 150 °C and 2 h are the optimum reaction temperature and time for the catalytic dehydration of fructose to 5-HMF on Zr-Ter. Higher temperatures and moderate reaction times can not only accelerate the conversion of fructose to the 5-HMF, but also side reactions. The most important side reaction is the polymerization of fructose

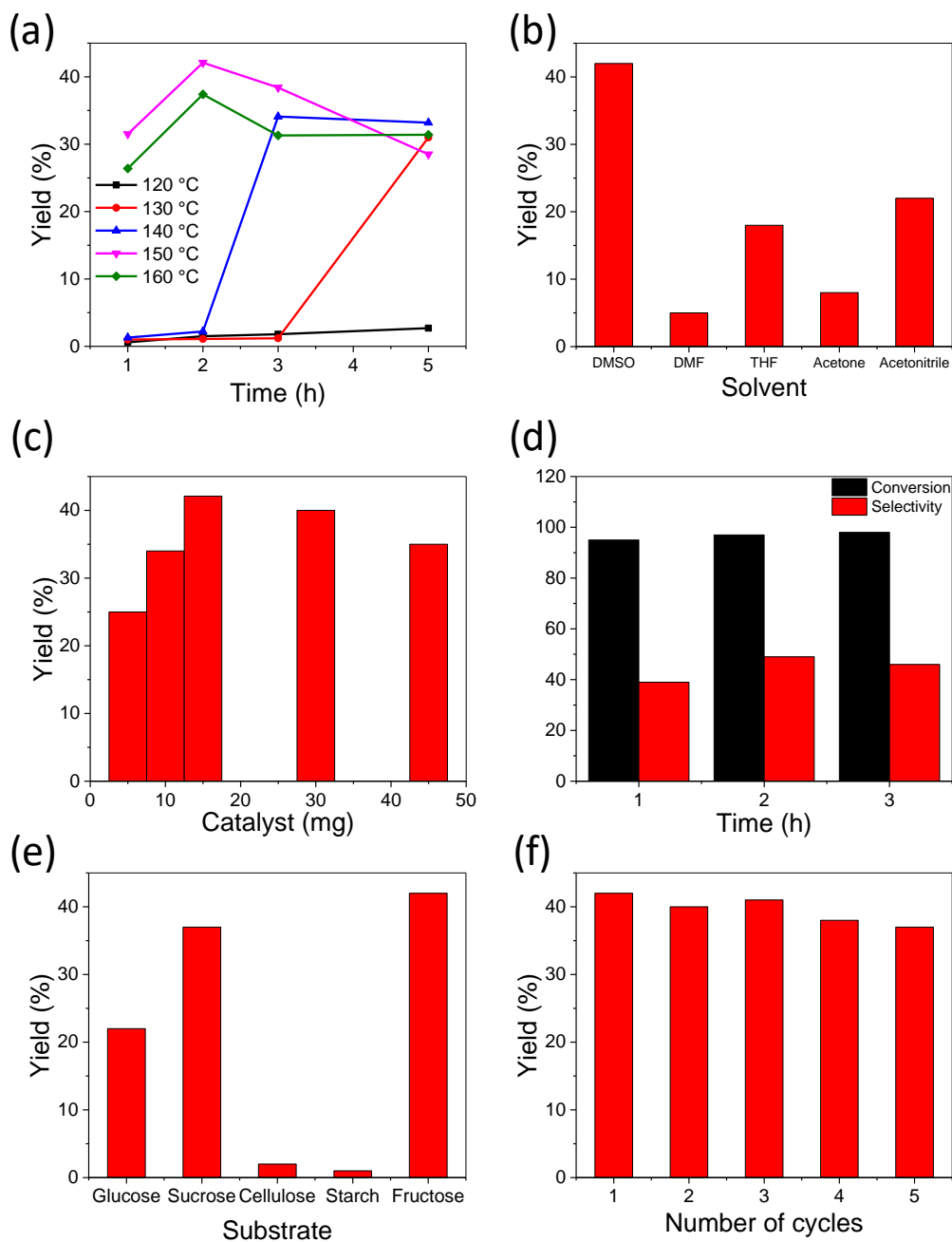


Figure 2-7. The effect of reaction temperature and time (a) on the yield of 5-HMF from the dehydration conversion of fructose in DMSO by Zr-Ter (15 mg). The effect of solvent (b) and catalyst amount (c) on the yield of 5-HMF. (d) Conversion of fructose and 5-HMF selectivity using 15 mg catalyst and fructose solution in DMSO at 150 °C. (e) The performance of catalyst on the conversion of various substrate solutions. (f) The reusability of the Zr-Ter catalyst in five consecutive runs (e). Unless the variable undergoing change, the amount of Zr-Ter was 15 mg, the solvent was DMSO, and the substrate was fructose.

and 5-HMF to humins, which were the major by-product in all catalytic tests in this work.<sup>53-55</sup>

#### 2.4.2. The effect of solvent and loading of the catalyst

There are several points that need to be considered for the effect of solvent on the conversion of fructose to 5-HMF. Water is a green and economical solvent; however, it can increase the rate of side reactions that convert 5-HMF to levulinic acid or formic acid.<sup>56, 57</sup> Thus, polar aprotic solvents should be used instead, for example, DMSO, DMF, THF, acetone or acetonitrile. Of these, DMSO is the most commonly used solvent for conversion of fructose to 5-HMF.<sup>57</sup> Ionic liquids are another option, but these are usually expensive, and the separation of the final product from the solvent is non-trivial.<sup>58</sup> In this study, the conversion of fructose to 5-HMF using 15 mg of Zr-Ter was carried out at 150 °C for 2 h in various polar aprotic solvents. The results of the conversion are shown in Figure 2-7 b. The best yield of 5-HMF was achieved with DMSO as the solvent. This could be due to limited conversion of 5-HMF to levulinic acid and formic acid, and high solubility and dispersity of fructose and Zr-Ter, respectively.

The influence of the quantity of Zr-Ter catalyst on the yield of 5-HMF after dehydration of fructose was also investigated. Various amounts of catalyst from 5 to 45 mg were utilized at the optimized conditions (i.e. 150 °C for 2 h in DMSO). As the amount of catalyst increases from 5 to 15 mg, the yield of 5-HMF increased due to the boost in the number of active sites of the catalyst available for reaction (Figure 2-7 c). However, increasing the quantity of catalyst to 30 mg had almost no change on the yield of 5-HMF, while the yield dropped by 7% after the catalyst was increased to 45 mg, which means the increased amount of catalyst had transformed fructose into undesirable products such as soluble polymers and humins instead of 5-HMF. Therefore, 15 mg of catalyst was considered optimum.

Finally, fructose conversion and 5-HMF selectivity were calculated to study the activity of the catalyst and results are shown in Figure 2-7 d. Conversion reached 95 % after 1 h of catalytic reaction and it increased to 98 % after 3 h of fructose dehydration under optimized condition (15 mg catalyst and fructose solution in DMSO at 150 °C) which considered a high conversion. However, the 5-HMF selectivity peaked after 2h at 49 %. It shows that the catalyst was very active for dehydration of fructose (98 % conversion), but it was accelerating side reactions that lead to humin production (49

% 5-HMF selectivity). As it was mentioned above, DMSO can prevent further dehydration of 5-HMF to levulinic and formic acids.<sup>49</sup>

#### 2.4.3. Conversion of other carbohydrate feedstocks to 5-HMF

Having optimized the catalytic reaction conditions, the conversion of other common carbohydrate feedstocks to 5-HMF was studied (Figure 2-7 e). The yield of 5-HMF from sucrose was 37 %, but when glucose was utilized as the substrate, only a 22 % yield was achieved. Glucose conversion to 5-HMF occurs in two steps: isomerization of glucose to fructose, which is a rate determining step, followed by conversion of fructose to 5-HMF.<sup>37, 55</sup> In order to achieve a high yield of 5-HMF, a base or Lewis acid acting as a catalyst is mandatory for the first step. An acid catalyst is then required for dehydration of fructose to the 5-HMF in the second step.<sup>55</sup> Since the surface of the zirconia is covered with functional groups, in this study, bound Ter molecules, a loss of Lewis acid sites likely resulted. This could explain the lower yield of 5-HMF from glucose compared to fructose or sucrose.<sup>3</sup> This may also explain the trace yields of 2 % and 1% obtained respectively using cellulose and starch as the substrate. Cellulose is a polysaccharide of beta-linked glucose molecules, whereas starch consists of various linear and branched glucose molecules linked via alpha linkages. Thus, bonds between the glucose molecules need to be broken before the glucose can even begin to react.

#### 2.4.4. Reusability of the catalyst

An essential factor in the development of a heterogenous catalyst for the dehydration of carbohydrates is reusability. The stability of the Zr-Ter catalyst was tested over 5 consecutive runs. The loss in 5-HMF yield was small, as shown in Figure 2-7 f. After each catalytic run the catalyst was separated by centrifuging, washed several times with water and ethanol, then dried in an oven at 60 °C overnight. The results would indicate that leaching of Ter during the catalysis process was limited. Therefore, catalytic activity was preserved over 5 cycles, showing the potential of the Zr-Ter catalyst as a reusable, active, solid-acid catalyst for biomass conversion.

## 2.5. Conclusion

Mesoporous spherical zirconia samples were prepared using sol-gel, templating, and solvothermal treatment with variation in pore size, surface area and crystal phase composition achieved by a change in the solvothermal temperature. Increasing the temperature from 100 to 200 °C, increased the pore size from 2.9 to 9.0 nm. The highest surface area of 84 m<sup>2</sup>g<sup>-1</sup> was achieved when the solvothermal temperature was 140 °C. All samples contained both tetragonal and monoclinic zirconia crystal phases with the highest percentage of monoclinic and tetragonal obtained at solvothermal temperatures of 160 and 200 °C, respectively. Possessing a surface area of 75 m<sup>2</sup>g<sup>-1</sup> and mesopore diameter of 6.1 nm, Zr-Sol160 was chosen for functionalization with various di-carboxylic acids and amino acids. The highest amount of grafting occurred with Ter (8.7 wt. %). Zr-Ter was studied for the acid catalysed dehydration conversion of d-fructose to 5-HMF. Reaction time, temperature, solvent and the amount of catalyst were optimized as 2 h, 150 °C, DMSO and 15 mg, respectively, for the highest yield of 42 % 5-HMF, fructose conversion 98 % and 5-HMF selectivity 49 %. Moreover, the Zr-Ter catalyst was shown to be reusable, with the 5-HMF yield decreasing slightly over 5 consecutive runs.

### 2.5.1. Comparing the catalytic performance of Zr-Ter with other catalysts

As mentioned in section 1.9, it is necessary to modify the surface of zirconia in order to increase the strength of the surface acidity. In this chapter, dicarboxylic acids were used to introduce acidic groups on the surface of zirconia. Based on the catalytic results, three major inferences can be drawn:

First, Zr-Ter appears active for the dehydration of fructose, glucose and sucrose to 5-HMF, but even under optimized conditions, the highest yield of 5-HMF was only 42% when fructose was used as the substrate. However, this yield is not high compared to other catalysts and research. For example, Wang et al. prepared high surface area Sn-based catalysts, SnO<sub>2</sub>-ZrO<sub>2</sub> and SO<sub>4</sub><sup>2-</sup>/SnO<sub>2</sub>-ZrO<sub>2</sub>, for the dehydration of hexose to 5-HMF.<sup>59</sup> After grafting sulfate, and under optimized conditions, a 75% yield of 5-HMF was obtained from a fructose solution in DMSO at 120 °C after 2.5 h. <sup>59</sup> In another report, SO<sub>4</sub><sup>2-</sup>/ZrO<sub>2</sub>-Al<sub>2</sub>O<sub>3</sub> with various Zr:Al mole ratios of 9:1, 7:3, 1:1, 3:7 and 1:9 were prepared for the conversion of glucose to 5-HMF by Yan et. al.<sup>7</sup> A 47% yield of 5-HMF

was obtained from glucose solution in DMSO at 130 °C after 4 h. The yield of 5-HMF was even higher (67%) when fructose was used as the substrate.<sup>7</sup> Thus, it would seem that using sulfate as a functional group is more effective than carboxylate.

The second inference is that a high surface area is an important factor for catalytic performance, since the number of functional group molecules that can be attached on the surface is dependent on it. The highest surface area of a zirconia sample in this chapter was for Zr-Sol140 (84 m<sup>2</sup>g<sup>-1</sup>), while that of Zr-Ter was lower (67 m<sup>2</sup>g<sup>-1</sup>). As mentioned above, the catalytic performance of SO<sub>4</sub><sup>2-</sup>/SnO<sub>2</sub>-ZrO<sub>2</sub> was better than both Zr-Ter (this thesis) and SO<sub>4</sub><sup>2-</sup>/ZrO<sub>2</sub>-Al<sub>2</sub>O<sub>3</sub>. This enhanced performance was due to the higher surface area (392 m<sup>2</sup>g<sup>-1</sup>) and using sulfate group as functional group. By contrast, the highest surface area of a SO<sub>4</sub><sup>2-</sup>/ZrO<sub>2</sub>-Al<sub>2</sub>O<sub>3</sub> catalyst (28 m<sup>2</sup>g<sup>-1</sup>) was much lower than the surface areas of both Zr-Sol140 and Zr-Ter, although the catalytic performance of SO<sub>4</sub><sup>2-</sup>/ZrO<sub>2</sub>-Al<sub>2</sub>O<sub>3</sub> was better than Zr-Ter due to grafted sulfate.

The third inference is that an alternative strategy could be used for introducing acidic groups, such as grafting phosphate on the surface of the catalyst (refer to section 1.9). For instance, Asghari and Yoshida prepared zirconium phosphate as a solid acid catalyst for dehydration of fructose to 5-HMF.<sup>60</sup> After optimizing conditions, a 50% yield was achieved, but it should be noted that the surface area of the catalyst was 38 m<sup>2</sup>g<sup>-1</sup>, lower than Zr-Ter.<sup>60</sup> Xu et al. reported the dehydration of fructose to 5-HMF by mesoporous zirconium phosphate.<sup>61</sup> Under optimal conditions, the yield of 5-HMF from fructose solution in DMSO was 69% at 140 °C after 2 h.<sup>61</sup> The surface area of this catalyst was 169 m<sup>2</sup>g<sup>-1</sup>. Hence, a zirconia surface grafted with phosphate seems more effective than carboxylate.

Therefore, the focus for the next two chapters will be on increasing surface area and replacing the carboxylate group with phosphate (chapter 3) and sulfate (chapter4).



## 2.6. References

1. T. Wang, M. W. Nolte and B. H. Shanks, *Green Chemistry*, 2014, **16**, 548-572.
2. D. M. Alonso, J. Q. Bond and J. A. Dumesic, *Green Chemistry*, 2011, **13**, 754-793.
3. A. Osatiashtiani, A. F. Lee, D. R. Brown, J. A. Melero, G. Morales and K. Wilson, *Catalysis Science & Technology*, 2014, **4**, 333-342.
4. N. Wang, Y. Yao, W. Li, Y. Yang, Z. Song, W. Liu, H. Wang, X.-F. Xia and H. Gao, *RSC Advances*, 2014, **4**, 57164-57172.
5. J. L. Roper-Vega, A. Aldana-Pérez, R. Gómez and M. E. Niño-Gómez, *Applied Catalysis A: General*, 2010, **379**, 24-29.
6. J. Navarrete, T. Lopez, R. Gomez and F. Figueras, *Langmuir*, 1996, **12**, 4385-4390.
7. H. Yan, Y. Yang, D. Tong, X. Xiang and C. Hu, *Catalysis Communications*, 2009, **10**, 1558-1563.
8. G. X. Yu, X. L. Zhou, F. Liu, C. L. Li, L. F. Chen and J. A. Wang, *Catalysis Today*, 2009, **148**, 70-74.
9. T. Y. Kim, D. S. Park, Y. Choi, J. Baek, J. R. Park and J. Yi, *Journal of Materials Chemistry*, 2012, **22**, 10021-10028.
10. Z. Wang, Q. Lu, X.-F. Zhu and Y. Zhang, *ChemSusChem*, 2011, **4**, 79-84.
11. S. K. Das and S. A. El-Safty, *ChemCatChem*, 2013, **5**, 3050-3059.
12. M. H. Sui and L. She, *Frontiers of Environmental Science & Engineering*, 2013, **7**, 795-802.
13. S. Tang, X. Huang, X. Chen and N. Zheng, *Advanced Functional Materials*, 2010, **20**, 2442-2447.
14. M. Hino and K. Arata, *Journal of the Chemical Society, Chemical Communications*, 1979, DOI: 10.1039/C39790001148, 1148-1149.
15. M. Hino, S. Kobayashi and K. Arata, *Journal of the American Chemical Society*, 1979, **101**, 6439-6441.
16. M. Hino and K. Arata, *Journal of the Chemical Society, Chemical Communications*, 1980, DOI: 10.1039/C39800000851, 851-852.
17. R. Srinivasan, T. Watkins, C. Hubbard and B. H. Davis, *Chemistry of Materials*, 1995, **7**, 725-730.
18. Y. Jiang, S. Yang, X. Ding, Y. Guo, H. Bala, J. Zhao, K. Yu and Z. Wang, *Journal of Materials Chemistry*, 2005, **15**, 2041-2046.
19. W. Li, F. Ma, F. Su, L. Ma, S. Zhang and Y. Guo, *ChemCatChem*, 2012, **4**, 1798-1807.
20. X. Song and A. Sayari, *Catalysis Reviews*, 1996, **38**, 329-412.
21. B. M. Reddy and M. K. Patil, *Chemical Reviews*, 2009, **109**, 2185-2208.
22. G. D. Yadav and J. J. Nair, *Microporous and Mesoporous Materials*, 1999, **33**, 1-48.
23. Y. T. Tao, *Journal of the American Chemical Society*, 1993, **115**, 4350-4358.
24. A. Corma, *Chemical Reviews*, 1995, **95**, 559-614.
25. J. P. Folkers, C. B. Gorman, P. E. Laibinis, S. Buchholz, G. M. Whitesides and R. G. Nuzzo, *Langmuir*, 1995, **11**, 813-824.
26. G. A. Buckholtz and E. S. Gawalt, *Materials*, 2012, **5**, 1206.

27. A. Raman, R. Quiñones, L. Barriger, R. Eastman, A. Parsi and E. S. Gawalt, *Langmuir*, 2010, **26**, 1747-1754.
28. I. V. Chernyshova, S. Ponnurangam and P. Somasundaran, *Langmuir*, 2011, **27**, 10007-10018.
29. S. Ponnurangam, I. V. Chernyshova and P. Somasundaran, *Langmuir*, 2012, **28**, 10661-10671.
30. K. Norén and P. Persson, *Geochimica et Cosmochimica Acta*, 2007, **71**, 5717-5730.
31. K. D. Dobson and A. J. McQuillan, *Spectrochimica Acta Part A: Molecular and Biomolecular Spectroscopy*, 2000, **56**, 557-565.
32. V. Zeleňák, Z. Vargová and K. Györyová, *Spectrochimica Acta Part A: Molecular and Biomolecular Spectroscopy*, 2007, **66**, 262-272.
33. P.-F. Guo, H.-B. Liu, X. Liu, H.-F. Li, W.-Y. Huang and S.-J. Xiao, *The Journal of Physical Chemistry C*, 2010, **114**, 333-341.
34. S. Eiden-Assmann, J. Widoniak and G. Maret, *Chemistry of Materials*, 2004, **16**, 6-11.
35. A. Parril, *Michigan State University Department of Chemistry*, 1997, 1-2.
36. K. D. Dobson and A. J. McQuillan, *Spectrochimica Acta Part A: Molecular and Biomolecular Spectroscopy*, 1999, **55**, 1395-1405.
37. Q. Yang, M. Sherbahn and T. Runge, *ACS Sustainable Chemistry & Engineering*, 2016, **4**, 3526-3534.
38. H. M. Mirzaei and B. Karimi, *Green Chemistry*, 2016, **18**, 2282-2286.
39. N. Balachander and C. N. Sukenik, *Langmuir*, 1990, **6**, 1621-1627.
40. S. Tunesi and M. A. Anderson, *Langmuir*, 1992, **8**, 487-495.
41. P. Behrens, *Angewandte Chemie International Edition in English*, 1996, **35**, 515-518.
42. G. Pacheco, E. Zhao, A. Garcia, A. Sklyarov and J. J. Fripiat, *Chemical Communications*, 1997, DOI: 10.1039/A607438C, 491-492.
43. P. Yang, D. Zhao, D. I. Margolese, B. F. Chmelka and G. D. Stucky, *Nature*, 1998, **396**, 152.
44. U. Ciesla, M. Fröba, G. Stucky and F. Schüth, *Chemistry of Materials*, 1999, **11**, 227-234.
45. J. Widoniak, S. Eiden-Assmann and G. Maret, *European Journal of Inorganic Chemistry*, 2005, **2005**, 3149-3155.
46. J.-H. Smått, N. Schüwer, M. Järn, W. Lindner and M. Lindén, *Microporous and Mesoporous Materials*, 2008, **112**, 308-318.
47. G. Sponchia, E. Ambrosi, F. Rizzolio, M. Hadla, A. D. Tedesco, C. R. Spina, G. Toffoli, P. Riello and A. Benedetti, *Journal of Materials Chemistry B*, 2015, **3**, 7300-7306.
48. I. Freris, P. Riello, F. Enrichi, D. Cristofori and A. Benedetti, *Optical Materials*, 2011, **33**, 1745-1752.
49. J. B. Joo, A. Vu, Q. Zhang, M. Dahl, M. Gu, F. Zaera and Y. Yin, *ChemSusChem*, 2013, **6**, 2001-2008.
50. W. Hertl, *Langmuir*, 1989, **5**, 96-100.
51. V. Bolis, C. Morterra, M. Volante, L. Orto and B. Fubini, *Langmuir*, 1990, **6**, 695-701.

52. V. Bolis, G. Cerrato, G. Magnacca and C. Morterra, *Thermochimica Acta*, 1998, **312**, 63-77.
53. K.-i. Shimizu, R. Uozumi and A. Satsuma, *Catalysis Communications*, 2009, **10**, 1849-1853.
54. S. Pujari, L. Pujari, A. T. M. Scheres, H. Marcelis and Zuilhof, *Angewandte Chemie (International ed.)*, 2014, **53**, 6322-6356.
55. L. Wang, H. Wang, F. Liu, A. Zheng, J. Zhang, Q. Sun, J. P. Lewis, L. Zhu, X. Meng and F.-S. Xiao, *ChemSusChem*, 2014, **7**, 402-406.
56. A. Najafi Chermahini, F. Shahangi, H. A. Dabbagh and M. Saraji, *RSC Advances*, 2016, **6**, 33804-33810.
57. X. Zheng, X. Gu, Y. Ren, Z. Zhi and X. Lu, *Biofuels, Bioproducts and Biorefining*, 2016, **10**, 917-931.
58. M. E. Zakrzewska, E. Bogel-Łukasik and R. Bogel-Łukasik, *Chemical Reviews*, 2011, **111**, 397-417.
59. Y. Wang, X. Tong, Y. Yan, S. Xue and Y. Zhang, *Catalysis Communications*, 2014, **50**, 38-43.
60. F. S. Asghari and H. Yoshida, *Carbohydrate Research*, 2006, **341**, 2379-2387.
61. H. Xu, Z. Miao, H. Zhao, J. Yang, J. Zhao, H. Song, N. Liang and L. Chou, *Fuel*, 2015, **145**, 234-240.



## Chapter 3. Phosphate-modified mesoporous zirconium titanium oxide for 5-HMF production from carbohydrates

### 3.1. Introduction

Biomass is produced from carbon dioxide and water during the process of photosynthesis. The primary products are monosaccharides (C<sub>5</sub> and C<sub>6</sub> sugars) and further progressing generates polymerized molecules such as cellulose and cross-linked polymers (lignin). Therefore, biomass can be considered as a source of carbohydrates that can be converted into potentially useful substances. Consequently, biomass has been heavily researched in recent years as a sustainable substrate that can be transformed to a variety of valuable and fine chemicals.<sup>1-5</sup> Glucose and fructose are the main monosaccharides found in biomass that can be utilized to produce biodiesel. In order to make the process of conversion of biomass to biofuel profitable, recent efforts have been focused on converting biomass to platform molecules (i.e. building block chemicals), which can subsequently be used for the production of various chemicals. One such platform molecule is 5-hydroxymethylfurfural (5-HMF), which is a strategic and valuable compound that can serve as a precursor to numerous products and chemical intermediates related to fuel, polymers, and pharmaceuticals.<sup>4,6-8</sup>

It is well known that 5-HMF can be obtained by acid catalyzed dehydration of carbohydrates. In most cases researchers have focused on the conversion of fructose to 5-HMF as a model reaction, since it is simple to run, and side reaction can be avoided.<sup>9-12</sup> Various heterogenous catalyst have been reported, for example, ion exchange resins<sup>13</sup>, phosphates<sup>14</sup>, heteropolyacids<sup>15</sup>, metal oxides (e.g. zirconia and titania)<sup>16,17</sup> and metal binary oxides ( For more information please refer to the chapter 1 section 1.7 and 1.8).<sup>18-21</sup>

The performance of a catalyst depends on its surface morphology and chemistry, including surface area, pore size and functional groups. Therefore, a rationally designed catalyst can enhance the number of active sites, which may lead to higher performance of the catalyst and better yield of the product.<sup>15</sup>

Various methods have been applied to functionalize the surfaces of materials, for example dip-coating, spin-coating, self-assembled monolayers, layer-by-layer assembly, vapor deposition, Langmuir–Blodgett deposition and plasma treatment,<sup>3,22,23</sup> for applications ranging from electronic to medical devices.<sup>22, 24, 25</sup> Based on the chemistry of the surface to be modified, different functional groups and modifiers can be employed.<sup>5, 23</sup> In the catalysis industry, long-term stability and reusability are two important factors that need to be considered, consequently strong covalent bonds are preferred over polymer coating or physisorption achieved by layer by layer coating. Among strongly covalent bonding functional groups, phosphonic acid (PA) is considered a powerful compound to modify metal oxide surfaces due to the formation of P-O-metal covalent bonds that present highly stable architectures, particularly for metal cations in high oxidation states.<sup>22, 26</sup> PA, phosphonate and its derivatives have been applied in different application such as anticorrosion surfaces, organic electronics, optical devices, optoelectronics, biosensors and catalysis.<sup>22, 24, 25, 27-31</sup>

PA, with general formula  $RPO_3H_2$  (where R is an organic group), can react with a wide variety of metal oxides. This reaction may proceed via an acid-base reaction, where the acidic OH groups of PA react with basic metal oxides to form strong P-O-M bonds.<sup>24, 26</sup> Consequently, phosphonate functionalised metal oxides have been used both in academia and industry in different applications. The advantage of PA over phosphonate derivatives is its solubility in water; however, it is feasible to use a phosphonate ester when the metal oxides are stable and non-soluble in water.<sup>22, 32</sup> Various methods have been used to graft PA on the surface of metal oxides.<sup>22</sup> In general, immersion-based surface modification works well and is reproducible on most of metal oxide surfaces. In almost all cases the number of hydroxyl groups on the surface is the key parameter. For instance, Giza et al. applied a water plasma prior surface modification to increase the number of hydroxy group on the surface of

aluminium oxide. As a result, the quantity of octadecyl phosphonic acid grafted was increased.<sup>33</sup>

In this work (As it was mentioned at the end of chapter 2 section 2.5.1.), mesoporous titanium zirconium oxide (TZ) spheres with surface areas of up to 420 m<sup>2</sup>/g were prepared via sol-gel chemistry and templating. Various Ti:Zr ratios, solvothermal and calcination temperatures were used to find the sample exhibiting optimal high surface area, mesopore size and a high quantity of surface hydroxyl groups. This best sample was modified with nitrilotri(methylphosphonic acid) (NPA) to prepare a solid acid catalyst. The functionalized compound was applied as a solid acid catalyst for the conversion of fructose to 5-HMF as a model reaction. Reaction time, temperature, solvent, and the amount of catalyst used were first optimized, then the catalyst was utilized for the conversion of other carbohydrates to 5-HMF. The reusability of the catalyst was also investigated. The featured characteristics of the NPA-functionalized TZ samples were high surface area with an open framework for catalytic chemical reaction, strong attachment of the functional group on the TZ sphere surface that made the catalyst highly reusable, well-maintained structural integrity, good dispersity in polar solvents and a strong acidic surface.

## 3.2. Experimental Section

### 3.2.1. Materials

Titanium(IV) isopropoxide (TIP, 97%), zirconium(IV) propoxide (ZrP, 70% in 1-propanol), hexadecylamine (HDA, 90%), D-Fructose (> 99%), glucose (> 99%), sucrose (> 99%), cellulose, starch, nitrilotri(methylphosphonic acid) (NPA), potassium chloride (AR) and dimethyl sulfoxide (DMSO, HPLC grade) were obtained from Sigma–Aldrich. Absolute ethanol (> 99.7%), tetrahydrofuran (THF), dimethylformamide (DMF), ammonia solution (28%), methanol, acetonitrile and acetone were from Merck. Milli-Q water was collected from a Millipore academic purification system with a resistivity higher than 18.2 MΩ cm. All chemicals and solvents were used as received.

### 3.2.2. Catalyst preparation

Spheres preparation: A sol-gel self-assembly process was used to prepare nonporous, mixed metal oxide precursor spheres using HDA as a structure directing agent,<sup>34</sup> and Ti to Zr atomic ratios of 7:3 (TZ30), 5:5 (TZ50), and 3:7 (TZ70). In a typical synthesis (TZ30), 7.95 g HDA was dissolved in 800 mL ethanol, followed by the addition of 3.2 mL aqueous KCl solution (0.1 M) and 5.44 mL water. Next, a mixture of 12.89 mL TIP and 7.96 mL ZrP was added under vigorous stirring for 1 min. The resulting milky white precursor suspension was kept static at room temperature for 18 h. The spheres were separated by centrifugation (Beckman Coulter Allegra 25R, 6000 rpm for 15 min) and washed with ethanol three times. Finally, the as-prepared sample was dried in a fume cupboard at ambient temperature for six days.

Solvothermal treatment and calcination: A solvothermal process was conducted on the amorphous nanospheres at different temperatures in the range 140-200 °C. In a typical procedure, 1.6 g of precursor spheres were dispersed in a mixed solution of 20 mL ethanol and 10 mL water, to which various amounts of ammonia solution (28%) (0, 0.5 and 1.0 mL) were added. The resulting mixture was sealed within a 50 mL Teflon-lined steel autoclave and heated at the selected temperature for 16 h in a Labec fan-forced oven. The products were separated by centrifugation, washed with ethanol three times and dried in an oven at 50 °C overnight. Finally, the dried TZ samples were calcined at 500, 600 or 700 °C (ramp rate of 1.6 °C min<sup>-1</sup>) for 2 h in air to obtain mesoporous TZ samples. The samples were labelled as TZ<sub>x</sub>-Solvo<sub>z</sub>-Clv, where *x*, *z* and *v* stand for the percentage of Zr in precursor solution, solvothermal and calcination temperatures, respectively. For instance, TZ30-Solvo180-Cl500 indicates mesoporous spheres prepared with 30% Zr (i.e. 7:3 Ti:Zr), solvothermal treatment at 180 °C and calcination at 500 °C. The TZ samples that underwent solvothermal treatment with ammonia were labelled with an "A" at the end of the name.

#### Functionalization of TZ30-Solvo160-Cl500

The surface of TZ30-Solvo160-Cl500 was functionalised with NPA to prepare a solid-acid catalyst. 1.56 mmol of NPA was dissolved in 10 mL of water, then 0.1 g of TZ30-



Solvo160-Cl500 spheres were added, sonicated for 10 min in an ultrasonic bath, followed by stirring overnight at ambient temperature. The functionalized spheres were collected by centrifugation (Beckman Coulter Allegra 25R, 6000 rpm for 15 min), washed several times with water and once with ethanol, then dried in an oven at 120 °C overnight.

### 3.2.3. Characterization

Scanning electron microscopy (SEM) using a field emission environmental scanning electron microscope (Quanta 200F FEI) with an accelerating voltage of 15 kV under low vacuum mode was used to investigate the morphology and particle size of the samples. Transmission electron microscopy (TEM) images were obtained on a transmission electron microscope (FEI Tecnai F20) operating at 200 kV. Powder X-ray diffraction (XRD; Bruker D8 Advance Diffractometer with Cu K $\alpha$  radiation) was used to determine the crystal phase of the products. The diffractometer was set at a 40 kV working voltage and 40 mA working current, with samples scanned from 5 to 80° in 2 $\theta$  at a step size of 0.02° and a scan-step time of 4 s. Thermogravimetric analysis (TGA) was conducted on a Mettler Toledo TGA/SDTA 851<sup>e</sup> Thermal Gravimetric analyzer with a heating ramp of 10 °C min<sup>-1</sup> under 30 mL min<sup>-1</sup> flowing nitrogen. Nitrogen gas sorption isotherms were measured at -196 °C using a Micromeritics Tristar 3000 Surface Area and Porosity Analyzer. Before measurement, calcined samples were degassed at 120 °C for 18 h on a vacuum line. The specific surface area was calculated by a standard multipoint Brunauer-Emmett-Teller (BET) method using the adsorption data in the P/P<sub>0</sub> range from 0.05 to 0.20. The Barrett-Joyner-Halenda (BJH) model was applied to the adsorption branch of the isotherm to determine pore size distributions. A Perkin Elmer IR Spectrum ASCII PEDS 1.60 FT-IR Spectrometer was employed to obtain Fourier transform infrared (FT-IR) spectra.

### 3.2.4. Catalytic activity test

The catalytic activity was tested by the dehydration of fructose to 5-HMF. Typically, 15 mg catalyst was added to a solution of fructose dissolved in DMSO (10 mL, 1.67 mM), then well-dispersed by ultrasonication for 5 min. The catalytic reaction was performed under stirring (800 rpm) in a 25 mL round-bottom flask in an oil bath at

temperatures of 120-170 °C for 1, 2 or 3 h. Following the reaction, the flask was cooled to room temperature, and the final products were separated from the catalyst by centrifugation. The products were examined using reverse phase preparatory high performance liquid chromatography (HPLC) on an Agilent 1200 series HPLC system. Fructose disappearance was monitored by a UV detector ( $\lambda = 285 \text{ nm}$ ) attached to an Eclipse Plus C18 column (150 mm x 2.1 mm x 5  $\mu\text{m}$ ), using an 88:12 water:methanol (v/v) gradient at a flow rate of 0.25 mL min<sup>-1</sup>. It was assumed that the volume changes were negligible after the dehydration reaction for all experiments. The 5-HMF yield was calculated as moles of 5-HMF produced based on a 5-HMF external standards curve. Variations in experiments using different solvents (acetonitrile, THF, ethanol, acetone and DMF), amounts of catalyst (5, 10, 30 and 45 mg) or the carbohydrate (glucose, sucrose, cellulose and starch) followed the same procedure. The mass spectroscopy (MS) analyses were performed using an Agilent 6500 Q-TOF LC/MS system in negative ion mode to calculate fructose conversion and 5-HMF selectivity. The 5-HMF yield, fructose conversion, and 5-HMF selectivity were calculated based on Equations 1- 3 in section 2.2.5.

Catalyst reusability tests: After each catalytic cycle (160 °C for 2 h), the catalyst (30 mg) was separated by centrifugation, washed thoroughly with ethanol and dried in an oven at 120 °C overnight. The fructose dehydration reaction was repeated with fresh substrate and solvent.

### 3.3. Results and discussion

The accessibility of catalytic sites in a mesoporous metal oxide is determined by pore size and pore morphology, which is important for functional group modification and catalytic chemical reactions in applications. Nitrogen sorption was carried out to study the textural properties of the TZ samples, and sorption isotherms (Figure 3-1), pore size distributions (Figure 3-2), and BET surface areas and the pore diameter distributions (Table 3-1) were obtained. Chen et al. reported mixing various amounts of ZrP and TIP can produce amorphous mesoporous TZ spherical particles with different surface areas, and that by increasing the percentage of ZrP from 30 to 70% the surface area of the final TZ particles decreased.<sup>34</sup> It was also reported that introducing ZrP as precursor with TIP at the first step of preparing spherical TZ

particles retarded crystallization of amorphous  $\text{TiO}_2$  to the anatase phase due to the substitution of  $\text{Ti}^{4+}$  ions by  $\text{Zr}^{4+}$ .<sup>34</sup> In this study, when the solvothermal and calcination temperatures were kept constant at 140 °C and 500 °C, respectively, the same results were obtained for various ZrP quantities (30, 50 or 70 %), and the TZ sample with a Ti:Zr atomic ratio of 7:3 (i.e. TZ30) was selected for further investigation due to having the highest surface area of  $420 \text{ m}^2\text{g}^{-1}$  and slightly larger pore diameter of 3.3 nm (Figure 3-1 a, Figure 3-2 a and Table 3-1). Further investigation was carried out on other factors such as the addition of ammonia to the solvothermal solution, solvothermal and calcination temperatures during the preparation of the TZ30 sample to gain more control over the textural properties of the TZ particles, and to optimize surface area, pore size and surface OH density.

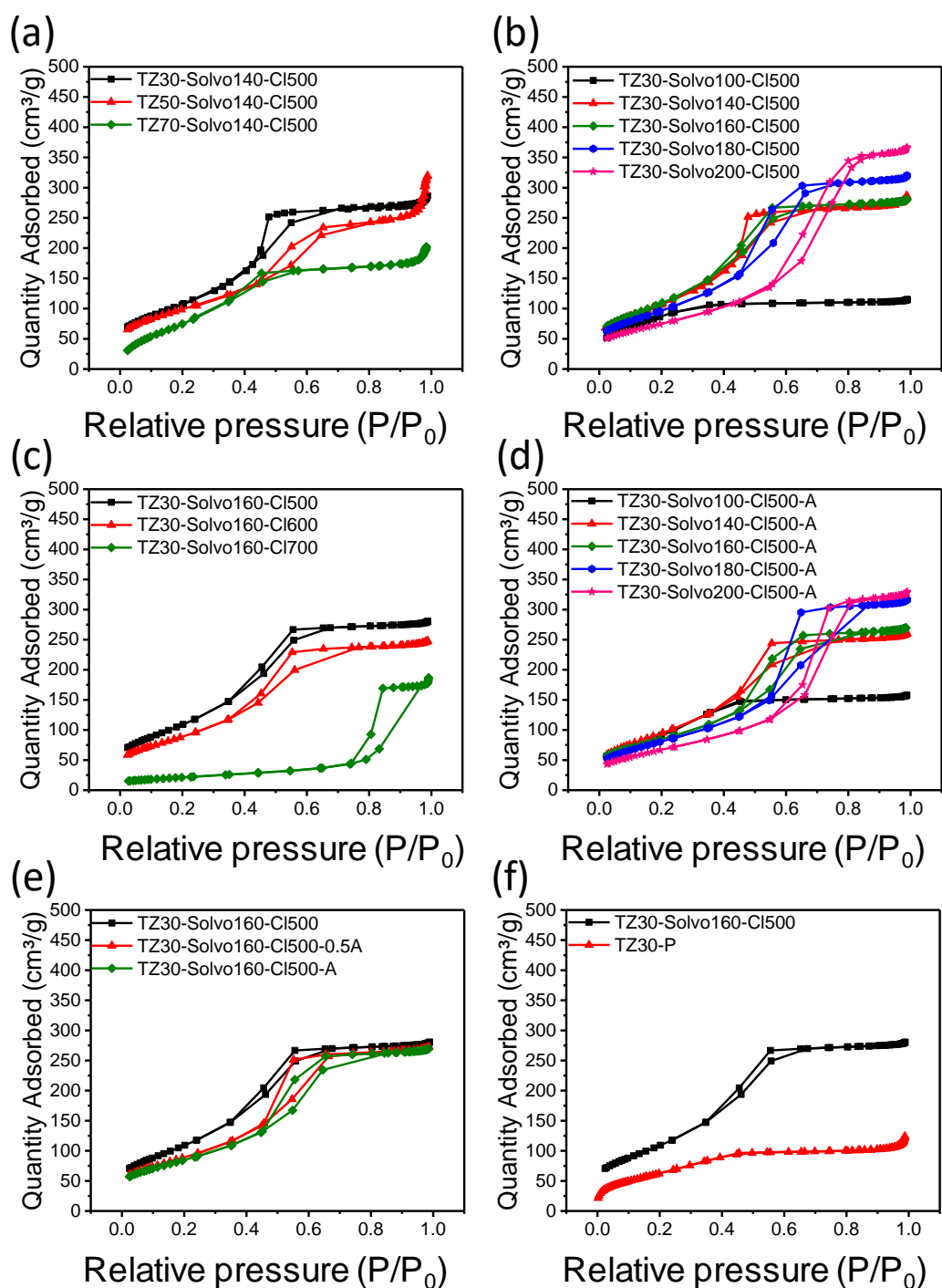


Figure 3-1. Nitrogen sorption isotherms: (a) TZx-Solvo140-Cl500 samples with various Zr quantities. The effect of (b) solvothermal temperature and (c) calcination temperature on TZ30-Solvoc-Clv samples. (d) The effect of solvothermal temperature on TZ30-Solvoc-Cl500 samples with the addition of 1 mL ammonia during solvothermal treatment and (e) the effect of ammonia (0, 0.5 and 1.0 mL) during solvothermal treatment. (f) TZ30-Sol160-Cl500 and after functionalization with NPA (TZ30-P).

All the obtained nitrogen sorption curves in Figure 3-1 can be classified as Type IV isotherms, which are commonly observed in mesostructured materials. For TZ30-Solvoz-CI500 samples, when the solvothermal temperature was increased from 100 to 140 °C the surface area of the TZ samples increased from 318 to 420 m<sup>2</sup>g<sup>-1</sup> (Table 3-1); however, further increases of the solvothermal temperature to 200 °C reduced the surface area of the TZ30 particles to just 268 m<sup>2</sup>/g. In contrast, increasing the solvothermal temperature from 100 to 200 °C enlarged the mesopore size from 1.9 to 6.4 nm (Figure 3-2 b and Table 3-1).

Table 3-1. The effects of Zr percentage, solvothermal temperature, calcination temperature, ammonia treatment, and NPA functionalization on the specific surface area ( $S_{\text{BET}}$ ), pore diameter (PD), OH amount, and surface OH density.

Sample	$S_{\text{BET}}^{(a)}$ (m <sup>2</sup> /g)	PD <sup>(b)</sup> [nm]	OH amount [mmol/g]	OH density [#/nm <sup>2</sup> ]
TZ30-Solvo100-CI500	318	2.9	2.7	5.1
TZ30-Solvo140-CI500	420	3.3	3.3	4.8
TZ30-Solvo160-CI500	380	3.8	3.3	5.1
TZ30-Solvo180-CI500	347	4.9	3.1	5.4
TZ30-Solvo200-CI500	268	6.4	2.4	5.5
TZ30-Solvo160-CI500- 0.5A	340	4.1	2.7	5.2
TZ30-Solvo100-CI500-A	330	2.3	2.8	5.2
TZ30-Solvo140-CI500-A	343	3.7	2.9	5.1
TZ30-Solvo160-CI500-A	303	4.8	2.8	5.5
TZ30-Solvo180-CI500-A	291	5.7	2.5	5.2
TZ30-Solvo200-CI500-A	242	6.6	2.0	5.1
TZ30-Solvo160-CI600	318	5.2	2.7	5.1
TZ30-Solvo160-CI700	76	10.7	0.75	6.0
TZ30-P	227	2.3	N/A	N/A

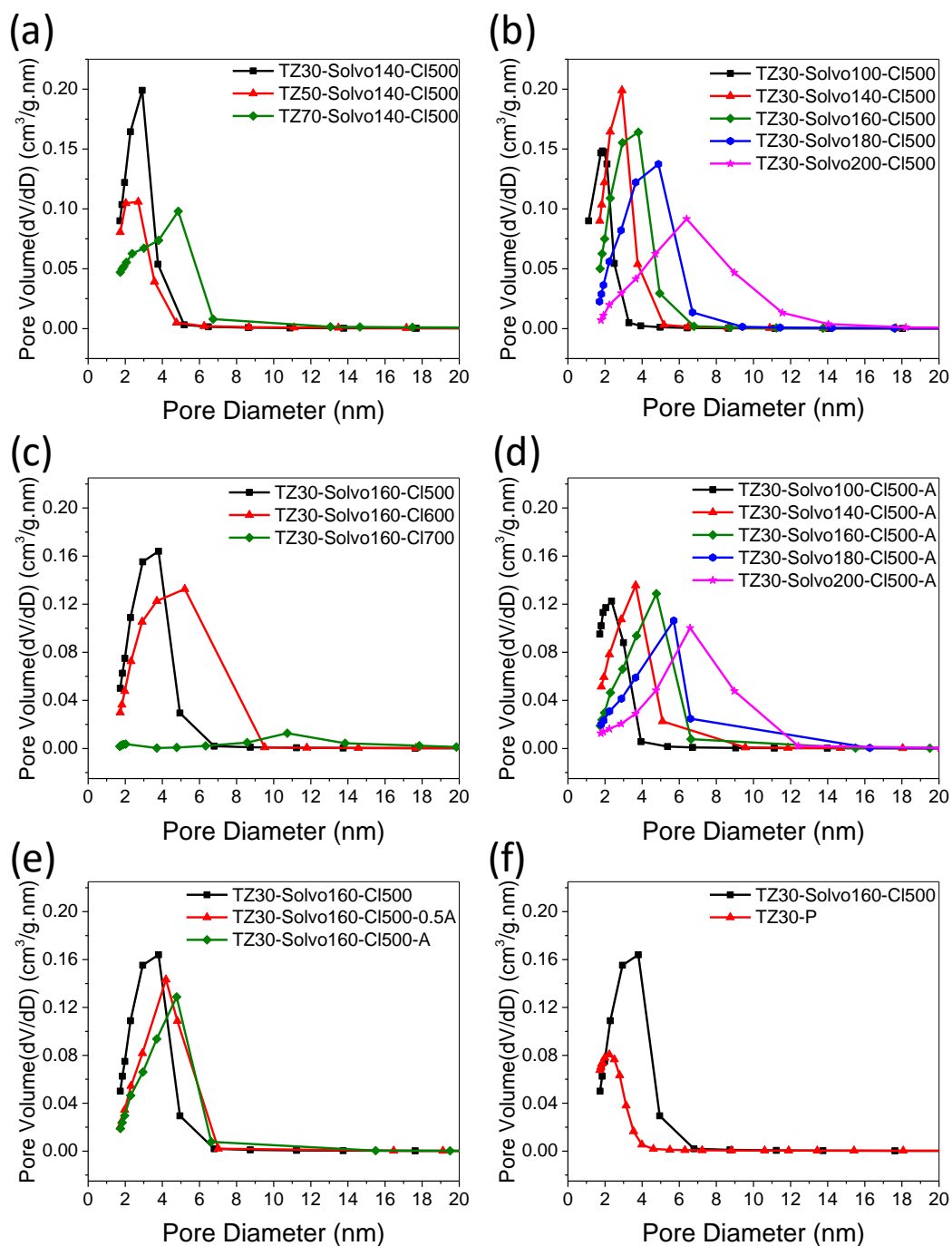


Figure 3-2. Pore size distributions: (a) TZx-Solvo140-CI500 samples with various Zr quantities. The effect of (b) solvothermal temperature and (c) calcination temperature on TZ30-Solvoz-CIv samples. (d) The effect of solvothermal temperature on TZ30-Solvoz-CI500 samples with the addition of 1 mL ammonia during solvothermal treatment and (e) the effect of ammonia (0, 0.5 and 1.0 mL) during solvothermal treatment. (f) TZ30-Sol160-CI500 and after functionalization with NPA (TZ30-P).

Altering the calcination temperature had a significant effect on the surface area and pore system of the TZ30-Solvo160-Clv samples. When the calcination temperature increased from 500 to 600 °C, the surface area dropped to 318 m<sup>2</sup>/g, but the mesopore size grew to 5.2 nm (Table 3-1). Increasing the calcination temperature to 700 °C resulted in a dramatic reduction of surface area (76 m<sup>2</sup>/g) and enlargement of pore size (10.7 nm), which was accompanied by a collapse in associated pore volume (Table 3-1 and Figure 3-2 c). These changes can be observed in the considerably different sorption isotherm of TZ30-Solvo160-Cl700 in Figure 3-1 c.

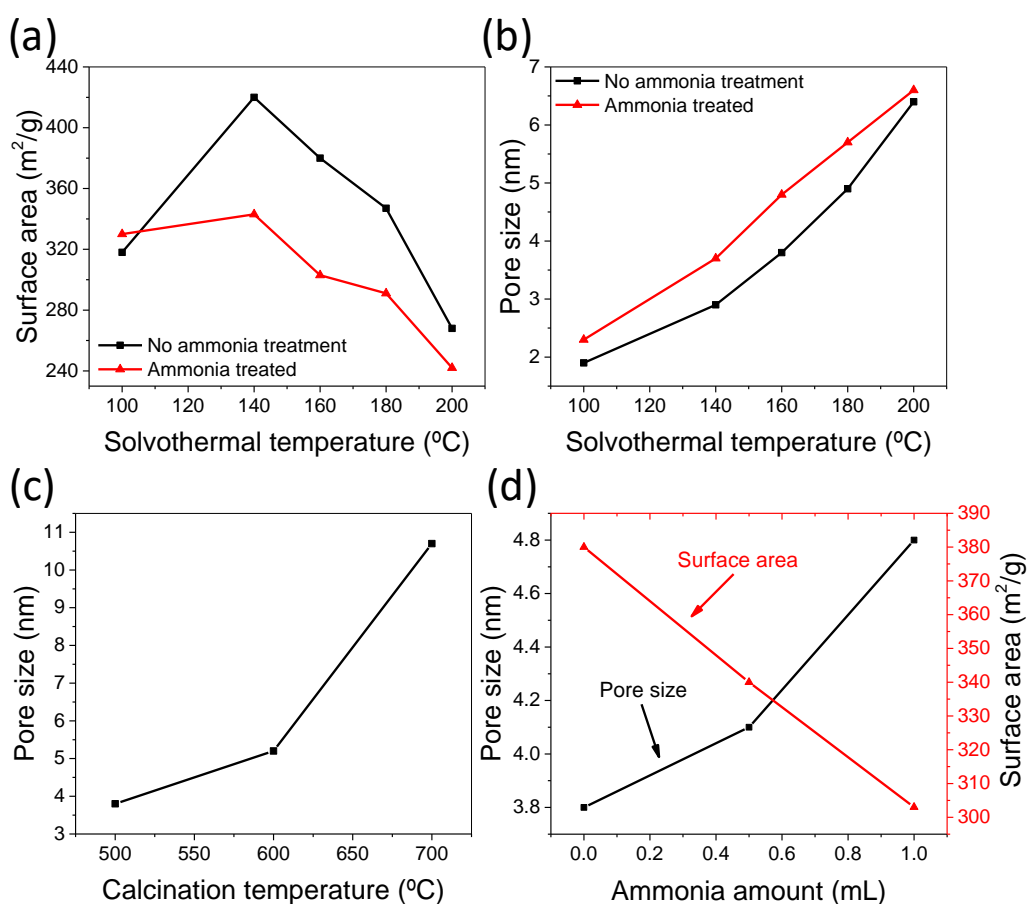


Figure 3-3. The effect of solvothermal temperature on (TZ30-Solvo160-Cl500 samples) surface area (a) and pore size (b), effect of calcination temperature on pore size (TZ30-Solvo160-Clv) (c), and the effect of addition of ammonia during solvothermal treatment (TZ30-Solvo160-Cl500 samples) on pore size and surface area (d)

Chen and co-workers previously demonstrated that addition of ammonia to a solvothermal solution can affect pore diameter.<sup>35,36</sup> For example, by addition of 1 mL

ammonia during the solvothermal step in the preparation of mesoporous titania, pore diameter increased from 14.1 to 23.0 nm.<sup>36</sup> In this study, the addition of different amounts of ammonia increased the pore size slightly; however, the surface area decreased by 30% when 1.0 mL of ammonia was added to the solvothermal solution for TZ30-Solvo160-CI500 (Figure 3-1 d and e, Figure 3-2 d and e, and Figure 3-3 d). To gain a better understanding of the impact of the addition of ammonia on pore size and surface area during the solvothermal process, solvothermal and calcination temperature, graphs were prepared from the information in Table 3-1 and are shown in Figure 3-3.

Out of all the prepared TZ samples, TZ30-Solvo160-CI500 was selected due to its high surface area (380 m<sup>2</sup>/g), pore size (3.8 nm), and high density of OH groups on the surface (5.1/nm<sup>2</sup>), for modification with NPA in order to a prepare solid-acid catalyst (TZ30-P). Nitrogen sorption isotherms of the sample before and after NPA grafting are presented in Figure 3-1 f. TZ30-P exhibited a Type IV isotherm that signified mesoporosity was preserved after introducing NPA; however, the surface area decreased to 227 m<sup>2</sup>/g which could be attributed to filling or blocking of pores by the functional group. The pore size was reduced from 3.8 nm for TZ30-Solvo160-CI500 to 2.3 nm for TZ30-P, and accompanied by a considerable loss of associated pore volume (Figure 3-2 f), which suggested that grafted NPA was occupying the mesopore space. Despite the reduction in pore size, the remaining pore diameter was sufficient for diffusion of the substrate (d-fructose) and product (5-HMF) during catalysis.

Pore size, surface area and surface OH density are the three crucial factors that control the quantity of grafting of NPA on the surface of the TZ samples. In 2003, Mueller et al. showed that by combining TGA and nitrogen sorption results, it was possible to calculate the surface density of OH groups on metal oxides.<sup>37</sup> More recently, Caruso and co-workers used this method to compute the amount of OH on the surface of the mesoporous titanium zirconium oxide spheres.<sup>34,38</sup> Thermal analysis was carried out for all TZ samples to enable calculation of surface OH densities, as well as determining the amount of NPA on the surface of TZ30-P (Figure 3-4).



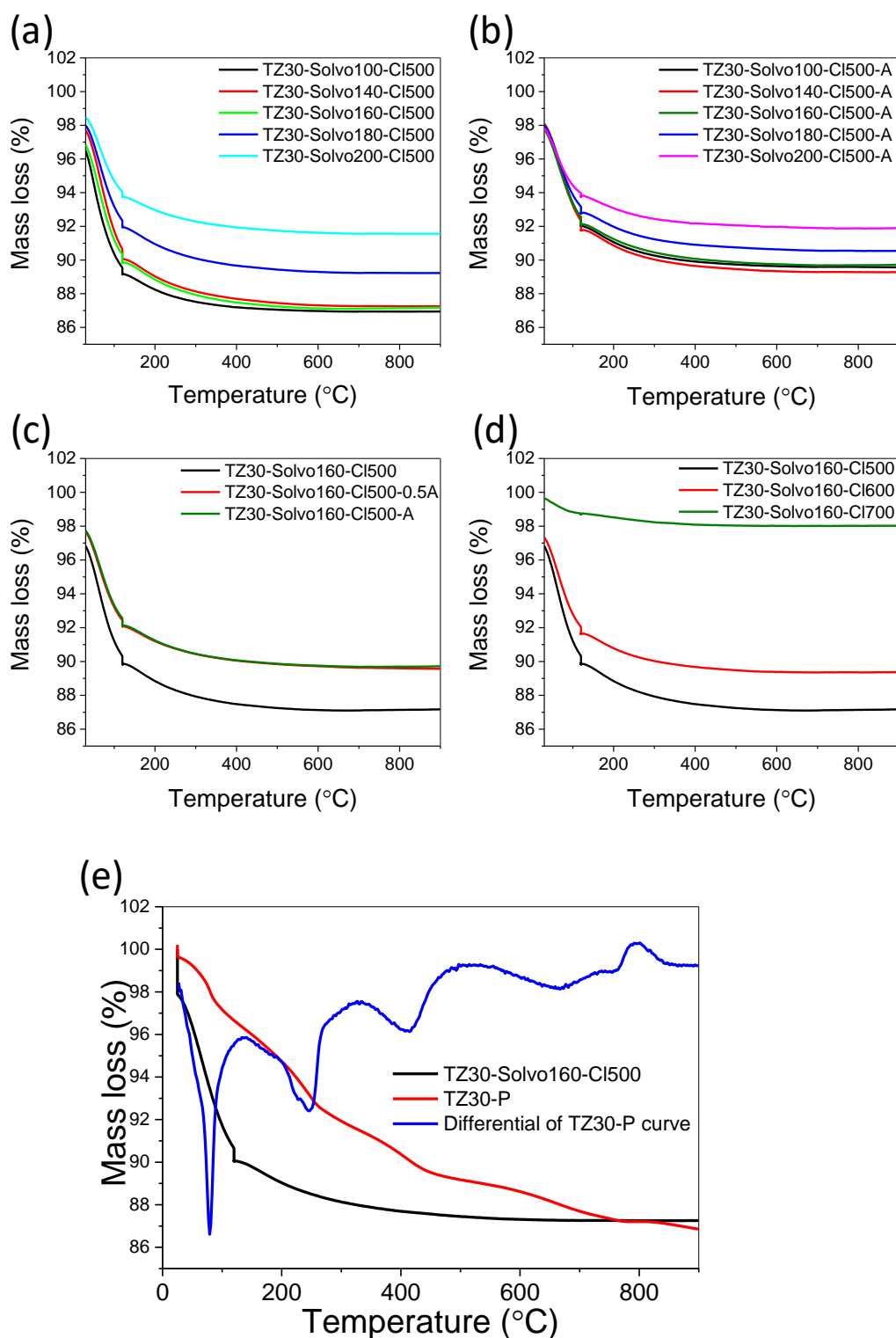


Figure 3-4. TGA: The effect of solvothermal temperature on (a) TZ30-Solvo-CI500 samples and (b) TZ30-Solvo-CI500 samples in the presence of 1.0 mL ammonia during solvothermal treatment. TZ30-Solvo160-CIv samples (c) treated with different amounts of ammonia (0, 0.5 and 1.0 mL) and (d) calcined at different temperatures. (e) TZ30-Solvo160-CI500 before and after modification with NPA (TZ30-P) plus differential of TZ30-P curve.

The TZ compounds experienced two main weight losses, the first below 120 °C, which could be related to physically adsorbed water, and the second in the range 120-500°C due to thermal removal of OH groups (Figure 3-4 a-d). The masses of the samples recorded at 120 and 500 °C were combined with previously obtained BET surface areas to calculate the surface density of OH groups (Table 3-1). From the results, samples prepared by solvothermal treatment that contained ammonia, had a lower quantity of OH on the surface, and high calcination temperature decreased the surface area and therefore decreased the overall amount of OH on the TZ particles. Furthermore, by increasing the percentage of zirconia the quantity of OH increased, despite the total surface area being reduced. Thus, TZ30-Solvo160-CI500 was selected to be functionalized with NPA, due to its high surface area, pore size and high surface OH density. The functionalised sample is labelled TZ30-P. The grafting percentage of NPA was measured by TGA (Figure 3-4 e). The mass loss below 120 °C was assigned to physically adsorbed water. The grafting percentage was calculated from the mass percentage decrease over the temperature range 150 to 900 °C. Three main degradation can be identified from the TGA of TZ30-P in the range of 150-900 °C that could be assigned to the attached NPA (Figure 3-4 e). Therefore, TGA confirmed the grafting percentage of NPA on the surface of the TZ30-Solvo160-CI500 was 6.3 wt%.

Electron microscopy was used to study the surface morphology and porosity of TZ30-Solvo160-CI500 before and after NPA functionalization, i.e. TZ30-P. SEM indicated that the TZ30-Solvo160-CI500 particles were spherical in shape, well-dispersed and homogeneous, with an average size of about 360 nm (Figure 3-5). TEM of TZ30-Solvo160-CI500 and TZ30-P (Figure 3-6) confirmed the spherical shape of the samples, while at higher magnification the 'worm-like' three-dimensional mesoporous network was observed at the outer-edge (less dense) of the spheres (Figure 3-6 c and d).

The crystallinity of TZ30-Solvo160-CI500 and TZ30-P was investigated by XRD (Figure 3-7). The pattern for TZ30-Solvo160-CI500 showed that despite solvothermal treatment at 160 °C followed by calcination in air at 500 °C, only an amorphous structure was obtained. No peaks corresponding to crystalline TiO<sub>2</sub> or ZrO<sub>2</sub> were detected, from which it was inferred that Ti and Zr were well-dispersed in the nanostructured network and thus prevented either metal oxide from crystallizing. This

result is explained by the addition of ZrP to the TIP precursor where  $Zr^{4+}$  ions can substitute for  $Ti^{4+}$  to produce Ti-O-Zr bonds. This bond inhibits the movement of the Ti and Zr atoms in the inorganic network, a movement which is necessary for metal oxide phase transition to occur.<sup>39</sup> After NPA grafting the amorphous structure was retained (Figure 3-7 a).

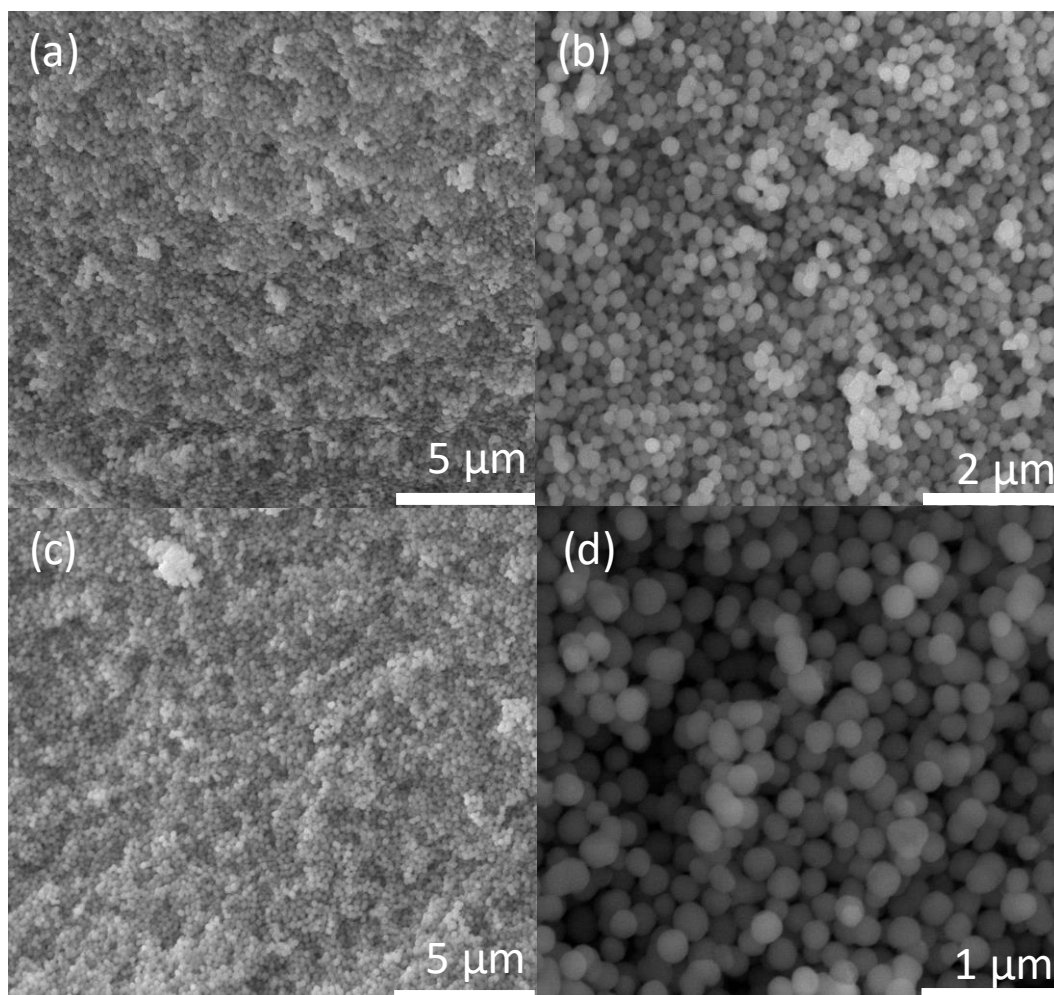


Figure 3-5. SEM images of TZ30-Solvo160-Cl500 (a and b) and TZ30-P (c and d).

FT-IR has previously been used to explore the attachment of PA and derivatives on the surface of the titania<sup>40-42</sup> and zirconia<sup>40, 43, 44</sup>. Thus, FT-IR was carried out to analyze the covalent grafting of NPA on the surface of TZ30-Solvo160-Cl500 (Figure 3-7 b). Peaks in the range  $500-700\text{ cm}^{-1}$  for TZ30-Solvo160-Cl500 and TZ30-P were identified, and were assigned to Zr-O and Ti-O stretching. Both samples also presented peaks around  $1600$  and  $3400\text{ cm}^{-1}$ , which were allocated to the bending and stretching vibrational modes of OH, respectively, and demonstrate the presence of water molecules on the surface of the particles. After modifying the metal oxide surface with

NPA, new peaks appeared: two peaks at around 2850 and 2920  $\text{cm}^{-1}$  and a single peak around 1430  $\text{cm}^{-1}$  that could be ascribed to the stretching vibrations of C-H and C-N bonds, respectively. Phosphonyl group peaks generally appear in the range 900-1300  $\text{cm}^{-1}$ : The typical stretch of P=O is around 1260  $\text{cm}^{-1}$ , while the two strong peaks at 1060 and 1150  $\text{cm}^{-1}$  could be related to P-O-Ti or P-O-Zr bonds.<sup>32, 45</sup> Therefore, based on the appearance and location of the peaks unique to TZ30-P, chemical attachment of NPA on the surface of TZ30-Solvo160-Cl500 was concluded.

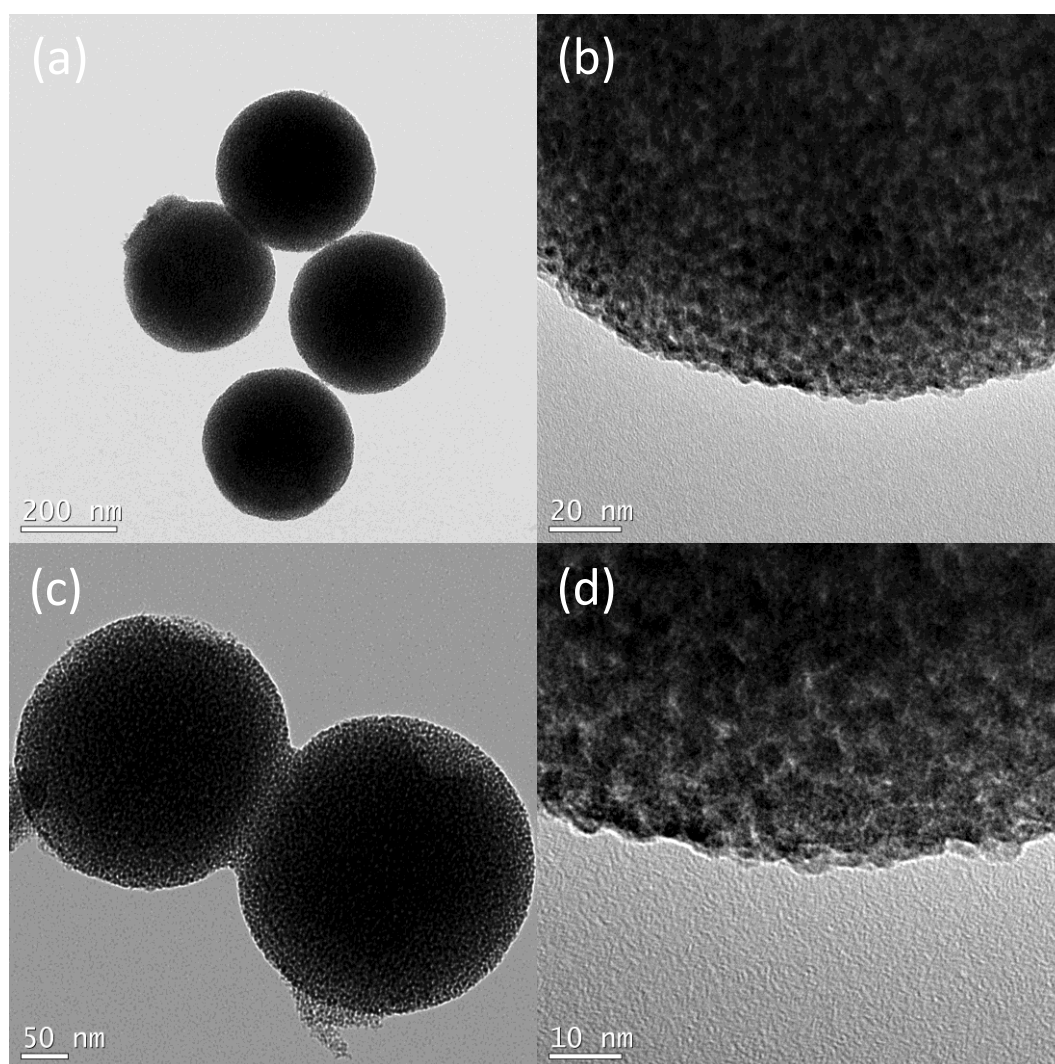


Figure 3-6. TEM images of TZ30-Solvo160-Cl500 (a and b) and TZ30-P (c and d).

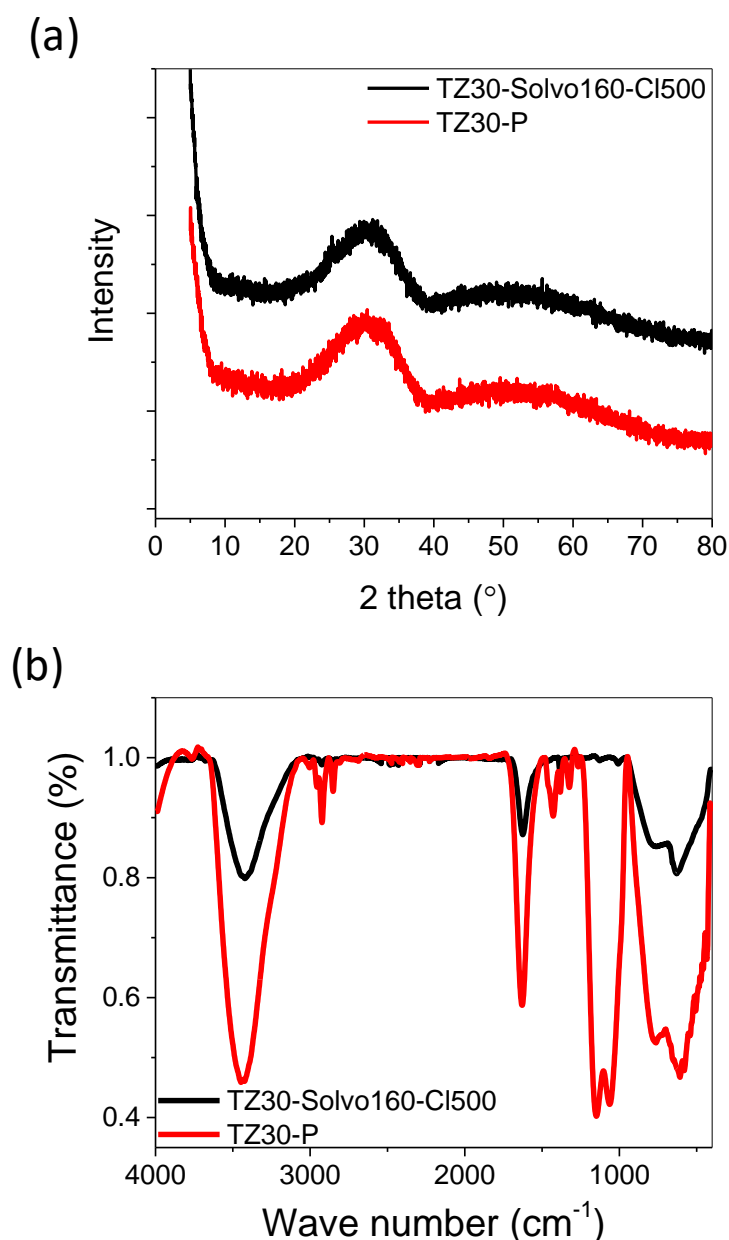


Figure 3-7. XRD patterns (a) and FT-IR spectra (b) of TZ30-Sol160-Cl500 and TZ30-P. The XRD pattern of TZ30-Solvo160-Cl500 was shifted up the y-axis for clarity.

### 3.4. Catalytic study

TZ30-P was used as a solid-acid catalyst to convert d-fructose to 5-HMF. The important features of TZ30-P are its high surface area, sufficient pore diameter for diffusion of the fructose substrate and 5-HMF product, acidic surface, and high quantity of the functional groups. NPA. The conversion of fructose to 5-HMF or other value-added products is affected by several factors, namely catalysis time, temperature, solvent choice and catalyst loading, which need to be optimized. It should be noted that the

main by-product in all of the catalytic tests in this work is a soluble polymer called “humin”, which is produced from the polymerization of fructose and 5-HMF. Characterizing the molecular structure, and quantifying the amount of humin is very difficult since a variety of structures and molecular weights may be formed.

#### 3.4.1. Effect of time and temperature

The dehydration reaction of fructose to 5-HMF was carried out at six different temperatures in the range 120-170 °C for 1 to 3 h. As shown in Figure 3-8 a, reaction temperature and duration had a significant influence on the yield of 5-HMF. As the reaction temperature increased from 120 to 160 °C, the 5-HMF yield increased from 15% to 57% after 2 h reaction, and remained constant even when the temperature was raised to 170 °C. The effect of time on the yield of the 5-HMF depended on the reaction temperature. When the temperature was below 160 °C prolonging the reaction time from 1 to 3 h boosted the yield of the 5-HMF. However, if the reaction temperature was at 160 or 170 °C, increasing the reaction time from 2 to 3 h had a negative effect on the yield. From these results it was concluded that the majority of conversion occurred within 2 h, and conversion was possible at any temperature between 120 and 170 °C. The conversion of fructose to the 5-HMF could be accelerated by increasing catalysis time and temperature; however, the rate of the side reaction such as polymerization to produce humin would also rise, especially for extended reaction durations or temperatures over 160 °C. A reaction temperature and time of 160 °C and 2 h, respectively, were optimum with a 57% yield of 5-HMF.

#### 3.4.2. The effect of solvent and loading of the catalyst

Solvent has a great impact on the conversion of the fructose to 5-HMF. In 2016, Zheng et al. reviewed the production of 5-HMF from various biomass sources in aqueous solution and in different solvents.<sup>46</sup> Water is a green and cost-effective solvent, and for the conversion of high molecular weight carbohydrates, such as cellulose is necessary.<sup>46, 47</sup> However, the drawback of using water is that it accelerates the conversion of 5-HMF to undesirable products like levulinic acid and formic acid.<sup>46, 48</sup>

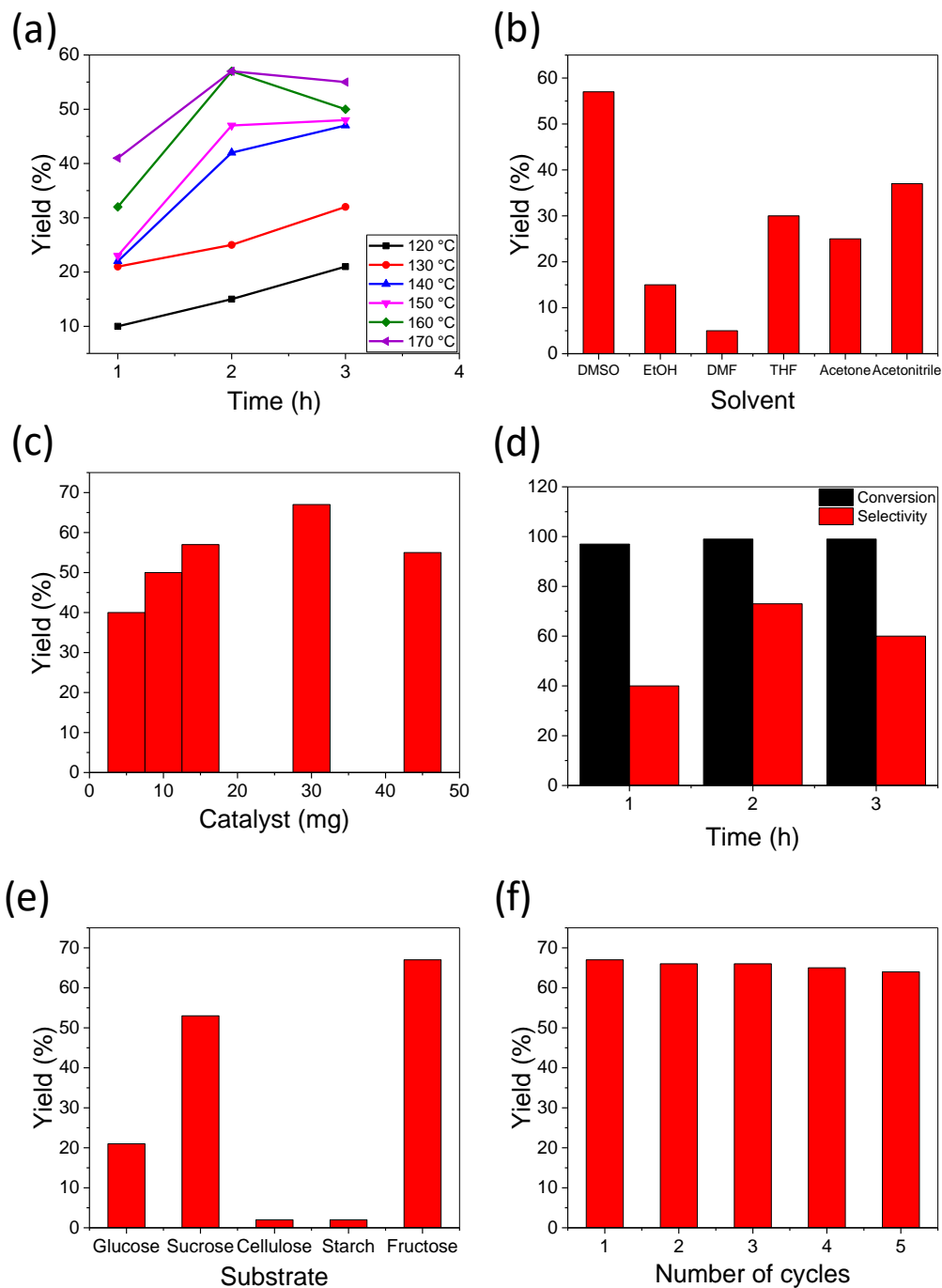


Figure 3-8. (a) The yield of 5-HMF from fructose dehydration of reaction temperature and time (reaction condition: fructose solution in DMSO (10 mL, 1.67 mM) and 15 mg catalyst), (b) different solvents (reaction condition: fructose solution in various solvents (10 mL, 1.67 mM), 15 mg catalyst at 160 °C for 2h), and (c) the catalyst amount (reaction condition: fructose solution in DMSO (10 mL, 1.67 mM), at 160 °C for 2h). (d) Conversion of fructose and 5-HMF selectivity using 30 mg catalyst and fructose solution in DMSO at 160 °C. (e) The effect of substrate on 5-HMF yield (reaction condition: substrate solution in DMSO (10 mL, 1.67 mM), 30 mg catalyst at 160 °C for 2h). (f) The reusability of the TZ30-P catalyst in five consecutive runs.

Thus, aprotic solvents such as DMSO, acetonitrile, DMF, acetone and THF are favored. Among these solvents DMSO has gained attention because of its high boiling point and ability to suppress conversion of 5-HMF to levulinic acid and formic acid. The aforementioned solvents, as well as ethanol, were used in the conversion of fructose to 5-HMF in a reaction occurring at 160 °C for 2 h, using 15 mg of TZ30-P as the catalyst. The results are shown in Figure 3-8 b. In agreement with the literature, DMSO was the best solvent for this reaction with a 5-HMF yield of 57%, followed by acetonitrile and THF with yields of 37 and 30%. DMSO was selected as the best solvent for studying the other factors that affect the dehydration of fructose to 5-HMF.

The catalyst loading is another crucial factor, which was investigated. By varying the amount of TZ30-P catalyst (5-45 mg), the yield of conversion of fructose to 5-HMF was affected due to the associated change in number of catalyst active sites (Figure 3-8 c). As the quantity of catalyst increased from 5 to 30 mg, the yield of 5-HMF increased from 40 to 67 %. However, increasing the amount to 45 mg reduced the yield. Although increasing the number of acid-sites can improve the rate of the reaction of fructose conversion to 5-HMF, it can raise the possibility of the transformation of fructose to undesired products such as humin, which ultimately reduces the 5-HMF yield. Therefore, 30 mg of TZ30-P is the optimum quantity of catalyst.

After optimization of the reaction conditions, the conversion of substrate and 5-HMF selectivity was tested ( Figure 3-8 d). 99 % fructose conversion and 73 % 5-HMF selectivity were obtained after 2 h fructose dehydration under optimized condition (30 mg of catalyst in DMSO at 160 °C) and it can be concluded the catalyst was highly active during the catalytic reactions. Further dehydration of 5-HMF to other products such as levulinic and formic acids was prevented due to using DMSO as solvent.<sup>4, 49</sup>

#### 3.4.3. Conversion of other feedstocks to 5-HMF and reusability of the catalyst

The promising results obtained from the dehydration of fructose serve as an inspiration to test the capability of TZ30-P for 5-HMF synthesis from other carbohydrates. In comparable reaction conditions (30 mg of catalyst in DMSO at 160 °C for 2 h) that were optimised for the fructose dehydration, sucrose, glucose, starch and cellulose were used as carbohydrate resources. Results of the 5-HMF yields are summarized in Figure 3-8 e. Reasonable yields were achieved for sucrose (53%) and



glucose (21%); however, the dehydration of cellulose and starch was not successful under the conditions. The dehydration of glucose to 5-HMF has two steps, the isomerization of glucose to fructose, and then dehydration of fructose to 5-HMF. The first step, which is rate-determining, needs a base or Lewis acid as a catalyst.<sup>50, 51</sup> It is conceivable that a loss of Lewis acid sites resulted from covering the surface of the TZ30-Solvo160-Cl500 with NPA. This may also explain the low yield of 5-HMF from cellulose and starch.

The stability of TZ30-P was tested by recycling of the catalyst in five consecutive runs to convert fructose. After each run, the catalyst was separated by centrifugation, washed with ethanol then dried in an oven overnight. Over the five runs the yield of the 5-HMF decreased from 67 to 64%, as shown in Figure 3-8 f. The small loss of activity could be caused by carbon deposition on the surface of the catalyst, or removal of functional groups from the surface. This demonstrates that the catalyst can be recycled. Thus, the mesoporous TZ30-P catalyst has promise to be utilized as a stable and highly active recyclable solid acid catalyst in biomass conversion.

### 3.5. Conclusion

Mesoporous titanium zirconium oxide was prepared via a sol-gel method using solvothermal and calcination treatments. The surface area and pore diameter were varied with the treatment temperatures, with maximum surface area and pore size achieved at solvothermal temperatures of 140 and 200 °C, respectively. A basic environment during the solvothermal process increased the pore size, but reduced the surface area. The most promising sample, TZ30-Solvo160-Cl500, was functionalized with NPA and then applied as a solid-acid catalyst for the dehydration of fructose to 5-HMF. Optimum conditions of 30 mg catalyst at 160 °C for 2 h in DMSO gave 99, 73 and 67 % fructose conversion, 5-HMF selectivity and yield of 5-HMF, respectively. The yields of 5-HMF from sucrose and glucose were 53 % and 21 %, respectively, but for cellulose and starch the yields were poor. The catalyst was used in 5 consecutive runs, with the yield of 5-HMF reduced by merely 3 %.

### 3.5.1. Comparing the catalytic performance of TZ30-P with other catalysts.

In chapter 2, Zr-Ter, which was functionalized with carboxylate and had a surface area of  $67 \text{ m}^2\text{g}^{-1}$ , was used as solid acid catalyst for dehydration of fructose to 5-HMF and the highest yield of 5-HMF was 42%. In section 2.5.1, it was concluded that to improve the yield of 5-HMF it was necessary to increase the surface area and replace carboxylate as the acidic functional group with either phosphate or sulfate. With the approach adopted in this chapter, surface area was successfully to  $380 \text{ m}^2\text{g}^{-1}$  for TZ30-Solvo160-Cl500 and the catalyst surface was then grafted with phosphate. Under optimized conditions, the yield of 5-HMF obtained from TZ30-P was 67%. However, the optimized temperature and amount of the catalyst employed was slightly greater for TZ30-P ( $160 \text{ }^\circ\text{C}$  and 30 mg) than Zr-Ter ( $150 \text{ }^\circ\text{C}$  and 15 mg). The yield of 5-HMF obtained from sucrose solution was also higher for TZ30-P (53%) than Zr-Ter (37%), but there was no significant increase in yield of 5-HMF when glucose was used as the substrate. In conclusion, TZ30-P was more successful than Zr-Ter for the conversion of fructose and sucrose to 5-HMF.

The novelty and catalytic effectiveness of the TZ30-P catalyst was further realized when it was compared with reported metal phosphate catalysts. As shown in Table 3-2, other phosphate-catalyst utilized in the catalytic conversion of fructose to 5-HMF produced yields of between 35% and 98%. Among the reported catalysts, the highest yield was obtained with phosphated titania,<sup>52</sup> but it should be noted that Luqman et al. used a mixture of solvents in a continuous flow reactor. Continuously separating 5-HMF from the reaction solution may be a very effective way to gain a high yield. Moreover, the catalytic reaction was performed under an argon atmosphere and 400 mg of catalyst was used for the dehydration of fructose to 5-HMF. Another high yield of 5-HMF was achieved by Liu et al. using chromium-incorporated mesoporous zirconium phosphate.<sup>53</sup> The reason for the high yield of 5-HMF could be related to the high surface area of the catalyst ( $386 \text{ m}^2\text{g}^{-1}$ ). One important conclusion that can be drawn from Table 3-2 is that using water or a water mixture as the solvent does not produce high yields of 5-HMF unless microwave or high temperature reaction conditions are employed.

Table 3-2. A comparison of the catalytic performance of TZ30-P with reported metal phosphate catalysts.

Catalyst	Solvent	Temperature (°C)	Time (min)	5-HMF yield (%)	Reference
Zirconium phosphate (ZrP)	Sub critical water	240	3	53	54
Copper phosphate nanostructures ( $\alpha$ -Cu <sub>2</sub> P <sub>2</sub> O <sub>7</sub> -900)	H <sub>2</sub> O	200	5	36	55
Titanium hydrogenphosphate	H <sub>2</sub> O-THF	140	180	55	56
Large pore mesoporous tin phosphate (LPSnP-1) <sup>(a)</sup>	H <sub>2</sub> O-methyl isobutyl ketone	150	20	77	57
Phosphated titania <sup>(b)</sup>	H <sub>2</sub> O/THF+ N-methyl-2-pyrrolidone	175	30	98	52
CaP <sub>2</sub> O <sub>6</sub>	Sub critical water	200	5	34	58
$\alpha$ -Sr(PO <sub>3</sub> ) <sub>2</sub>	Sub critical water	200	5	39	58
Mesoporous niobium phosphate	H <sub>2</sub> O	130	30	45	59
Cr-incorporated mesoporous ZrP	DMSO	120	120	86	53
Ordered mesoporous ZrP	DMSO	120	90	69	60
TZ30-P	DMSO	160	120	67	This work

<sup>(a)</sup> Microwave-assisted reaction.

<sup>(b)</sup> Flow reactor setup was used. NaCl was also added.

Therefore, by carefully controlling the surface area, pore diameter, OH surface density, and grafted surface functional groups, versatile mesoporous phosphated-TZ particles could be considered as promising options for the conversion of biomass to high value chemicals.

### 3.6. References

1. G. W. Huber, S. Iborra and A. Corma, *Chemical Reviews*, 2006, **106**, 4044-4098.
2. A. J. Ragauskas, C. K. Williams, B. H. Davison, G. Britovsek, J. Cairney, C. A. Eckert, W. J. Frederick, J. P. Hallett, D. J. Leak, C. L. Liotta, J. R. Mielenz, R. Murphy, R. Templer and T. Tschaplinski, *Science*, 2006, **311**, 484-489.
3. A. Corma, S. Iborra and A. Velty, *Chemical Reviews*, 2007, **107**, 2411-2502.
4. T. Wang, M. W. Nolte and B. H. Shanks, *Green Chemistry*, 2014, **16**, 548-572.
5. L. Wang and F.-S. Xiao, *Green Chemistry*, 2015, **17**, 24-39.
6. D. M. Alonso, J. Q. Bond and J. A. Dumesic, *Green Chemistry*, 2011, **13**, 754-793.
7. L. Hu, G. Zhao, W. Hao, X. Tang, Y. Sun, L. Lin and S. Liu, *RSC Advances*, 2012, **2**, 11184-11206.
8. R.-J. van Putten, J. C. van der Waal, E. de Jong, C. B. Rasrendra, H. J. Heeres and J. G. de Vries, *Chemical Reviews*, 2013, **113**, 1499-1597.
9. J. Chen, K. Li, L. Chen, R. Liu, X. Huang and D. Ye, *Green Chemistry*, 2014, **16**, 2490-2499.
10. N. Wang, Y. Yao, W. Li, Y. Yang, Z. Song, W. Liu, H. Wang, X.-F. Xia and H. Gao, *RSC Advances*, 2014, **4**, 57164-57172.
11. B. Karimi, H. M. Mirzaei, H. Behzadnia and H. Vali, *ACS Applied Materials & Interfaces*, 2015, **7**, 19050-19059.
12. H. Xu, Z. Miao, H. Zhao, J. Yang, J. Zhao, H. Song, N. Liang and L. Chou, *Fuel*, 2015, **145**, 234-240.
13. X. Qi, M. Watanabe, T. M. Aida and R. L. Smith Jr, *Green Chemistry*, 2008, **10**, 799-805.
14. P. Daorattanachai, P. Khemthong, N. Viriya-empikul, N. Laosiripojana and K. Faungnawakij, *Carbohydrate Research*, 2012, **363**, 58-61.
15. K.-i. Shimizu and A. Satsuma, *Energy & Environmental Science*, 2011, **4**, 3140-3153.
16. C.-H. Kuo, A. S. Poyraz, L. Jin, Y. Meng, L. Pahalagedara, S.-Y. Chen, D. A. Kriz, C. Guild, A. Gudz and S. L. Suib, *Green Chemistry*, 2014, **16**, 785-791.
17. A. Osatiashtiani, A. F. Lee, D. R. Brown, J. A. Melero, G. Morales and K. Wilson, *Catalysis Science & Technology*, 2014, **4**, 333-342.
18. T. Y. Kim, D. S. Park, Y. Choi, J. Baek, J. R. Park and J. Yi, *Journal of Materials Chemistry*, 2012, **22**, 10021-10028.
19. H. Yan, Y. Yang, D. Tong, X. Xiang and C. Hu, *Catalysis Communications*, 2009, **10**, 1558-1563.
20. G. X. Yu, X. L. Zhou, F. Liu, C. L. Li, L. F. Chen and J. A. Wang, *Catalysis Today*, 2009, **148**, 70-74.
21. Z. Li, R. Wnetrzak, W. Kwapinski and J. J. Leahy, *ACS Applied Materials & Interfaces*, 2012, **4**, 4499-4505.
22. C. Queffelec, M. Petit, P. Janvier, D. A. Knight and B. Bujoli, *Chemical Reviews*, 2012, **112**, 3777-3807.
23. S. Pujari, L. Pujari, A. T. M. Scheres, H. Marcelis and Zuilhof, *Angewandte Chemie (International ed.)*, 2014, **53**, 6322-6356.

24. S. A. Paniagua, A. J. Giordano, O. N. L. Smith, S. Barlow, H. Li, N. R. Armstrong, J. E. Pemberton, J.-L. Brédas, D. Ginger and S. R. Marder, *Chemical Reviews*, 2016, **116**, 7117-7158.
25. A. Cattani-Scholz, *ACS Applied Materials & Interfaces*, 2017, **9**, 25643-25655.
26. A. Clearfield, in *Metal Phosphonate Chemistry: From Synthesis to Applications*, The Royal Society of Chemistry, 2012, DOI: 10.1039/9781849733571-00001, pp. 1-44.
27. A. Bulusu, S. A. Paniagua, B. A. MacLeod, A. K. Sigdel, J. J. Berry, D. C. Olson, S. R. Marder and S. Graham, *Langmuir*, 2013, **29**, 3935-3942.
28. D. Liu, X. Xu, Y. Su, Z. He, J. Xu and Q. Miao, *Angewandte Chemie International Edition*, 2013, **52**, 6222-6227.
29. L. Sang, A. Mudalige, A. K. Sigdel, A. J. Giordano, S. R. Marder, J. J. Berry and J. E. Pemberton, *Langmuir*, 2015, **31**, 5603-5613.
30. F. Forato, H. Liu, R. Benoit, F. Fayon, C. Charlier, A. Fateh, A. Defontaine, C. Tellier, D. R. Talham, C. Queffélec and B. Bujoli, *Langmuir*, 2016, **32**, 5480-5490.
31. E. S. Skibinski, W. J. I. DeBenedetti and M. A. Hines, *The Journal of Physical Chemistry C*, 2017, **121**, 14213-14221.
32. G. M. Pavel and V. L. Georgii, *Russian Chemical Reviews*, 2006, **75**, 541.
33. M. Giza, P. Thissen and G. Grundmeier, *Langmuir*, 2008, **24**, 8688-8694.
34. D. Chen, L. Cao, T. L. Hanley and R. A. Caruso, *Advanced Functional Materials*, 2012, **22**, 1966-1971.
35. D. Chen, F. Huang, Y.-B. Cheng and R. A. Caruso, *Advanced Materials*, 2009, **21**, 2206-2210.
36. D. Chen, L. Cao, F. Huang, P. Imperia, Y.-B. Cheng and R. A. Caruso, *Journal of the American Chemical Society*, 2010, **132**, 4438-4444.
37. R. Mueller, H. K. Kammler, K. Wegner and S. E. Pratsinis, *Langmuir*, 2003, **19**, 160-165.
38. X. Wang, D. Chen, L. Cao, Y. Li, B. J. Boyd and R. A. Caruso, *ACS Applied Materials & Interfaces*, 2013, **5**, 10926-10932.
39. F. Xia, D. Chen, N. V. Y. Scarlett, I. C. Madsen, D. Lau, M. Leoni, J. Ilavsky, H. E. A. Brand and R. A. Caruso, *Chemistry of Materials*, 2014, **26**, 4563-4571.
40. J. Randon, P. Blanc and R. Paterson, *Journal of Membrane Science*, 1995, **98**, 119-129.
41. G. Guerrero, P. H. Mutin and A. Vioux, *Chemistry of Materials*, 2001, **13**, 4367-4373.
42. A. Raman, R. Quiñones, L. Barriger, R. Eastman, A. Parsi and E. S. Gawalt, *Langmuir*, 2010, **26**, 1747-1754.
43. J. F. Smalley, K. Chalfant, S. W. Feldberg, T. M. Nahir and E. F. Bowden, *The Journal of Physical Chemistry B*, 1999, **103**, 1676-1685.
44. S. Pawsey, K. Yach and L. Reven, *Langmuir*, 2002, **18**, 5205-5212.
45. D. Geldof, M. Tassi, R. Carleer, P. Adriaensens, A. Roevens, V. Meynen and F. Blockhuys, *Surface Science*, 2017, **655**, 31-38.
46. X. Zheng, X. Gu, Y. Ren, Z. Zhi and X. Lu, *Biofuels, Bioproducts and Biorefining*, 2016, **10**, 917-931.
47. K. Y. Nandiwale, N. D. Galande, P. Thakur, S. D. Sawant, V. P. Zambre and V. V. Bokade, *ACS Sustainable Chemistry & Engineering*, 2014, **2**, 1928-1932.

48. A. Najafi Chermahini, F. Shahangi, H. A. Dabbagh and M. Saraji, *RSC Advances*, 2016, **6**, 33804-33810.
49. L. T. Mika, E. Cséfalvay and Á. Németh, *Chemical Reviews*, 2018, **118**, 505-613.
50. L. Wang, H. Wang, F. Liu, A. Zheng, J. Zhang, Q. Sun, J. P. Lewis, L. Zhu, X. Meng and F.-S. Xiao, *ChemSusChem*, 2014, **7**, 402-406.
51. Q. Yang, M. Sherbahn and T. Runge, *ACS Sustainable Chemistry & Engineering*, 2016, **4**, 3526-3534.
52. A. Luqman, S. Abhijit, M. Swathi, M. Qing, K. Muxina and B. Jorge, *ChemSusChem*, 2015, **8**, 2907-2916.
53. B. Liu, C. Ba, M. Jin and Z. Zhang, *Industrial Crops and Products*, 2015, **76**, 781-786.
54. F. S. Asghari and H. Yoshida, *Carbohydrate Research*, 2006, **341**, 2379-2387.
55. P. Khemthong, P. Daorattanachai, N. Laosiripojana and K. Faungnawakij, *Catalysis Communications*, 2012, **29**, 96-100.
56. M. I. Alam, S. De, B. Singh, B. Saha and M. M. Abu-Omar, *Applied Catalysis A: General*, 2014, **486**, 42-48.
57. D. Arghya, G. Dinesh, P. A. K., S. Basudeb and B. Asim, *ChemSusChem*, 2014, **7**, 925-933.
58. P. Daorattanachai, P. Khemthong, N. Viriya-empikul, N. Laosiripojana and K. Faungnawakij, *Carbohydrate Research*, 2012, **363**, 58-61.
59. Y. Zhang, J. Wang, J. Ren, X. Liu, X. Li, Y. Xia, G. Lu and Y. Wang, *Catalysis Science & Technology*, 2012, **2**, 2485-2491.
60. H. Xu, Z. Miao, H. Zhao, J. Yang, J. Zhao, H. Song, N. Liang and L. Chou, *Fuel*, 2015, **145**, 234-240.



## Chapter 4. Functionalized mesoporous zirconium titanium oxide spheres as acid catalysts for the conversion of fructose into 5-HMF

### 4.1. Introduction

Biomass has attracted attention due to its considerable potential as a raw material for the production of green chemicals, fuels and fuel additives, with an estimated global production of around 100 billion tons per year.<sup>1-3</sup> Biomass feedstocks are sourced from the non-edible components of crops such as stems, leaves and husks, cellulose from agricultural or forestry waste, or high yield, short rotation, non-food crops such as switchgrass or willow trees, which require minimal cultivation.<sup>4</sup> Biomass offers the only renewable source of organic molecules for the manufacture of bulk, fine and specialty chemicals necessary to secure the future needs of society.<sup>2,5</sup> Carbohydrates are the major component of biomass. Thus, the selective conversion of sugars under mild conditions to platform molecules (i.e. building block chemicals), which can subsequently be used for the production of various chemicals, is highly sought.

Among the biomass-derived platform chemicals, 5 hydroxymethylfurfural (5-HMF) is considered to be a key multipurpose building block for the biorefinery. Valuable chemicals, such as 2,5-dimethylfuran, 2,5-diformylfuran, 2,5-furandicarboxylic acid, levulinic acid, 1,6-hexanediol, adipic acid, caprolactam and caprolactone, with high potential in fuel, polymer and solvent applications can all be derived from 5-HMF( please for more information refer to chapter 1 section 1.5).<sup>6-8</sup> Therefore, the development of a sustainable procedure for the conversion of biomass and carbohydrates into 5-HMF has become increasingly important to fill the growing gap between the demand for biofuels and chemicals.

Over the past five years, extensive research has been conducted on the efficient preparation of 5-HMF from carbohydrates.<sup>6-14</sup> Although this research has tended to focus on the simple conversion of fructose (as a model saccharide) to 5-HMF,<sup>10, 11, 14</sup> and so avoid the formation of side products such as oligosaccharides. Homogeneous



mineral acids such as sulfuric acid and metal chloride salts have been used for the synthesis of 5-HMF from carbohydrates traditionally<sup>15</sup> and are known to be very efficient. However, there are disadvantages to this approach, including catalyst separation, reactor corrosion and recyclability. The replacement of liquid acids by solid alternatives may overcome the drawbacks of the homogenous catalysts. Solid-acid catalysis is highly desirable for designing green chemical approaches with a significant reduction in pollution compared to typical liquid acids.<sup>16-18</sup> In the pursuit of economical, simple, efficient and environmentally friendly 5-HMF production, many solid-acid catalysts have been investigated, including acidic polyoxometalate,<sup>19</sup> polymer-based acid,<sup>20</sup> zeolite,<sup>21</sup> metal oxides (e.g. zirconia and titania)<sup>12, 13, 22, 23</sup> and metal binary oxides.<sup>24-28</sup>

Among these heterogeneous catalysts, acidified TiO<sub>2</sub> and ZrO<sub>2</sub> have substantial potential as catalytic materials.<sup>10, 13, 25, 29-31</sup> For example, de Almeida et al. prepared sulfated TiO<sub>2</sub> via a sol-gel process with different concentrations of sulfate group on the surface for the methanolysis of soybean and castor oils.<sup>16</sup> Compared to TiO<sub>2</sub>, solid acid ZrO<sub>2</sub> is more widely used and has provoked interest in carbohydrate dehydration procedures. Sulfated ZrO<sub>2</sub> has two significant advantages with the strength of the acid and the type of acidity,<sup>32</sup> both Brønsted and Lewis. These advantages enable enhanced activity and selectivity. Furthermore, Tominaga et al. found that Lewis and Brønsted mixed-acid systems were more efficient for dehydrating carbohydrates.<sup>33</sup> As a result much research has been devoted to synthesizing a highly active sulfated ZrO<sub>2</sub> catalyst. However, the surface area of the ZrO<sub>2</sub> catalyst is limited because of crystallization during the solvothermal process or calcination, which affects the loading of the sulfate group on the surface. The performance of metal oxide solid-acid catalysts depends on the morphological properties of the materials such as specific surface area, porosity and pore volume, as well as the surface chemistry. Since chemical reactions typically occur on the surface of the catalysts, a rationally designed catalyst featuring high surface area and pore volume would maximize the catalytically-active surface area.

We have previously studied titanium zirconium oxides for potential application in dye adsorption, drug delivery, heavy metal ion and radioactive waste sequestration.<sup>34-39</sup>

Compared to individual  $\text{ZrO}_2$  or  $\text{TiO}_2$ , a zirconium titanium binary oxide with the presence of the Zr–O–Ti network retards the nucleation and crystallization of the individual oxides, instead producing an amorphous binary metal oxide framework with adjustable porosity and high surface area.<sup>35</sup> Moreover, zirconium titanium oxides exhibit modifiable surface properties that could be exploited during application of the binary oxide as a high-performance catalyst. For example, Li et al. prepared  $\text{ZrO}_2/\text{TiO}_2$  nanocomposites for the esterification reaction between levulinic acid and ethanol,<sup>28</sup> and concluded that introducing  $\text{ZrO}_2$  on the surface of the  $\text{TiO}_2$  nanorods increased the surface content of sulfate groups.

Therefore, high potential exists for using zirconium titanium binary oxide as a solid-acid catalyst to convert biomass to platform chemicals. In this chapter, high surface area, mesoporous titanium zirconium oxide (TZ) spheres with variable Ti to Zr ratios were functionalized with sulfate groups and then applied as a catalyst for the conversion of fructose to 5-HMF. The influence of acid concentration, duration of the acid treatment, surface area and zirconia content on the loading of the sulfate groups on the surface were studied. The sample with the highest loading of sulfate groups was then applied as an acid catalyst for the conversion of fructose to 5-HMF. A study of the catalytic dehydration of fructose was also carried out. The resulting sulfated TZ sample featured characteristics advantageous to catalysis, including a well-maintained structural integrity, good dispersity in polar solvents, favourable mesoporous structure and a strongly acidic surface. The presence of more surface area facilitated sulfate functionalization, while the open framework provides easy access to the active sites for the chemical reactions.

## 4.2. Experimental Section

### 4.2.1. Materials

Titanium(IV) isopropoxide (TIP, 97%), zirconium(IV) propoxide (ZrP, 70% in 1-propanol), hexadecylamine (HDA, 90%), D-Fructose (>99%), glucose (>99%), sucrose (>99%), cellulose, starch, potassium chloride (AR) and dimethyl sulfoxide (DMSO) were obtained from Sigma–Aldrich. Absolute ethanol (>99.7%), sulfuric acid (>95%), tetrahydrofuran (THF), and dimethylformamide (DMF) were from Merck. Milli-Q

water was collected from a Millipore academic purification system with a resistivity higher than 18.2 MΩ cm. All chemicals and solvents were used as received.

#### 4.2.2. Preparation of the TZ Spheres.

Sphere preparation: The nonporous precursor spheres were prepared via sol–gel chemistry in the presence of HDA.<sup>35</sup> Ti:Zr atomic ratios of 7:3 (TZ30), 1:1 (TZ50), and 3:7 (TZ70) were used in the preparation. In a typical synthesis (TZ30), 7.95 g HDA was dissolved in 790 mL ethanol, followed by the addition of 3.20 mL aqueous KCl solution (0.1 M) and 5.44 mL water. To this solution, a mixture of 12.89 mL TIP and 7.96 mL ZrP was quickly added under vigorous stirring which was maintained for 1 min. After stirring ceased, the resulting milky white precursor suspension was kept undisturbed at room temperature for 18 h. The spheres were collected by centrifugation (Beckman Coulter Allegra 25R) and washed with ethanol three times. Finally, the as-prepared sample was covered with low lint cellulose paper (Kimwipes) and dried in a fume cupboard at ambient temperature for 6 days.

Solvothermal treatment: A solvothermal process was conducted on the amorphous spheres at 140, 160, 180 or 200 °C. In a typical procedure, 1.6 g of the precursor spheres were dispersed in a mixed solution of 20 mL ethanol and 10 mL water. The resulting mixture was sealed within a 50 mL Teflon-lined steel autoclave and heated at the desired temperature for 16 h in a Labec fan-forced oven. The products were separated by centrifugation (Beckman Coulter Allegra 25R), washed with ethanol three times and dried in an oven at 50 °C overnight.

Sulfuric acid treatment and calcination: 0.3 g of dried powder was dispersed in an aqueous solution of H<sub>2</sub>SO<sub>4</sub> (0.1, 1.0 or 2.0 M, 15 mL) and stirred for either 1 h or 3 h to investigate the loading of the sulfate group on the surface of the spheres. The resulting samples were filtered by centrifugation, washed with water and ethanol, and dried in an oven at 100 °C overnight. Finally, the dried TZ samples were calcined at 500, 550, 600 or 650 °C (ramp rate of 1.6 °C min<sup>-1</sup> from room temperature) for 2 h in air to obtain sulfated TZ samples. The final materials were labelled as TZ<sub>x</sub>-Solvo<sub>y</sub>-zMch-Cl<sub>v</sub>, where *x*, *y*, *z*, *c* and *v* represent the Zr content, temperature of the solvothermal treatment, acid concentration, duration of the acid treatment and calcination temperature, respectively. For example, TZ30-Solvo140-2M1h-Cl500

indicates the nonporous precursor spheres were prepared with a Ti:Zr atomic ratio of 7:3, solvothermally treated at 140 °C that underwent sulfuric acid treatment in aqueous 2.0 M H<sub>2</sub>SO<sub>4</sub> for 1 h before calcination at 500 °C.

#### 4.2.3. Characterization

The morphology and particle size of the samples were observed by scanning electron microscopy (SEM) using a FEI Quanta 200 environmental scanning electron microscope under low vacuum mode and with an accelerating voltage of 15 kV. SEM images were obtained without metal sputter coating. EDX (energy dispersive X-ray spectroscopy) was performed using an INCA SDD X-ray microanalysis system. Transmission electron microscopy (TEM) images were obtained on a FEI Tecnai F20 transmission electron microscope operated at 200 kV. Powder X-ray diffraction (XRD) patterns were acquired using a Bruker D8 Advance Diffractometer with Cu K $\alpha$  radiation. The diffractometer was set at 40 kV working voltage and 40 mA working current, with samples scanned from 5 to 80° in 2 $\theta$  at a step size of 0.02° and a scan-step time of 4 s. Thermogravimetric analysis (TGA) measurements were conducted on a Mettler Toledo TGA/SDTA 851<sup>e</sup> Thermogravimetric Analyzer with a heating ramp of 10 °C min<sup>-1</sup> under 30 mL min<sup>-1</sup> flowing nitrogen from 25 to 900 °C. Nitrogen gas sorption isotherms were measured at -196 °C using a Micromeritics Tristar 3000 Surface Area and Porosity Analyzer. Before the measurement, samples were degassed at 160 °C for 18 h on a vacuum line. The specific surface area was calculated by a standard multipoint Brunauer-Emmett-Teller (BET) method using adsorption data in the P/P<sub>0</sub> range from 0.05 to 0.20. The Barrett-Joyner-Halenda (BJH) model was applied to the adsorption branch of the isotherm to determine pore size distributions. X-ray photoelectron spectroscopy (XPS) was conducted with a VG ESCALAB 220i-XL X-ray spectrometer equipped with a twin crystal monochromated Al K $\alpha$  X-ray source emitting photon energy of 1486.6 eV at 10 kV and 22 mA. Samples were secured onto Al holders and were measured in the analysis chamber at a typical operating pressure of approximately 7 $\times$ 10<sup>-9</sup> mbar. An electron flood gun was used to compensate the charging effect of nonconductive materials. Spectra were obtained at a step size of either 1.0 eV (survey scans) or 0.05 eV (regional scans). The C 1s peak at 285.0 eV was used as a reference for the calibration of the binding energy scale. Fourier transform

infrared spectroscopy (FTIR) was carried out on a PE IR Spectrum ASCII PEDS 1.60 FTIR spectrometer. Spectra were acquired as the average of 8 scans. To measure the acidity of the samples, temperature programmed desorption of ammonia (TPD-NH<sub>3</sub>) was performed using a Belsorp equipped with a thermal conductivity detector (TCD). Prior to adsorption of ammonia, 15 mg of sample was first preheated at 120 °C under He flow for 1.5 h to remove undesirable physisorbed species, followed by heating under the He environment at 350 °C for 1 h, then cooled to 120 °C. Samples were heated linearly from 120 °C to 650 °C at 10 °C min<sup>-1</sup>.

#### 4.2.4. Catalytic activity test

The catalytic activity of the sulfated TZ samples was evaluated by the dehydration reaction of fructose to 5-HMF. Typically, 15 mg of catalyst was added to a solution of fructose (3 mg) dissolved in DMSO (10 mL, 1.67 mM) in a 25 mL round bottom flask, and well dispersed by ultrasonication (in an ultrasonic bath) for 5 min. The reactor was then heated at 110, 120, 130, 140, 150 or 160 °C for 1, 2, 3 or 6 h in an oil bath. The final products were separated by centrifugation, before the reaction samples were analyzed using a reverse phase preparatory HPLC on an Agilent 1200 series HPLC system. Fructose disappearance was monitored with an Eclipse Plus C18 column (150 mm x 2.1 mm x 5 μm), using 88:12 v/v (water:CH<sub>3</sub>OH) gradient at a flow rate of 0.25 mL min<sup>-1</sup> and a UV detector (λ = 285 nm). It was assumed that the volume changes were negligible after the dehydration reaction for all experiments. Carbohydrate conversion was calculated as moles of fructose reacted per mole of carbohydrate fed, based on an external standard. The 5-HMF yield was calculated as moles of 5-HMF produced based on a 5-HMF external standards curve. Variations in experiments using different solvents (acetonitrile, THF, ethanol and DMF), amounts of catalyst (5, 10, 30 and 45 mg) or the organic substrate (glucose, sucrose, inulin, cellulose and starch) followed the above procedure. The mass spectroscopy (MS) analyses were performed using an Agilent 6500 Q-TOF LC/MS system in negative ion mode to calculate fructose conversion and 5-HMF selectivity. The 5-HMF yield, fructose conversion, and 5-HMF selectivity were calculated based on Equations 1- 3 in section 2.2.5.

Catalyst reusability tests: After each catalytic cycle (150 °C for 6 h), the catalyst (5 mg) was separated by centrifugation, washed thoroughly with ethanol and dried in an

oven at 100 °C overnight. Then the recovered catalyst was heated in a furnace at 200 °C for 4 h before the fructose dehydration reaction was repeated with fresh substrate and solvent.

### 4.3. Results and discussion

Amorphous TZ spheres were synthesized by a sol-gel self-assembly process using HDA as a structure directing agent, followed by ethanolic solvothermal treatment between 140 and 200 °C. Nanostructures comprising both Brønsted and Lewis acid sites were prepared by the addition of sulfate ions (from H<sub>2</sub>SO<sub>4</sub>) to the surface of the TZ nanoparticles followed by high temperature calcination. There were five factors that affected sulfate loading: zirconia content in the TZ composite, solvothermal temperature, H<sub>2</sub>SO<sub>4</sub> concentration, duration of the acid treatment and calcination temperature. Optimization of each feature was required in order to obtain the highest amount of sulfate groups on the TZ surface.

#### 4.3.1. Optimization of the Zr content and H<sub>2</sub>SO<sub>4</sub> treatment conditions

To optimize the Zr content, H<sub>2</sub>SO<sub>4</sub> concentration, and the duration of the acidification process, the solvothermal and calcination temperatures were kept constant at 160 and 500 °C, respectively. The Ti:Zr synthesis ratios were 7:3, 1:1 and 3:7, while the spheres were immersed in 0.1, 1.0 or 2.0 M H<sub>2</sub>SO<sub>4</sub> for either 1 or 3 h. Thermal analysis was used to determine the loading of the sulfate group based on the mass loss from 600 to 850 °C. Figure 4-1 shows the TGA curves for the range of TZx-Solvo160-zMch-Cl500 samples. Curve profiles were similar for all samples. Mass loss up to 600 °C primarily occurred before 200 °C and was attributed to the desorption of physically and chemically adsorbed water molecules and the dehydroxylation process on the surface of the TZ samples. The mass loss between 600 and 850 °C was related to the decomposition of the surface-bound sulfate species, which was believed to be removed as sulfur oxide.<sup>40-42</sup> Figure 4-1 and Figure 4-2 show the sulfate grafting percentage (which is the difference in the mass percentage of the samples at 600 and 850 °C obtained from TGA). Control samples prepared without acid immersion showed negligible mass loss in this range. The sample with a Ti:Zr atomic ratio of 1:1 during preparation that was treated with 2.0 M H<sub>2</sub>SO<sub>4</sub> for 3 h exhibited the biggest mass loss (Figure 4-1 f and Figure 4-2), from which it can be concluded that this sample

had the highest amount of sulfate groups per gram of sample. It was expected that samples with the highest surface area would have more functional groups. However, increasing the Zr content from Ti:Zr atomic ratios of 7:3, 1:1 to 3:7 during synthesis decreased the surface area yet boosted the quantity of sulfate groups present. When the acidification step was extended to 6 h the quantity of functional groups was less than obtained for 3 h, which may be due to partial digestion of the TZ sample matrix. Therefore, a Ti:Zr synthesis ratio of 1:1 was considered optimum for the fabrication of the TZ spheres followed by immersion in 2.0 M H<sub>2</sub>SO<sub>4</sub> for 3 h during the acid treatment step.

#### 4.3.2. Optimization of the solvothermal and calcination temperatures

The effects of varying the solvothermal and calcination temperatures on the loading of the functional group were also investigated by TGA, and the results are shown in Figure 4-3 a and b, respectively. For these experiments, synthesis with a Ti:Zr 1:1 and acid treatment with 2.0 M H<sub>2</sub>SO<sub>4</sub> for 3 h were kept constant. With increasing solvothermal temperature from 140 to 200 °C, the quantity of sulfate groups on the surface decreased. This could be related to a decrease in the surface area (Table 4-1). When the calcination temperature was increased from 500 to 650 °C, the quantity of the functional group decreased dramatically, which implied that the sulfate group had been partially decomposed during calcination. This is evident from the shift to higher temperature for the onset of sulfate removal (Figure 4-3). For the sample calcined at 650 °C, most of the functional group was already decomposed, leading to a small mass of 2.4 wt % associated to remnants of the sulphate functionalization. Thus, the optimum solvothermal and calcination temperatures for retaining the sulfate grafting on the TZ spheres were 140 °C and 500 °C, respectively. Using these optimized

conditions, sample TZ50- Solvo140-2M3h-CI500 had the highest sulfate loading of 10.7 wt%.

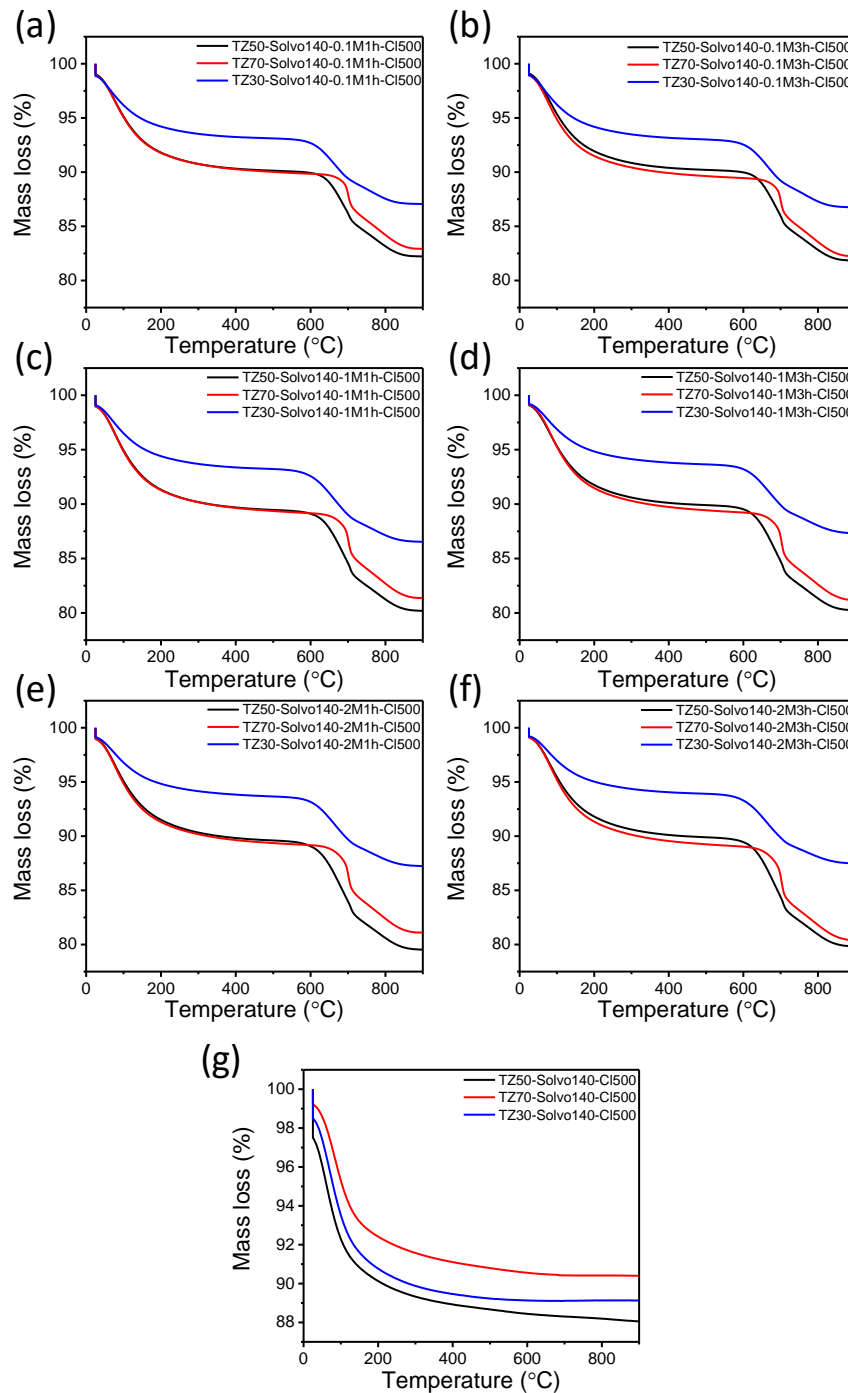


Figure 4-1. TGA results of TZx-Solvo160-zMch-CI500 samples for optimizing Zr content, H<sub>2</sub>SO<sub>4</sub> concentration and duration of the H<sub>2</sub>SO<sub>4</sub> treatment.



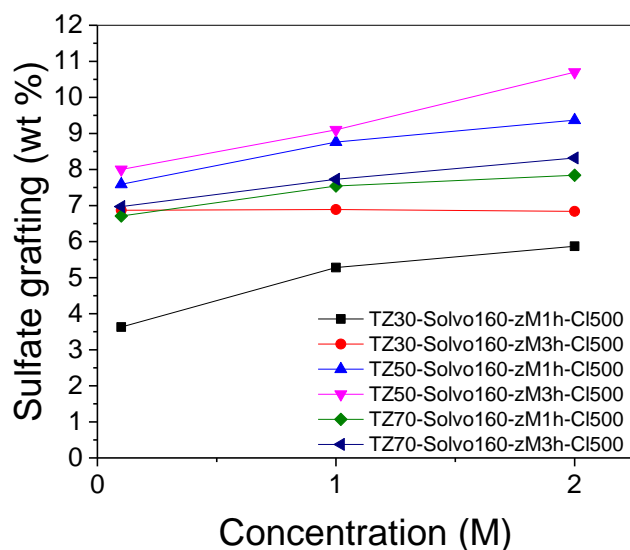


Figure 4-2. The effect of the  $\text{H}_2\text{SO}_4$  concentration, duration of acidification process and Zr content on sulfate grafting percentage.

#### 4.3.3. Surface acidity of the TZ spheres

The acidity of the surface of the TZ spheres, with or without grafting of sulfate group, was evaluated by TPD- $\text{NH}_3$ . An upper limit of 600 °C was chosen for desorption experiments, because TGA of the catalyst had shown a substantial mass loss at higher temperatures due to decomposition of the sulfate group (Figure 4-1). Figure 4-4 shows typical TPD- $\text{NH}_3$  curves of the catalyst prepared under various reaction conditions.

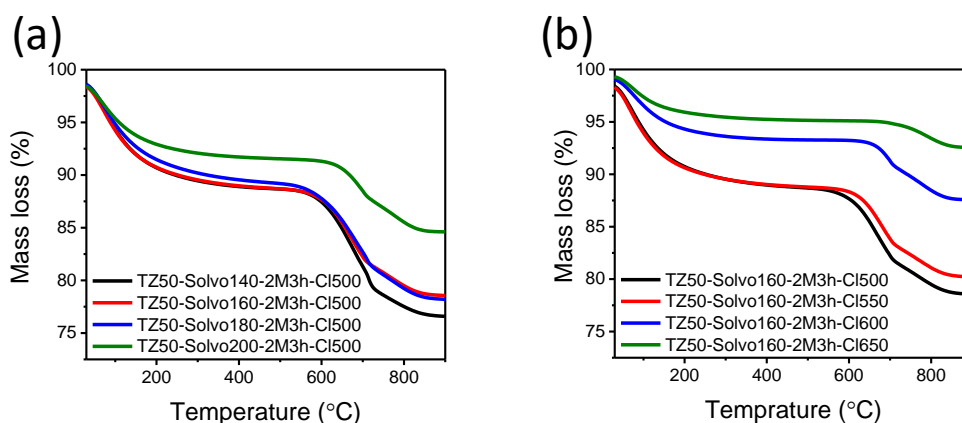


Figure 4-3. TGA results for TZ50-Solvoy-2M3h-Clv samples at different solvothermal (a) and calcination (b) temperatures.

Two main  $\text{NH}_3$  desorption peaks were observed around 200 °C and 570 °C. The quantity of acidity was calculated from the peak areas of the TPD- $\text{NH}_3$  curves and the

results are shown in Table 4-1. Based on Figure 4-4 a, where the solvothermal and calcination temperatures were 140 and 500 °C, respectively, the inclusion of zirconia in the catalyst was crucial for the effective functionalizing of the surface with sulfate groups. This is because the acidified pure Ti sample, i.e., Ti-Solvo140-2M3h-CI500, only showed weak acidity (Table 4-1). By adding zirconia during synthesis of the catalyst (Ti:Zr atomic ratio of 7:3) the surface area increased, but the quantity of acidity was still lower than the acidified pure Zr sample, Zr-Solvo140-2M3h-CI500, Table 4-1. Increasing the zirconia content further (Ti:Zr of 1:1 during synthesis) reduced the surface area slightly (Table 4-1). When the zirconia content in the binary oxide was highest, Ti:Zr 3:7, the quantity of acidity decreased due to reduced surface area (Table 4-1 and Table 4-2). Raising the solvothermal temperature from 140 °C to 200 °C led to a decline in surface area and a decrease in the acidity loading (Figure 4-4 c and Table 4-1). When the calcination temperature increased from 500 °C to 650 °C, as shown in Figure 4-4 d, sulfate groups started to decompose. At 650 °C almost no surface acidity was indicated, which made this sample essentially equivalent in the amount of acidity to both the non-sulfated TZ50 and acidified pure Ti samples (Table 4-1).

Table 4-1. Surface acidity for TZ spheres prepared under various conditions determined from TPD-NH<sub>3</sub> measurements.

Sample name	Acidity (mmol/g)
Zr-Solvo140-2M3h-CI500	0.38
Ti-Solvo140-2M3h-CI500	0.07
TZ30-Solvo140-2M3h-CI500	0.36
TZ70-Solvo140-2M3h-CI500	0.47
TZ50-Solvo140-2M3h-CI500	0.62
TZ50-Solvo160-2M3h-CI500	0.52
TZ50-Solvo180-2M3h-CI500	0.47
TZ50-Solvo200-2M3h-CI500	0.40
TZ50-Solvo140-2M3h-CI550	0.45
TZ50-Solvo140-2M3h-CI600	0.13
TZ50-Solvo140-2M3h-CI650	0.09
TZ50-Solvo140-CI500	0.08

Table 4-2. Surface area and pore diameter of the mesoporous TZ spheres.

Sample	$S_{\text{BET}}^{(a)}$ ( $\text{m}^2\text{g}^{-1}$ )	$PD^{(b)}$ (nm)
TZ30-Solvo140-CI500	420	2.9
TZ50-Solvo140-CI500	392	3.1
TZ70-Solvo140-CI500	305	2.9
TZ50-Solvo140-2M3h-CI500	292	3.1

- <sup>(a)</sup>  $S_{\text{BET}}$  = BET surface area obtained from adsorption data in the  $P/P_0$  range 0.05-0.20.
- <sup>(b)</sup> PD = pore diameter determined by using BJH model from the adsorption branch.

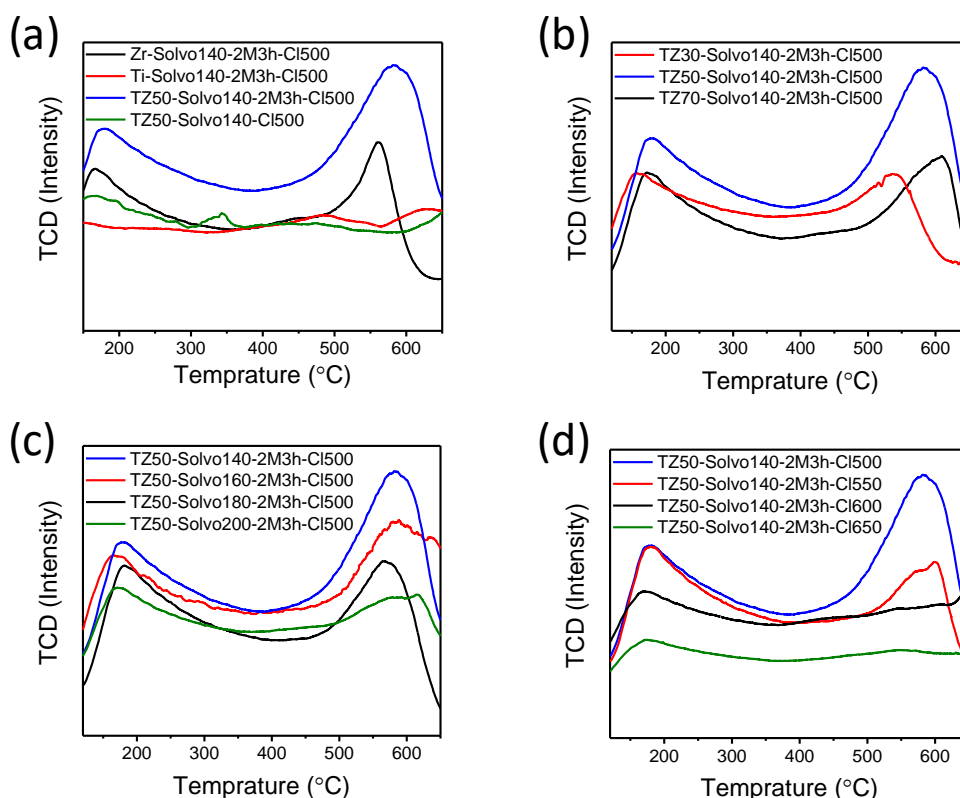


Figure 4-4. TPD-NH<sub>3</sub> curves of (a) non-acidified TZ50 and sulfated pure Ti and Zr control samples, (b) samples with different Zr percentages, the TZ50 catalyst prepared at different (c) solvothermal and (d) calcination temperatures contrasted with the TPD-NH<sub>3</sub> curve of TZ50-Solvo140-2M3h-CI500.

The TPD-NH<sub>3</sub> acidity results obtained are in keeping with the amounts of sulfate grafting as determined by TGA. Therefore, having the strongest surface acidity and highest loading of sulfate groups, TZ50-Solvo140-2M3h-CI500 was considered the

most promising sample for the catalytic dehydration reaction of fructose to 5-HMF. The following section investigates the physical and chemical properties of TZ50-Solvo140-2M3h-CI500.

#### 4.3.4. Characterisation of TZ spheres

Electron microscopy was used to observe the surface morphology and internal structure of TZ50-Solvo140-2M3h-CI500 (Figure 4-5 a). The particles were spherical in shape with a mean diameter of 360 nm. EDX spectra confirmed that the TZ50 spheres contained Ti, Zr and O, and after sulfate grafting, S (Figure 4-5 b).

The crystal phase of the TZ spheres was investigated by XRD. The XRD patterns of TZ50-Solvo140-2M3h-CI500 and TZ50-Solvo140-CI500 (TZ50 samples, prepared by solvothermal treatment at 140 °C with or without grafted sulfate groups) are shown in Figure 4-5 c. Even after calcination at 500 °C the materials remained amorphous, with no crystal phases of either titania or zirconia detected. This result suggests that Ti and Zr were well-distributed within the nanostructure preventing either metal oxide from crystallizing. Moreover, coordination of sulfate groups on the surface did not induce crystallization.

TEM showed that the spheres contained an interconnected “worm-like” porous network, which formed a three-dimensional mesoporous network (Figure 4-6). Significantly, the spherical shape, size and internal morphology were retained after incorporating sulfate groups on the surfaces. The porosity of the spheres is discussed in more detail below. Furthermore, no obvious crystallinity was observed (Figure 4-6), despite calcination at 500 °C.

Nitrogen gas sorption isotherms of the TZ spheres are shown in Figure 4-7. All samples displayed type IV isotherms with a hysteresis loop, indicating mesoporous characteristics.<sup>43</sup> With the introduction of Zr (IV) into the TiO<sub>2</sub> matrix, the crystallization of TiO<sub>2</sub> during solvothermal treatment and calcination ceased. The formation of Ti-O-Zr bonds inhibits Ti atom mobility.<sup>35</sup> With an increasing zirconia content, the surface area of the TZ spheres following solvothermal processing decreased (Error! Reference source not found.), which was in keeping with previous s

tudies.<sup>35,37</sup> A high surface area is one significant factor that can affect the amount of sulfate loading on the surface.

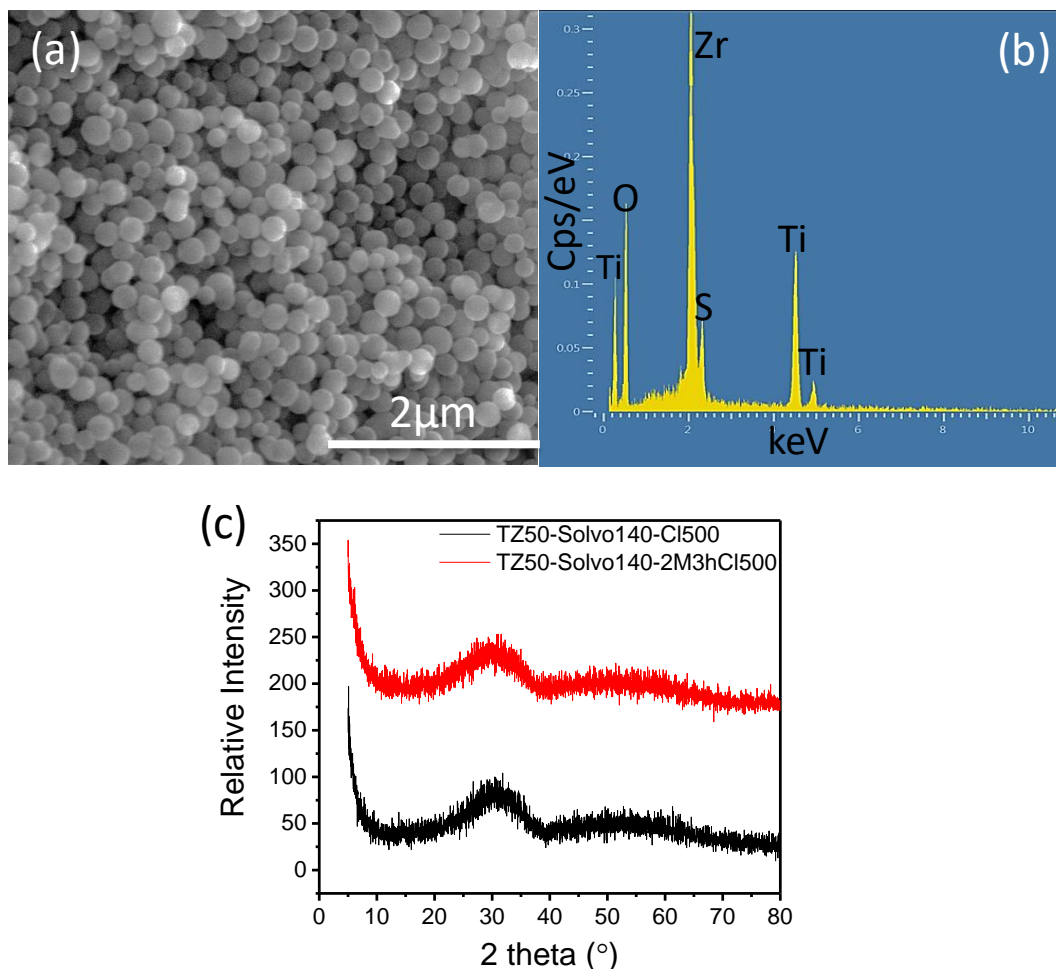


Figure 4-5. (a) SEM image and (b) EDX spectrum (cps/eV is counts per second per eV) of TZ50-Solvo140-2M3h-CI500. (c) XRD patterns of TZ50-Solvo140-2M3h-CI500 and TZ50-Solvo140-CI500. The XRD pattern of TZ50-Solvo140-2M3h-CI500 was shifted up the y-axis for clarity.

For instance, of a series of mesoscopically-assembled, sulfated zirconia nanoparticles prepared by Wang et al.<sup>14</sup> for the dehydration of fructose to 5-HMF, the sample with the highest surface area ( $95.4 \text{ m}^2\text{g}^{-1}$ ) had the highest sulfate loading ( $0.165 \text{ mmolg}^{-1}$ ). Additionally, Joo et al. reported the synthesis of sulfated  $\text{ZrO}_2$  hollow nanostructures with controllable physical and chemical properties. This catalyst was also applied to the dehydration of fructose to 5-HMF.

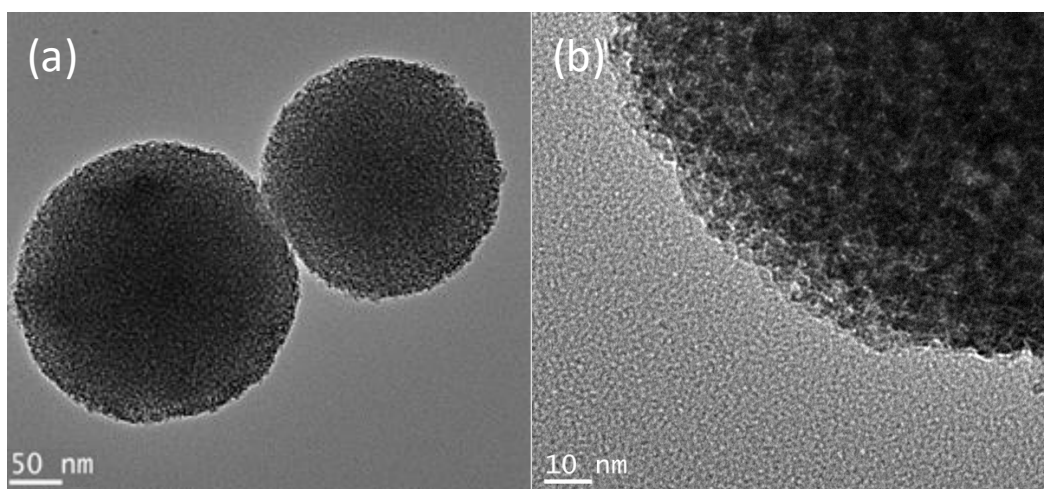


Figure 4-6. TEM images of TZ50-Solvo140-2M3h-Cl500 (a and b).

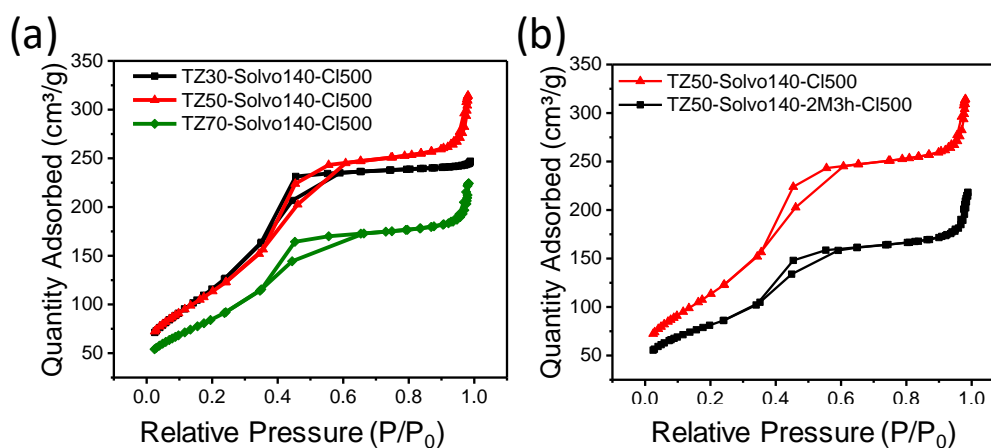


Figure 4-7. Nitrogen sorption isotherms of (a) TZ samples with different Zr content and (b) the TZ50 sample before and after sulfate functionalization.

Compared with a solid ZrO<sub>2</sub> nanostructure (with surface area 50 m<sup>2</sup>g<sup>-1</sup>), the hollow ZrO<sub>2</sub> nanostructure had a higher quantity of sulfate groups on the surface since its surface area was almost double.<sup>10</sup> The leading sample of this work, TZ50-Solvo140-Cl500, has an advantage over the aforementioned materials, with a high surface area of 392 m<sup>2</sup> g<sup>-1</sup> and quantity of acidity (0.62 mmolg<sup>-1</sup>). Hence, TZ50-Solvo140-2M3h-

CI500 is capable of exposing a larger number of acid sites on the surface of the material for the dehydration reaction of fructose to 5-HMF.

XPS was utilized to investigate the surface of the two samples (Figure 4-8). Binding energies for TZ50-Solvo140-CI500, i.e. the sample without sulfate groups, were 458.7, 182.5 and 530.2 eV for Ti 2p, Zr 3d and O 1s, respectively, whereas for TZ50-Solvo140-2M3h-CI500, i.e. the sulfated sample, the binding energies for Ti 2p, Zr 3d, O 1s and S 2p were 459.2, 182.9, 530.7 and 169.4 eV, respectively. The presence of sulfur only in the latter sample was in keeping with the EDX and FT-IR results. It is believed that  $\text{SO}_4^{2-}$  is the only type of S species on the surface of the catalyst.<sup>13, 14</sup> Moreover, the effect of S inclusion on the binding energies of Ti, Zr and O was noticeable from the XPS spectra (Figure 4-8), with all three binding energies slightly increasing because of the stronger electron withdrawing ability of S atoms in TZ50-Solvo140-2M3h-CI500.

Figure 4-8 f shows the FT-IR spectra of the TZ50-Solvo140-CI500 and TZ50-Solvo140-2M3h-CI500 samples, that is, before and after functionalization with a sulfate group. Both samples exhibited absorption peaks in the range of 500-700  $\text{cm}^{-1}$ , which were allocated to Zr-O and Ti-O stretching.<sup>43</sup> The peaks around 3400 and 1600  $\text{cm}^{-1}$  were attributed to the stretching and bending vibrational modes of OH respectively, and indicate the presence of hydroxyl groups and  $\text{H}_2\text{O}$  molecules on the surface of the nanoparticles. Exclusive to TZ50-Solvo140-2M3h-CI500 were the vibrational bands at 1140 and 1240  $\text{cm}^{-1}$  that are characteristic of bidentate or tridentate  $\text{SO}_4^{2-}$  ions, in this case attached to the surface of the TZ50 nanostructure in  $\text{C}_{2v}$  symmetry with a  $\nu_3$  vibration, indicating a strongly super-acidic surface.<sup>43, 44</sup> This accords with EDX (Figure 4-5 b) and XPS (Figure 4-8 a-e) results. Thus, spheres of TZ50-Solvo140-2M3h-CI500 could potentially serve as solid-acid catalysts.

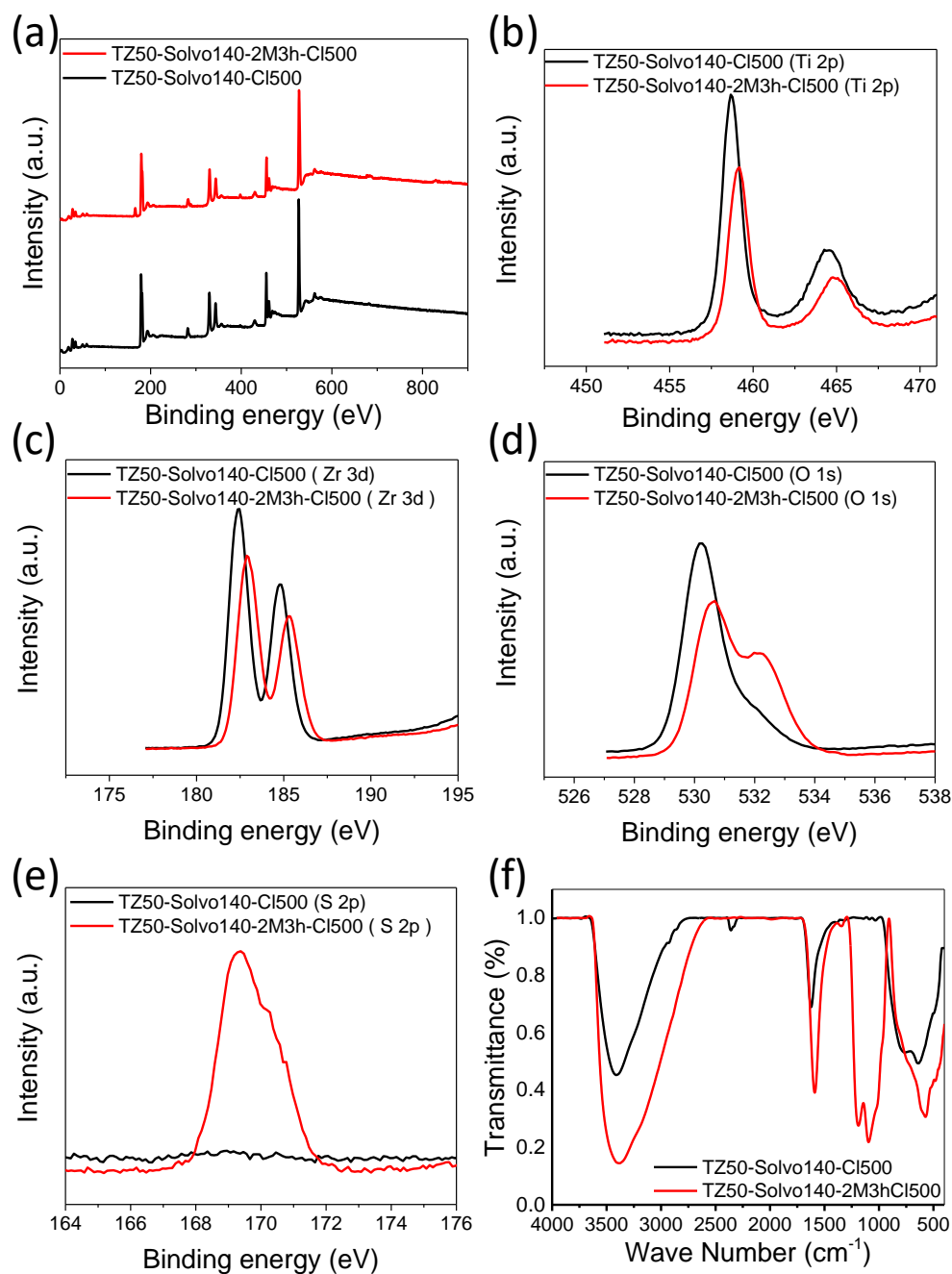


Figure 4-8. XPS (a) and high-resolution XPS spectra of spectra of (b) Ti 2p, (c) Zr 3d, (d) O 1s and (e) S 2p for TZ50-Solvo140-CI500 and TZ50-Solvo140-2M3h-CI500. FT-IR spectra (f) TZ50-Solvo140-CI500 and TZ50-Solvo140-2M3h-CI500.

#### 4.4. Catalytic conversion of fructose to 5-HMF

In this study, fructose was converted to 5-HMF by a catalytic dehydration reaction using TZ50-Solvo140-2M3h-CI500 as a solid-acid catalyst. As discussed above, this sample was selected



#### 4.4.1. Solvent effects on the conversion of fructose to 5-HMF

Water is the most economical solvent for the synthesis of 5-HMF; however, it can accelerate undesired side reactions that decrease the yield. Thus, polar aprotic solvents are used instead. Sugars typically have very low solubility in organic solvents, with the exception of polar coordinating solvents such as DMSO. This solvent was first used in 1980 for preparing 5-HMF by employing an ion-exchange resin with a 90 % yield.<sup>45</sup> In this work, DMSO and other common solvents were initially studied for their effect on the 5-HMF yield after 1 h reaction at 150 °C using TZ50-Solvo140-2M3h-Cl500 as the catalyst (Figure 4-9 a). Among the various solvents trialled, pure DMSO had by far the best results for fructose conversion (99 %) and 5-HMF yield (80 %), from which it was concluded that DMSO was the best solvent for converting fructose to 5-HMF.

#### 4.4.2. The effects of time, temperature and catalyst amount on dehydration of fructose to 5-HMF

Using 15 mg of TZ50-Solvo140-2M3h-Cl500 as the catalyst, a series of dehydration reactions of fructose were carried out between 110 and 160 °C for durations of 1 to 6 h. The results in Figure 4-9 b show that substrate conversion and the yield of 5-HMF in the dehydration reaction of fructose were dependent on the time and temperature of the reaction. The yield of the reaction increased with time as the temperature rose from 110 to 150 °C before moderating at 160 °C. For example, catalytic yields after 1 h reaction were a mere 2 % at 110 °C, enhanced to 80 % at 150 °C, but reduced to 66 % at 160 °C. The greatest 5-HMF yield, 91 %, was achieved at 150 °C for 6 h. The reduced yield at the highest temperature and generally slow increase in yield at all temperatures above 130 °C can be explained by the rapid formation of insoluble humins on the surface of the catalyst, thus shielding some acid reaction sites and limiting the transformation of fructose, perhaps by pore blocking.<sup>46, 47</sup>

Next, the influence of catalyst loading on the dehydration reaction of fructose was evaluated (Figure 4-9 c). Catalyst amounts between 5 and 45 mg were utilized with set reaction conditions of 150 °C for 6 h. When the quantity of the catalyst was less than 15 mg, the 5-HMF yields were nearly the same at 90 % or greater. However, when the catalyst loading was 30 or 45 mg the 5-HMF yield reduced, meaning that the

increased amount of catalyst has transformed fructose into undesired products such as soluble polymers and humins instead of 5-HMF. Based on these results, the efficient conversion of fructose and highest yield of 5-HMF were obtained by running the catalytic dehydration at 150 °C for 6 h and using 5 mg of the TZ50-Solvo140-2M3h-Cl500 catalyst. Finally, conversion and selectivity of the catalyst also were investigated. High fructose conversion (more than 97 %) and 5-HMF selectivity (more than 86 %) were achieved when 5 mg of the catalyst were used for conversion of fructose solution to 5-HMF in DMSO at 150 °C. It shows the catalyst is completely active for dehydration of fructose and it is also very selective towards 5-HMF. It should be noted that one of the advantages of using DMSO as solvent is preventing further dehydration of 5-HMF to the other products such as levulinic and formic acids.<sup>48-50</sup>

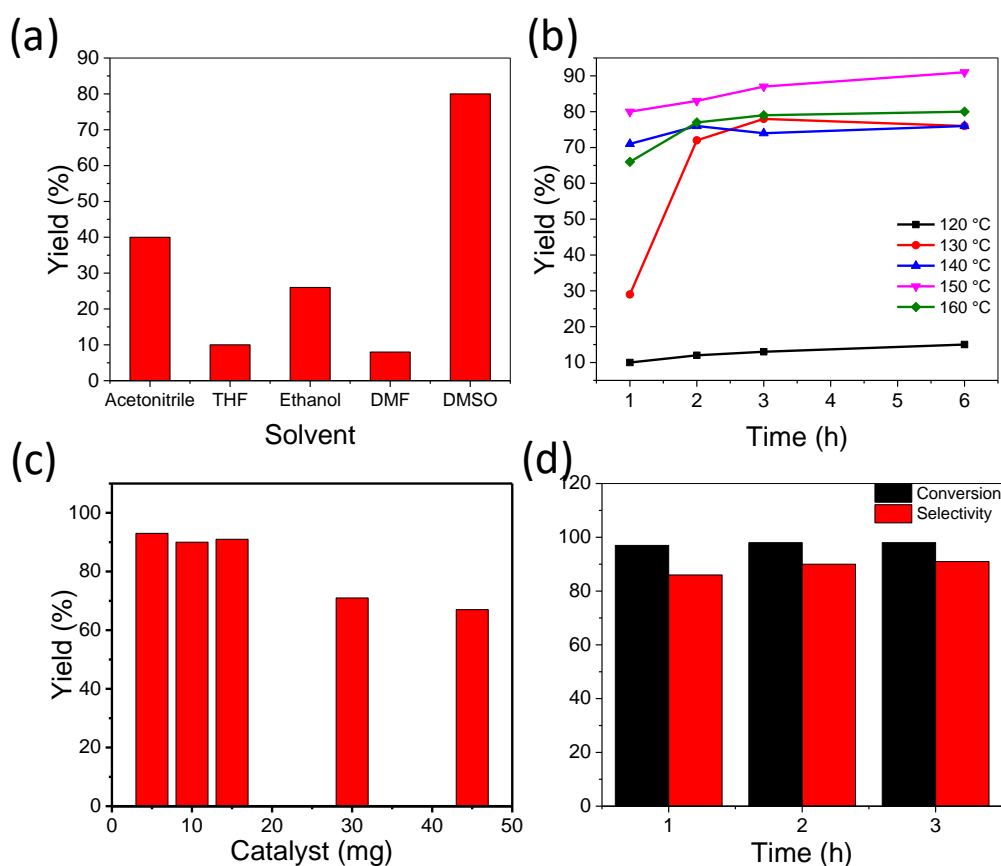


Figure 4-9. The effect of (a) different solvents (15 mg catalyst and fructose solution in DMSO at 150 °C 1 h), (b) reaction temperature and time (15 mg catalyst and fructose solution in DMSO) and (c) the catalyst amount on the yield of production of 5-HMF (fructose solution in DMSO at 150 °C 6 h). (d) Conversion of fructose and 5-HMF selectivity using 5 mg catalyst and fructose solution in DMSO at 150 °C.

#### 4.4.3. Conversion of other feedstocks to 5-HMF

Following the success of the TZ50-Solvo140-2M3h-Cl500 catalyst in the conversion of fructose to 5-HMF, other readily available carbohydrates were trialled as possible feedstocks of 5-HMF. Using only 5 mg of catalyst and run at 150 °C for 6 h, the results of the catalyst performance on various substrates are summarized in Figure 4-10 a. Under the same conditions, the conversion and yield from glucose was approximately half that of sucrose. Glucose converts to 5-HMF in two steps: isomerization of glucose to fructose, which is rate-limiting, followed by catalytic dehydration of fructose to 5-HMF by an acid catalyst. A base or Lewis acid is required for isomerization in order to obtain a reasonable yield.<sup>51, 52</sup> However, the high coverage of sulfate group on the surface of the catalyst can cause a loss of Lewis acidity.<sup>13</sup> Therefore, suppression of the isomerization step may explain the lower yield of 5-HMF from glucose. This may also account for the trace conversion and yields found using cellulose and starch as substrates.

It is worth to mention that higher yield of 5-HMF was obtained when sucrose was used as substrate compared to the glucose (Figure 4-9 c). Sucrose is a disaccharide molecule composed of two monosaccharides: glucose and fructose. So, a mixture of fructose and glucose can be obtained when it is subjected to the acidic environment.<sup>53, 54</sup> For example, Tan-Soetedjo et. al reported the acid-catalyzed conversion of sucrose to levulinic acid recently.<sup>54</sup> They developed a kinetic model which explains 5-HMF formation as well as the dehydration of 5-HMF to form levulinic acid. As a result of sucrose decomposition fructose and glucose can be produced. Fructose molecules could be converted to the 5-HMF efficiently. However, glucose molecules still needed to pass the two-step path that was explained in previous paragraph of this section. Therefore, the yield of 5-HMF was higher when sucrose was used as substrate due to its structure.

#### 4.4.4. Investigation of the catalyst reusability

The ability to recycle a catalyst is important in industrial applications. As discussed above, a reduction or loss of activity on the heterogeneous, solid-acid TZ50-Solvo140-2M3h-Cl500 catalyst is likely caused by the formation of humin deposits on the catalyst surface. To test the reusability of TZ50-Solvo140-2M3h-Cl500, the catalyst

was used in five consecutive runs with limited activity loss observed (Figure 4-10 b). After each catalytic cycle, the catalyst was washed in water and ethanol, dried at 60 °C overnight, then heated in a furnace at 200 °C for 4 h to remove any possible accumulation of humin. After the fifth run the yield of 5-HMF had decreased by just 3 %. Therefore, catalytic activity was maintained over multiple cycles and this catalyst has potential as a reusable, active, solid-acid catalyst in the biomass industries.

The catalyst was stable and maintained its activity due to the preparation method. As it was explained in section 4.2.2, a calcination step needed to be done after acidification process. It also mentioned that calcination temperature played a role in the quantity of sulfate on the surface (Please refer to section 4.3.2 and Figure 4-3 b). So, the calcination temperature was optimized at 500 °C. The calcination process was removed HDA and physically adsorbed sulfate from the surface of TZ spheres. As it can be seen from the TGA results, no mass loss was observed below 600 °C. Therefore, the catalyst activity maintained over multiple cycles due to the strong bond of the sulfate groups with TZ spheres.

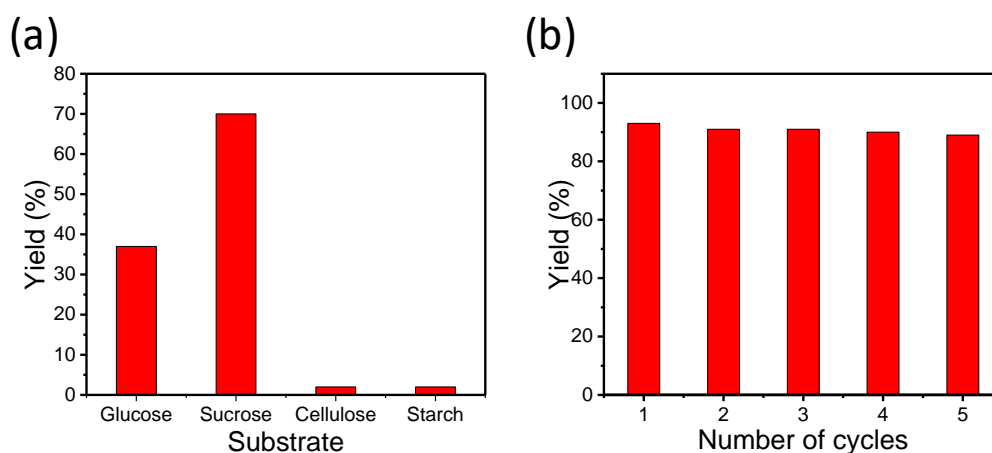


Figure 4-10. The effect of substrate (a) on the dehydration of fructose. (b) The reusability of the TZ50-Solvo140-2M3h-Cl500 catalyst in five consecutive runs.

#### 4.5. Conclusion

Amorphous, mesoporous zirconium titanium oxide spheres were prepared by sol-gel chemistry and solvothermal treatment before being functionalized with sulfate groups to fabricate solid-acid catalysts. The zirconia content played an important role

on the sulphate loading. When the Ti:Zr atomic ratio changed from 7:3 to 1:1 to 3:7 the surface area decreased; however, sulfate grafting was greatest at 10.7 wt% when the Ti:Zr was 1:1 during synthesis and these TZ50 spheres were exposed to a high concentration of H<sub>2</sub>SO<sub>4</sub> (2.0 M) for 3 h. Solvothermal treatment (140 °C) and post-H<sub>2</sub>SO<sub>4</sub> calcination (500 °C) were also optimized, with further increases in temperature for either step reducing the quantity of sulfate. The most promising sample, TZ50-Solvo140-2M3h-CI500, had a surface area of 292 m<sup>2</sup>g<sup>-1</sup> and total surface acid quantity of 0.62 mmol g<sup>-1</sup>, and was applied to the dehydration reaction of fructose to 5-HMF. After optimization of the reaction conditions (5 mg catalyst at 150 °C for 6 h in DMSO), a 93 % yield of 5-HMF for the catalytic reaction was obtained. Under optimized conditions, 99 and 91 % of conversion of fructose and 5-HMF selectivity, respectively, were achieved after 3h. The catalyst was also reusable, preserving activity after five consecutive cycles, with the 5-HMF yield diminished by only 3 %. Yields for the conversion of sucrose and glucose to 5-HMF were decent (70 and 35 %, respectively), but for other common carbohydrate feedstocks (starch and cellulose) relatively poor yields resulted, possibly due to the high coverage of sulfate on the catalyst surface interfering with the isomerisation reaction of glucose to fructose.

#### 4.5.1. Comparing catalytic performance of TZ50-Solvo140-2M3h-CI500 with other catalysts.

The catalytic performance of TZ50-Solvo140-2M3h-CI500 for the conversion of fructose, sucrose and glucose was much higher than TZ30-P and Zr-Ter. Under optimized conditions the yields of 5-HMF from a fructose solution were 93, 67 and 42 %, respectively. Therefore, achieving a high surface area and having selected acidic functional groups present on the catalyst surface are key factors that impact the catalytic reaction. This is consistent with the inferences made in section 2.5.1.

In comparing between a phosphated catalyst and sulfated catalyst, the procedure of phosphate grafting on the surface of metal oxides is easier and greener than sulfate attachment. Metal-O-P bonds are very strong and can be made through the simple mixing of metal oxides and phosphoric acid solution, and without needing a calcination step to promote functional group attachment. On the other hand, the

acidity strength of sulfate-metal oxides is generally higher than phosphate-metal oxides.

TZ50-Solvo140-2M3h-Cl500 showed superior performance in comparison with other sulfated catalysts in the literature (Table 4-3). For example, Wang et al. prepared mesoscopically assembled sulfated zirconia for the conversion of carbohydrates to 5-HMF.<sup>14</sup> This catalyst had much lower acid concentration and surface area ( $0.165 \text{ mmol g}^{-1}$  and  $95.4 \text{ m}^2\text{g}^{-1}$ ) compared to TZ50-Solvo140-2M3h-Cl500. Additionally, yields of 5-HMF obtained from sucrose and glucose solution were respectively 70 and 35% using TZ50-Solvo140-2M3h-Cl500 as the catalyst, compared with just 43.7 and 7.4% for sulfated zirconia.<sup>14</sup> On the other hand, Qi et al. gained an excellent yield of 5-HMF (88%) using a sulfated zirconia catalyst,<sup>55</sup> but the ionic liquid solvent ([BMIM][Cl]) is very expensive and made separation of the final product difficult.

Table 4-3. A comparison of catalytic performance of the TZ50-Solvo140-2M3h-Cl500 with those of reported sulfated catalyst.

Catalyst	Solvent	Temperature (°C)	Time (h)	5-HMF yield (%)	Reference
$\text{SO}_4^{2-}/\text{ZrO}_2\text{-Al}_2\text{O}_3$	DMSO	130	4	68	25
$\text{SO}_4^{2-}/\text{ZrO}_2$	DMSO	130	4	64	25
$\text{SO}_4^{2-}/\text{ZrO}_2$ hollow nanostructure	DMSO	120	1	65	56
Mesoscopically assembled $\text{SO}_4^{2-}/\text{ZrO}_2$	DMSO	120	2	92	14
Sulfated $\text{TiO}_2$	Methanol	175	1	33	57
$\text{SO}_4^{2-}/\text{ZrO}_2\text{-SnO}_2$	DMSO	120	2.5	75	58
$\text{SO}_4^{2-}/\text{ZrO}_2$	DMSO-acetone	180	0.3	73	59
$\text{SO}_4^{2-}/\text{ZrO}_2$	Ionic liquid ([BMIM][Cl])	100	0.5	88	55
TZ50-Solvo140-2M3h-Cl500	DMSO	150	6	93	This work

Therefore, through careful control of morphology, composition and surface functional groups, versatile mesoporous zirconium titanium oxides could open new avenues for cost effective, sustainable biomass refinery processes, and so lead to the production of affordable biochemicals and biofuels.

## 4.6. References

1. A. J. Ragauskas, C. K. Williams, B. H. Davison, G. Britovsek, J. Cairney, C. A. Eckert, W. J. Frederick, J. P. Hallett, D. J. Leak, C. L. Liotta, J. R. Mielenz, R. Murphy, R. Templer and T. Tschaplinski, *Science*, 2006, **311**, 484-489.
2. A. Corma, S. Iborra and A. Velty, *Chemical Reviews*, 2007, **107**, 2411-2502.
3. P. Daorattanachai, P. Khemthong, N. Viriya-empikul, N. Laosiripojana and K. Faungnawakij, *Carbohydrate Research*, 2012, **363**, 58-61.
4. C.-H. Zhou, X. Xia, C.-X. Lin, D.-S. Tong and J. Beltramini, *Chemical Society Reviews*, 2011, **40**, 5588-5617.
5. P. N. R. Vennestrøm, C. M. Osmundsen, C. H. Christensen and E. Taarning, *Angewandte Chemie International Edition*, 2011, **50**, 10502-10509.
6. D. M. Alonso, J. Q. Bond and J. A. Dumesic, *Green Chemistry*, 2011, **13**, 754-793.
7. L. Hu, G. Zhao, W. Hao, X. Tang, Y. Sun, L. Lin and S. Liu, *RSC Advances*, 2012, **2**, 11184-11206.
8. R.-J. van Putten, J. C. van der Waal, E. de Jong, C. B. Rasrendra, H. J. Heeres and J. G. de Vries, *Chemical Reviews*, 2013, **113**, 1499-1597.
9. X. Qi, H. Guo, L. Li and R. L. Smith, *ChemSusChem*, 2012, **5**, 2215-2220.
10. J. B. Joo, A. Vu, Q. Zhang, M. Dahl, M. Gu, F. Zaera and Y. Yin, *ChemSusChem*, 2013, **6**, 2001-2008.
11. J. Chen, K. Li, L. Chen, R. Liu, X. Huang and D. Ye, *Green Chemistry*, 2014, **16**, 2490-2499.
12. C.-H. Kuo, A. S. Poyraz, L. Jin, Y. Meng, L. Pahalagedara, S.-Y. Chen, D. A. Kriz, C. Guild, A. Gudz and S. L. Suib, *Green Chemistry*, 2014, **16**, 785-791.
13. A. Osatiashtiani, A. F. Lee, D. R. Brown, J. A. Melero, G. Morales and K. Wilson, *Catalysis Science & Technology*, 2014, **4**, 333-342.
14. N. Wang, Y. Yao, W. Li, Y. Yang, Z. Song, W. Liu, H. Wang, X.-F. Xia and H. Gao, *RSC Advances*, 2014, **4**, 57164-57172.
15. B. F. M. Kuster, *Starch - Stärke*, 1990, **42**, 314-321.
16. R. M. de Almeida, L. K. Noda, N. S. Gonçalves, S. M. P. Meneghetti and M. R. Meneghetti, *Applied Catalysis A: General*, 2008, **347**, 100-105.
17. A. J. Crisci, M. H. Tucker, M.-Y. Lee, S. G. Jang, J. A. Dumesic and S. L. Scott, *ACS catalysis*, 2011, **1**, 719-728.
18. E. Nikolla, Y. Román-Leshkov, M. Moliner and M. E. Davis, *ACS catalysis*, 2011, **1**, 408-410.
19. D. S. Park, B. K. Kwak, N. D. Kim, J. R. Park, J.-H. Cho, S. Oh and J. Yi, *ChemCatChem*, 2012, **4**, 836-843.
20. A. Takagaki, M. Ohara, S. Nishimura and K. Ebitani, *Chemical Communications*, 2009, DOI: 10.1039/B914087E, 6276-6278.
21. M. S. Holm, S. Saravanamurugan and E. Taarning, *Science*, 2010, **328**, 602-605.
22. C. Morterra, G. Cerrato, F. Pinna and M. Signoretto, *Journal of Catalysis*, 1995, **157**, 109-123.
23. K. Saravanan, B. Tyagi and H. C. Bajaj, *Catalysis Science & Technology*, 2012, **2**, 2512-2520.



24. J. Navarrete, T. Lopez, R. Gomez and F. Figueras, *Langmuir*, 1996, **12**, 4385-4390.
25. H. Yan, Y. Yang, D. Tong, X. Xiang and C. Hu, *Catalysis Communications*, 2009, **10**, 1558-1563.
26. G. X. Yu, X. L. Zhou, F. Liu, C. L. Li, L. F. Chen and J. A. Wang, *Catalysis Today*, 2009, **148**, 70-74.
27. T. Y. Kim, D. S. Park, Y. Choi, J. Baek, J. R. Park and J. Yi, *Journal of Materials Chemistry*, 2012, **22**, 10021-10028.
28. Z. Li, R. Wnetrzak, W. Kwapinski and J. J. Leahy, *ACS Applied Materials & Interfaces*, 2012, **4**, 4499-4505.
29. Q. Lu, W.-M. Xiong, W.-Z. Li, Q.-X. Guo and X.-F. Zhu, *Bioresource Technology*, 2009, **100**, 4871-4876.
30. B. Krishnakumar and M. Swaminathan, *Journal of Organometallic Chemistry*, 2010, **695**, 2572-2577.
31. J. L. Roper-Vega, A. Aldana-Pérez, R. Gómez and M. E. Niño-Gómez, *Applied Catalysis A: General*, 2010, **379**, 24-29.
32. T. Wang, Y. J. Pagán-Torres, E. J. Combs, J. A. Dumesic and B. H. Shanks, *Topics in Catalysis*, 2012, **55**, 657-662.
33. K.-i. Tominaga, A. Mori, Y. Fukushima, S. Shimada and K. Sato, *Green Chemistry*, 2011, **13**, 810-812.
34. M. Chee Kimling, N. Scales, T. L. Hanley and R. A. Caruso, *Environmental Science & Technology*, 2012, **46**, 7913-7920.
35. D. Chen, L. Cao, T. L. Hanley and R. A. Caruso, *Advanced Functional Materials*, 2012, **22**, 1966-1971.
36. J. Choi, A. Ide, Y. B. Truong, I. L. Kyratzis and R. A. Caruso, *Journal of Materials Chemistry A*, 2013, **1**, 5847-5853.
37. X. Wang, D. Chen, L. Cao, Y. Li, B. J. Boyd and R. A. Caruso, *ACS Applied Materials & Interfaces*, 2013, **5**, 10926-10932.
38. M. C. Kimling, D. Chen and R. A. Caruso, *Journal of Materials Chemistry A*, 2015, **3**, 3768-3776.
39. B. M. Reddy and A. Khan, *Catalysis Reviews*, 2005, **47**, 257-296.
40. J. R. Satam and R. V. Jayaram, *Catalysis Communications*, 2008, **9**, 1033-1039.
41. X. Qi, M. Watanabe, T. M. Aida and R. L. Smith Jr, *Catalysis Communications*, 2009, **10**, 1771-1775.
42. B. M. Reddy and M. K. Patil, *Chemical Reviews*, 2009, **109**, 2185-2208.
43. K. S. Sing, *Pure and applied chemistry*, 1985, **57**, 603-619.
44. X. Li, K. Nagaoka, R. Olindo and J. A. Lercher, *Journal of Catalysis*, 2006, **238**, 39-45.
45. Y. Nakamura and S. Morikawa, *Bulletin of the Chemical Society of Japan*, 1980, **53**, 3705-3706.
46. B. Karimi, H. M. Mirzaei, H. Behzadnia and H. Vali, *ACS Applied Materials & Interfaces*, 2015, **7**, 19050-19059.
47. H. M. Mirzaei and B. Karimi, *Green Chemistry*, 2016, **18**, 2282-2286.
48. J. Zhao, C. Zhou, C. He, Y. Dai, X. Jia and Y. Yang, *Catalysis Today*, 2016, **264**, 123-130.
49. X. Zheng, X. Gu, Y. Ren, Z. Zhi and X. Lu, *Biofuels, Bioproducts and Biorefining*, 2016, **10**, 917-931.

50. L. T. Mika, E. Cséfalvay and Á. Németh, *Chemical Reviews*, 2018, **118**, 505-613.
51. J. B. Binder, A. V. Cefali, J. J. Blank and R. T. Raines, *Energy & Environmental Science*, 2010, **3**, 765-771.
52. Y. Román-Leshkov, M. Moliner, J. A. Labinger and M. E. Davis, *Angewandte Chemie International Edition*, 2010, **49**, 8954-8957.
53. S. Bower, R. Wickramasinghe, N. J. Nagle and D. J. Schell, *Bioresource Technology*, 2008, **99**, 7354-7362.
54. J. N. M. Tan-Soetedjo, H. H. van de Bovenkamp, R. M. Abdilla, C. B. Rasrendra, J. van Ginkel and H. J. Heeres, *Industrial & Engineering Chemistry Research*, 2017, **56**, 13228-13239.
55. X. Qi, H. Guo and L. Li, *Industrial & Engineering Chemistry Research*, 2011, **50**, 7985-7989.
56. J. J. Bong, V. Austin, Z. Qiao, D. Michael, G. Minfen, Z. Francisco and Y. Yadong, *ChemSusChem*, 2013, **6**, 2001-2008.
57. J. Zhang, S. B. Wu and B. Li, *Advanced Materials Research*, 2013, **666**, 131-142.
58. Y. Wang, X. Tong, Y. Yan, S. Xue and Y. Zhang, *Catalysis Communications*, 2014, **50**, 38-43.
59. X. Qi, M. Watanabe, T. M. Aida and R. L. Smith, *Catalysis Communications*, 2009, **10**, 1771-1775.



## Chapter 5. Conclusion and future work

According to the International Energy Outlook 2017, total world energy consumption is expected to increase 28% by 2040.<sup>1</sup> The shortage of carbon-based fuels and the time required for their replacement has motivated research for the development of renewable resources to replenish petroleum derivatives. 5-(hydroxymethyl)furfural (5-HMF) has been identified as both an energy source and a versatile platform molecule for the chemical and petroleum industries (refer to chapter 1, sections 1.3 to 1.5). This thesis focused on synthesizing 5-HMF from carbohydrates using a solid acid catalyst. The motivations for the research were presented in section 1.10, forming a single objective, to *prepare, functionalize and characterize mesoporous titania, zirconia and binary titanium zirconium oxides for the conversion of carbohydrates to 5-HMF*. To fulfil that objective, six aims were set:

- vii. Synthesise zirconium dioxide spheres by controlling the physical properties of pore diameter and surface area, then modify the zirconia surface with aliphatic di-carboxylic acids, aromatic di-carboxylic acids or amino acids to prepare a multifunctional catalyst that contains both Lewis and Brønsted acid and base sites for the conversion of sugars to 5-HMF.
- viii. Control the crystal structure of zirconia to tune the acid strength of the surface.
- ix. Prepare mesoporous titanium zirconium oxide spheres and control the physicochemical properties of pore diameter, surface area and surface hydroxyl group density, and study the effect of Ti:Zr ratio, solvothermal temperature and calcination temperature on the physicochemical properties.
- x. Functionalize the surface of high surface area mesoporous titanium zirconium oxide spheres with phosphonic acid derivatives to prepare a multifunctional solid acid catalyst for the dehydration of carbohydrates to 5-HMF.
- xi. Graft sulfate groups on the surface of the mesoporous titanium zirconium oxide spheres to prepare a solid acid catalyst for the conversion of carbohydrates to 5-HMF, studying the effect of sulfuric acid concentration, duration of acid treatment, calcination temperature and Ti:Zr ratio on the grafting percentage of sulfate on the surface.

- xii. Apply the prepared solid acid catalysts for the conversion of fructose to 5-HMF, and study the effect of time, temperature, solvent, substrate and loading of the catalyst on the 5-HMF yield.

This chapter includes a summary of the key research findings and how they have addressed the thesis aims, and future work for this thesis research within a global carbohydrate catalysis context.

## 5.1. Research summary

Mesoporous zirconia and titanium zirconium oxide samples were prepared via a sol-gel method followed by solvothermal and calcination treatments to form the base structure of three kinds of functionalized solid-acid catalysts. Mesopore size, surface area, crystal phase composition and hydroxyl group surface density were tuned via the solvothermal temperature and calcination temperature, as well as the Ti:Zr atomic ratio for the titanium zirconium oxide spheres. As discussed in section 1.9, the strength of the acid on the catalyst surface for bare metal oxides such as zirconia and titania is weak, and requires modification with acidic functional groups to increase surface acidity. In this context, after preparing the mesoporous samples, the surfaces of promising samples were modified with functional groups of dicarboxylic acids, phosphate derivatives or sulfate.

The pore size of the mesoporous zirconia spheres increased from 2.9 to 9.0 nm when the solvothermal temperature was increased from 100 to 200 °C. At a solvothermal temperature of 140 °C the highest surface area ( $84 \text{ m}^2\text{g}^{-1}$ ) was gained; however, the pore size was only 3.8 nm. In comparison, the surface area of the zirconia spheres solvothermally treated at 160 °C (Zr-Sol160) decreased from 84 to  $75 \text{ m}^2 \text{ g}^{-1}$ , but the mesopore size grew to 6.1 nm. Hence, this sample was selected for functionalization with dicarboxylic and amino acids.

The Lewis acidity of zirconia depends on the percentage of the monoclinic phase present, since Lewis acidity is predominately associated with this phase. Additionally, Lewis acidity plays a key role in the conversion of glucose to 5-HMF. All zirconia samples contained a mix of tetragonal and monoclinic crystal phases; the phase composition was controlled via the solvothermal temperature. The highest

percentage of monoclinic phase (61%) was attained at a solvothermal temperature of 160 °C. Solvothermal treatment at 200 °C produced largely tetragonal phase zirconia. Zr-Sol160 was functionalized with different di-carboxylic acids and amino acids: The quantity of functional groups grafted onto the surface was higher with an aromatic dicarboxylic acid (i.e., terephthalic acid, Ter) than with either aliphatic dicarboxylic acids (i.e., Adipic acid and Succinic acid) or amino acids (i.e., Aspartic acid and Glutamic acid). After functionalizing with Ter (Zr-Ter) the highest grafting percentage of 8.7 wt% was obtained. Therefore, this research has met aims (i) and (ii). Zr-Ter was used as a solid acid catalyst for the conversion of carbohydrates to 5-HMF. At optimized conditions, the yield of 5-HMF was 42% from fructose solution in a dimethyl sulfoxide (DMSO) solvent at 150 °C after 2 h. Yields of 5-HMF from sucrose and glucose were 37 and 22%, respectively. The catalyst was used for five consecutive runs with only a small loss in activity.

Mesoporous titanium zirconium oxide was prepared using the same methods and strategies. After addition of the titania precursor to the zirconia precursor, the textural properties of the final mesoporous compounds were massively changed compared to the zirconia spheres. When the Ti:Zr atomic ratio was 7:3 (sample TZ30), a surface area of 420 m<sup>2</sup> g<sup>-1</sup> resulted, which was the highest in this thesis. Other factors that had a considerable impact on surface area and mesopore diameter were the solvothermal and calcination temperatures. By raising the solvothermal temperature from 100 to 140 °C the surface area was increased; however, further enhancement to 200 °C caused a decline in the surface area of the TZ30 samples. On the other hand, the mesopore size was enlarged from 1.9 to 6.4 nm with increasing solvothermal temperature. Furthermore, a basic environment (from the addition of ammonia) during the solvothermal process enlarged the pore size but decreased the surface area. This research (Chapter 4) satisfies aim (iii). Following solvothermal treatment at 160 °C and calcination at 500 °C, the most promising TZ30 sample was modified with nitrilotri(methylphosphonic acid) (NPA) (a surface loading of 0.3 mmol g<sup>-1</sup>), then used as a solid-acid catalyst (TZ30-P) for the dehydration of fructose to 5-HMF. This part of the study realized aim (iv). The highest yield of 5-HMF from a fructose solution in DMSO was 67% using 30 mg catalyst at 160 °C for 2 h. Yields of 5-HMF from sucrose

and glucose were 53% and 21%, respectively. The catalyst was reusable and recycled five times, with the yield of 5-HMF reduced by a mere 3%.

One of the common types of solid acid catalyst for the dehydration of carbohydrates to 5-HMF is sulfated-metal oxide. In this thesis, mesoporous zirconium titanium oxide spheres were prepared by sol-gel chemistry, solvothermally treated at different temperatures, functionalized with sulfate groups, and finally calcined to fabricate solid-acid catalysts. Unlike the preceding research, catalyst calcination occurred after functionalization, because calcination is necessary for effective sulfate grafting. The zirconia content, sulfuric acid concentration and duration of acid treatment all had a great impact on sulfate loading. Sulfate grafting was highest at 10.7 wt% when the Ti:Zr atomic ratio was 1:1 (sample TZ50), and these TZ50 spheres were exposed to a high concentration of H<sub>2</sub>SO<sub>4</sub> (2 M) for 3 h. When the temperatures of the solvothermal treatment and calcination were increased above 140 °C and 500 °C, respectively, the quantity of sulfate on the surface of the TZ50 samples was reduced. The best sample, TZ50-Solvo140-2M3h-Cl500, had a total surface acid quantity of 0.62 mmol g<sup>-1</sup> and was utilized in the dehydration reaction of fructose to 5-HMF. This research has successfully satisfied aim (v). The dehydration reaction was affected by the factors of time, temperature, solvent, substrate and the amount of catalyst. Under optimized reaction conditions of 5 mg catalyst at 150 °C for 6 h in DMSO the yield of 5-HMF was 93%. The catalyst was recycled five times with only a 3% loss in 5-HMF yield in the fifth cycle. The yields for the conversion of sucrose and glucose to 5-HMF were 70 and 37%, respectively.

The acid functional group, optimized reaction conditions and 5-HMF yields of the three best performing solid-acid catalysts prepared in this thesis are compared. As can be seen, TZ50-Solvo140-2M3h-Cl500 was best across all three carbohydrate substrates, even after just 1 h of reaction, followed by TZ30-P and then Zr-Ter. Additionally, five major inferences can be made:

- 1- The three catalysts were successful in converting fructose to 5-HMF by a dehydration reaction, which collectively have realized aim (vi).
- 2- All catalysts showed a reasonable to high performance for the conversion of sucrose to 5-HMF.

Table 5-1. Comparison of the best performing solid-acid catalysts.

	Zr-Ter	TZ30-P	TZ50-Solvo140- 2M3h-Cl500
Functional group	Ter	NPA	Sulfate
Solvent	DMSO	DMSO	DMSO
Temperature (°C)	150	160	150
Time (h)	2	2	6
Amount of catalyst (mg)	15	30	5
Yield (%) of 5-HMF for substrate: fructose, sucrose and glucose	42, 37 and 22	67, 53 and 21	93, 70 and 37
Loss in 5-HMF yield (%) in fifth cycle	5	3	3

- 3- The yields of 5-HMF obtained from the dehydration of glucose were not high. The reason for this is explained in section 4.4.3. Briefly, the process of glucose conversion is a two-step process in which the first, rate determining step needs a base or Lewis acid catalyst.
- 4- The catalysts were unsuccessful for the conversion of cellulose and starch. These carbohydrates have complex structures and are insoluble in many conventional solvents which make the process of dehydration more difficult.<sup>2</sup> To depolymerize these compounds to simpler molecules such as glucose requires employing concentrated salt additives, toxic heavy metals and/or ionic liquids, which are expensive.<sup>3-5</sup>
- 5- All catalysts were capable of consecutive catalytic runs, with only a small loss of 5-HMF yield in the fifth cycle.

In conclusion, by careful control of morphology, metal oxide composition, mesopore size and surface functional group, mesoporous zirconia and binary titanium zirconium oxides could open a new pathway for the cost effective and sustainable biomass refinery production of high value chemicals and biofuels.



## 5.2. Future work

### 5.2.1. Mechanism of the catalytic system

The production of platform chemicals from carbohydrates depends on the catalytic system. Therefore, understanding the catalytic system at the molecular level, in addition to recognizing and characterizing key intermediates of the catalytic reaction is vital to surpassing the performance of existing methods and processes. To achieve deeper insights and design better catalyst, in-situ spectroscopy or isotope labeling methods could be useful.

### 5.2.2. Designing multifunctional catalysts that include both acidic and basic sites

The main component of lignocellulosic biomass is cellulose, and the efficient conversion of cellulose to 5-HMF is the chief limitation for using complex biomass as a chemical feedstock. Model sugars such as fructose are simple materials for proof-of-concept, but commercially the successful conversion of non-edible resources is crucial. In this context, preparing a multifunctional catalyst with a high quantity of Lewis and Brønsted acidic and basic sites on the surface, little or no loss of activity after multiple catalytic cycles, and very low leaching of catalyst during the catalytic reaction is highly sought.

### 5.2.3. Scaling-up the process of 5-HMF production

The conversion of fructose or glucose to 5-HMF is a significant research area. Although excellent catalyst activity was demonstrated in this thesis, and in the literature, the scale-up and economic production of 5-HMF, including solvent and catalyst recycling, and product purification, remains a challenge. Thus, investigation of scaling-up procedures is demanded.

### 5.3. References

1. INTERNATIONAL ENERGY OUTLOOK 2017, <https://www.eia.gov/outlooks/ieo/#1>).
2. R. Rinaldi and F. Schüth, *ChemSusChem*, 2009, **2**, 1096-1107.
3. J. B. Binder and R. T. Raines, *Journal of the American Chemical Society*, 2009, **131**, 1979-1985.
4. Y. Zhang, J. Pan, M. Gan, H. Ou, Y. Yan, W. Shi and L. Yu, *RSC Advances*, 2014, **4**, 11664-11672.
5. B. R. Caes, M. J. Palte and R. T. Raines, *Chemical Science*, 2013, **4**, 196-199.



Minerva Access is the Institutional Repository of The University of Melbourne

**Author/s:**

Motevalizadeh, Seyed Farshad

**Title:**

Functionalized mesoporous metal oxide spheres as catalysts for efficient conversion of carbohydrates into 5-hydroxymethylfurfural

**Date:**

2018

**Persistent Link:**

<http://hdl.handle.net/11343/218095>

**File Description:**

Functionalized mesoporous metal oxide spheres as catalysts for efficient conversion of carbohydrates into 5-hydroxymethylfurfural

**Terms and Conditions:**

Terms and Conditions: Copyright in works deposited in Minerva Access is retained by the copyright owner. The work may not be altered without permission from the copyright owner. Readers may only download, print and save electronic copies of whole works for their own personal non-commercial use. Any use that exceeds these limits requires permission from the copyright owner. Attribution is essential when quoting or paraphrasing from these works.